NPS-57Bp76051

NAVAL POSTGRADUATE SCHOOL
Monterey, California

STRUCTURAL RESPONSE OF FLUID-CONTAINING-TANKS TO PENETRATING PROJECTILES (HYDRAULIC RAM) - A COMPARISON OF EXPERIMENTAL AND ANALYTICAL RESULTS

R. E. BALL

MAY 1976

Prepared for:
Naval Weapons Center
China Lake, CA 93555
and the
Joint Technical Coordinating Group/Aircraft Survivability

NAVAL POSTGRADUATE SCHOOL

Monterey, California

Rear Admiral I. W. Linder
Superintendent

Jack R. Borsting
Provost

The work reported herein was supported by the Naval Weapons Center, China Lake, California.

This report was prepared by:

R. E. BALL
Associate Professor of Aeronautics

Reviewed by:

R. W. BELL, Chairman
Department of Aeronautics

Released by:

R. R. FOSSUM
Dean of Research

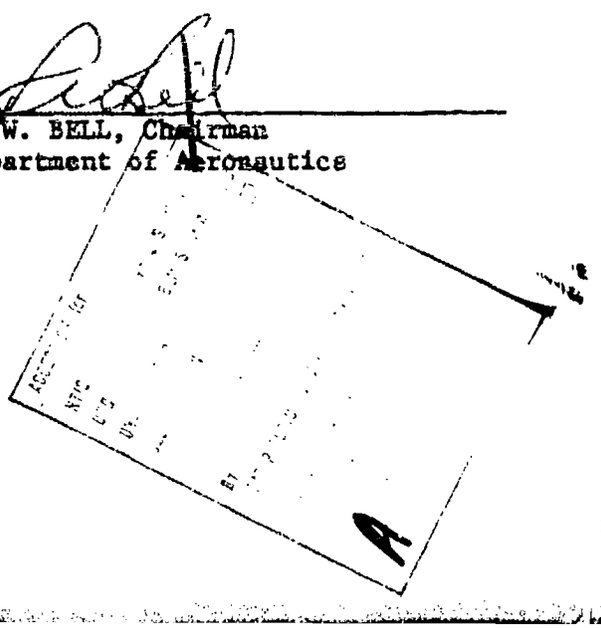

UNCLASSIFIED
SECURITY CLASSIFICATION OF THIS PAGE (When Data Entered)

REPORT DOCUMENTATION PAGE	READ INSTRUCTIONS BEFORE COMPLETING FORM
(14) NPS-57Bp76051 / 2. GOVT ACCESSION NO.	3. RECIPIENT'S CATALOG NUMBER (9)
4. TITLE (and Subtitle) (6) STRUCTURAL RESPONSE OF FLUID CONTAINING TANKS TO PENETRATING PROJECTILES (HYDRAULIC RAM) - A COMPARISON OF EXPERIMENTAL AND ANALYTICAL RESULTS,	5. TYPE OF REPORT & PERIOD COVERED Final Report 1 July 1974 — 30 June 76
	6. PERFORMING ORG. REPORT NUMBER
7. AUTHOR(s) (10) R. E. BALL (11) May 76	8. CONTRACT OR GRANT NUMBER(s) (12) 102 p.
9. PERFORMING ORGANIZATION NAME AND ADDRESS Naval Postgraduate School Monterey, California 93940 (16)	10. PROGRAM ELEMENT, PROJECT, TASK AREA & WORK UNIT NUMBERS 61152N, WSL22-001 N6053076WR30071
11. CONTROLLING OFFICE NAME AND ADDRESS Naval Weapons Center China Lake, California and the Joint Technical Coordinating Group/Aircraft Survivability	12. REPORT DATE
	13. NUMBER OF PAGES 107
14. MONITORING AGENCY NAME & ADDRESS (if different from Controlling Office) (17) WSL22001	15. SECURITY CLASS. (of this report)
	15a. DECLASSIFICATION/DOWNGRADING SCHEDULE

16. DISTRIBUTION STATEMENT (of this Report)

Approved for public release; distribution unlimited.

17. DISTRIBUTION STATEMENT (of the abstract entered in Block 20, if different from Report)

18. SUPPLEMENTARY NOTES

19. KEY WORDS (Continue on reverse side if necessary and identify by block number)

Aircraft Survivability
Aircraft Vulnerability
Hydraulic Ram
Fluid-Structure Interaction

20. ABSTRACT (Continue on reverse side if necessary and identify by block number)

This report presents the results of a study of 1) the fluid hydraulic ram pressures in a fluid-containing-tank caused by a penetrating projectile, and 2) the transient response of the entry and exit walls of the tank due to the fluid pressure. The experimental and analytical hydraulic ram and structural response programs at the Naval Weapons Center (NWC) and the Naval Postgraduate School (NPS) are briefly described. The computer analyses for the fluid pressure at the entry and exit walls and the

OVER

DD FORM 1 JAN 73 1473 EDITION OF 1 NOV 65 IS OBSOLETE
S/N 0102-014-6601 | ii

UNCLASSIFIED
SECURITY CLASSIFICATION OF THIS PAGE (When Data Entered)

251450

transient entry and exit wall strains are described in detail. Comparisons are made of the predicted wall strains with the circular entry wall strains, measured at NPS, and the square exit wall strains, measured at NWC. Good agreement in the form of the strain histories is obtained, but the magnitudes of the predicted strains are smaller than those of the measured strains. This study contributes to the knowledge of the hydraulic ram phenomenon and associated fluid-structure interaction, and should provide some useful information for the design of aircraft fuel tanks.

TABLE OF CONTENTS

I. INTRODUCTION

The recent conflict in Southeast Asia dramatically revealed the vulnerability of sophisticated and expensive aircraft to small arms ground fire and to surface-to-air missiles. Since the fuel tanks of tactical aircraft have the largest presented area of all of the vulnerable components, engineering estimates of fuel tank response to penetrating ballistic projectiles are required in order to design more survivable tanks. Projectiles that penetrate tanks containing fuel cause more severe damage to the tank than those that pass through empty tanks. The reason for this is that the passage of the projectile through the fuel causes an intense pressure pulse to propagate in the fuel and strike the walls of the tank. This large internal fluid pressure on the walls can cause severe petaling of the walls, usually at the entrance and exit points of the projectiles. The development of the pressure pulse in the fuel by the ballistic penetrator is known as the hydraulic ram effect, and the fluid pressure is referred to as the hydraulic ram pressure.

The hydraulic ram effect can be divided into three phases; the early shock phase, the later drag phase, and the cavity phase. The shock phase is initiated when the projectile penetrates the wall and impacts the fluid. As energy is transferred to the fluid, a strong hemispherical shock wave centered at the point of impact is formed. This creates an impulsive load on the inside of the entry wall in the vicinity of the entry hole which may cause the entry wall to crack and petal. As the projectile travels through the fluid, its energy is transformed into kinetic energy of fluid motion as the projectile is slowed by viscous drag. A pressure field is generated as fluid is displaced from the projectile path. In contrast to the pressures developed in the shock

phase, the fluid is accelerated gradually rather than impulsively, so that the peak pressure is much lower; however, the duration of the pressure pulse is considerably longer. A cavity develops behind the projectile as it passes through the fluid which is filled with liquid vapor evaporated from the cavity surface and air which can enter the cavity through the entry hole. As the fluid seeks to regain its undisturbed condition, the cavity will oscillate. The concomitant pressures will pump fluid from any holes in the tank and they may be sufficient to damage fuel cell components. This cavity oscillation is called the "cavity phase."

The structural response of the fuel tank walls to the hydraulic ram pressure is a complicated process. The pressure in the fuel caused by the penetrating projectile acts on the tank walls, causing them to displace. This displacement in turn affects the pressure in the fuel, thus leading to a complex interaction between the fuel and the tank walls.* This interaction phenomenon is referred to as fluid-structure interaction.

Considerable research effort has been expended to develop an understanding of the hydraulic ram effect and the associated fluid-structure interaction. References 1 and 2 contain extensive bibliographies of most of the work on hydraulic ram. Of particular interest here is the Hydraulic Ram Project that has been conducted at the Naval Weapons Center (NWC), China Lake, California. The first phase of that project involved the characterization of the pressure waves, generated by the projectile during fluid penetration through a rectangular tank. An analytical model for predicting the drag phase pressure field was presented in Ref. 3. During FY 1973, an extensive series of ballistic tests were performed at NWC to obtain detailed fluid pressure measurements at

*Any cracking and petaling of the walls will also change the pressure in the fluid, and hence the subsequent loading on the walls.

were performed at NWC to obtain detailed fluid pressure measurements at several locations for a variety of projectiles under a wide range of impact conditions. The results of these tests is reported in Ref. 4. A digital computer code for predicting the drag phase fluid pressure in a rectangular tank due to ballistic penetrators, based upon the theory of Ref. 3 and the empirical data of Ref. 4, was subsequently developed by Lundstrom and Fung. Information on the code and its use is given in Ref. 5. This code will be referred to hereafter as the NWC hydraulic ram pressure code. One very significant feature of this code is the fact that the wall surfaces of the rectangular fluid volume are treated either as free surfaces or as fixed surfaces when considering wave reflections from the walls.

The second phase of the NWC Hydraulic Ram Project involved the characterization of the fluid-structure interaction during the loading of the fuel tank walls by the hydraulic ram pressure. In support of this goal, an extensive series of ballistic penetration tests were conducted on fluid-filled, rectangular tanks in March, 1974, to obtain detailed measurements of the strains at several locations on the exit wall of the tank. A detailed description of the test set-up and the complete set of results are given in Ref. 6.

An analytical and experimental hydraulic ram program has been conducted at the Naval Postgraduate School (NPS) in conjunction with the NWC program for approximately three years. A ballistic range has been built consisting of a 22 caliber rifle and a cubic fluid-containing tank. Fluid pressures and entry wall strains have been measured for various projectile sizes and energy levels. The results of these experiments are given in Refs. 7-17. The analytical phase of the NPS program has been devoted to the development of methods of analysis

that will accurately predict the structural response of the tank walls to the hydraulic ram loading. The results of this effort are given in Refs. 10 and 17-21.

As a consequence of the complexity of the fluid-structure interaction while the projectile is penetrating the tank, and after it exits the tank, an approximate theory was proposed in Ref. 10 that allows the solution for the fluid pressures to be obtained separately from the solution for the wall response.* This theory is known as the "piston theory." It is an exact theory for the one-dimensional acoustic fluid-structure interaction problem. In the piston theory the response of the wall is computed using the conventional structural response equations, with the normal pressure on the wall q given by $2p_o - \rho c \dot{w}$ where p_o is the incident fluid pressure at the wall, ρ is the fluid density, c is the acoustic velocity in the fluid, and $\dot{w}$ is the wall velocity**. The values for p_o during the drag phase can be obtained from the NWC hydraulic ram pressure code. For the shock phase pressure, the theory developed by Yurkovich, (Ref. 22,) can be used to determine the incident pressure field.

Two structural response digital computer codes, BR-1 and SATANS, have been modified by the author to include the piston theory. The modification consisted of incorporating the $-\rho c \dot{w}$ loading component into the equations of motion of the structure. The BR-1 code, Ref. 23, is a finite element code for predicting the inelastic, large deflection, transient response of combat aircraft skin-rib-stringer structures when subjected to internal airblast loading. The finite elements are flat rectangular plates and beam stiffeners. The modified

*An exact method for determining the response of the fluid-structural system was presented in Ref. 3. However, this method requires simultaneous solution for the fluid pressures and the wall deflections. This approach does not appear to be practical at this time.
**A dot above a variable denotes a derivative with respect to time.

code is called BR-1HR. A description of the modification to BR-1 and a User's Manual for BR-1HR are presented in Ref. 24. The code SATANS is a finite difference - Fourier series code for the geometrically nonlinear static and dynamic analysis of arbitrarily loaded shells of revolution. A detailed description of SATANS is given in Ref. 25. Instructions for its use are given in Ref. 26. For this study the code is used to analyze flat circular plates.

This report presents the results of our efforts to determine the accuracy of the structural response codes with piston theory when predicting the entry and exit wall strains due to the fluid pressures predicted by the NWC hydraulic ram pressure code and the Yurkovich shock pressure theory. A modification to the piston theory is also considered that accounts for cavitation at the interface due to tension in the fluid. Section II contains a description of the NWC exit wall and the NPS entry wall test programs. Section III presents various aspects of the fluid-structure interaction, including cavitation at the interface, and Section IV describes the features of BR-1HR and SATANS and the proposed structural models of the tank walls. Section V describes the NWC hydraulic ram pressure code and presents the predicted pressure on the entry and exit walls. The entry and exit wall strains computed using SATANS with piston theory and piston theory with cavitation are presented and compared to the measured strains in Section VI. The conclusions with regard to the accuracy of the analyses are given in Section VII.

II. EXPERIMENTAL PROGRAMS

A. Naval Weapons Center Exit Wall Test Program

Mr. Wallace Fung (Code 5114) has conducted a series of hydraulic ram effects tests on simulated aircraft fuel tanks at the Naval Weapons Center (NWC), China Lake, California, in which 12.7mm API ballistic projectiles were fired at a fluid filled, rectangular tank. The tank is 60 inches wide by 60 inches high, with 22 inches between the entry and exit walls. The top of the tank is open. A schema of the test set-up is shown in Fig. 1. The central portion of the entry wall is a stretched rubber membrane. The central portion of the exit wall is a 20 inch by 20 inch by 0.125 inch 2024-T3 aluminum test plate clamped to a 0.25 inch steel wall. The edge clamping was obtained by compression (friction) between two rubber gaskets around the outer perimeter of the plate. Additional edge support was provided by a pin through the plate at two diametrically opposed corners.

Fourteen 12.7mm API projectiles were fired at the tank with velocities between 1300 fps and 2900 fps. The exit point of each shot is shown in Fig. 2. The strains on the wet and dry surfaces of the exit wall were measured at the four locations shown in Fig. 2 for each shot. The strains at each location were measured in the two directions indicated by the short lines in Fig. 2. Pressures were measured at five locations along the trajectory and high-speed motion pictures were taken looking at the dry side of the exit wall. Table 1 lists the projectile velocity and the extent of damage for each shot. In general, low velocity projectiles caused some bulging of the exit wall accompanied by short cracks approximately three inches in length. The high velocity projectiles caused severe tearing of the wall with several cracks

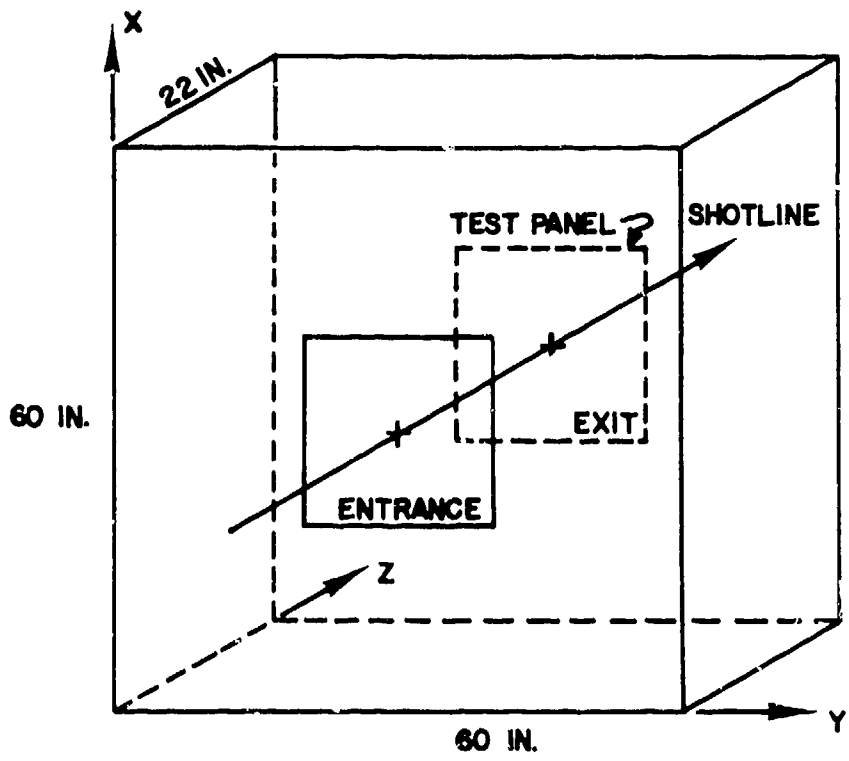

FIG. 1. Schema of the NWC Exit Wall Test Tank

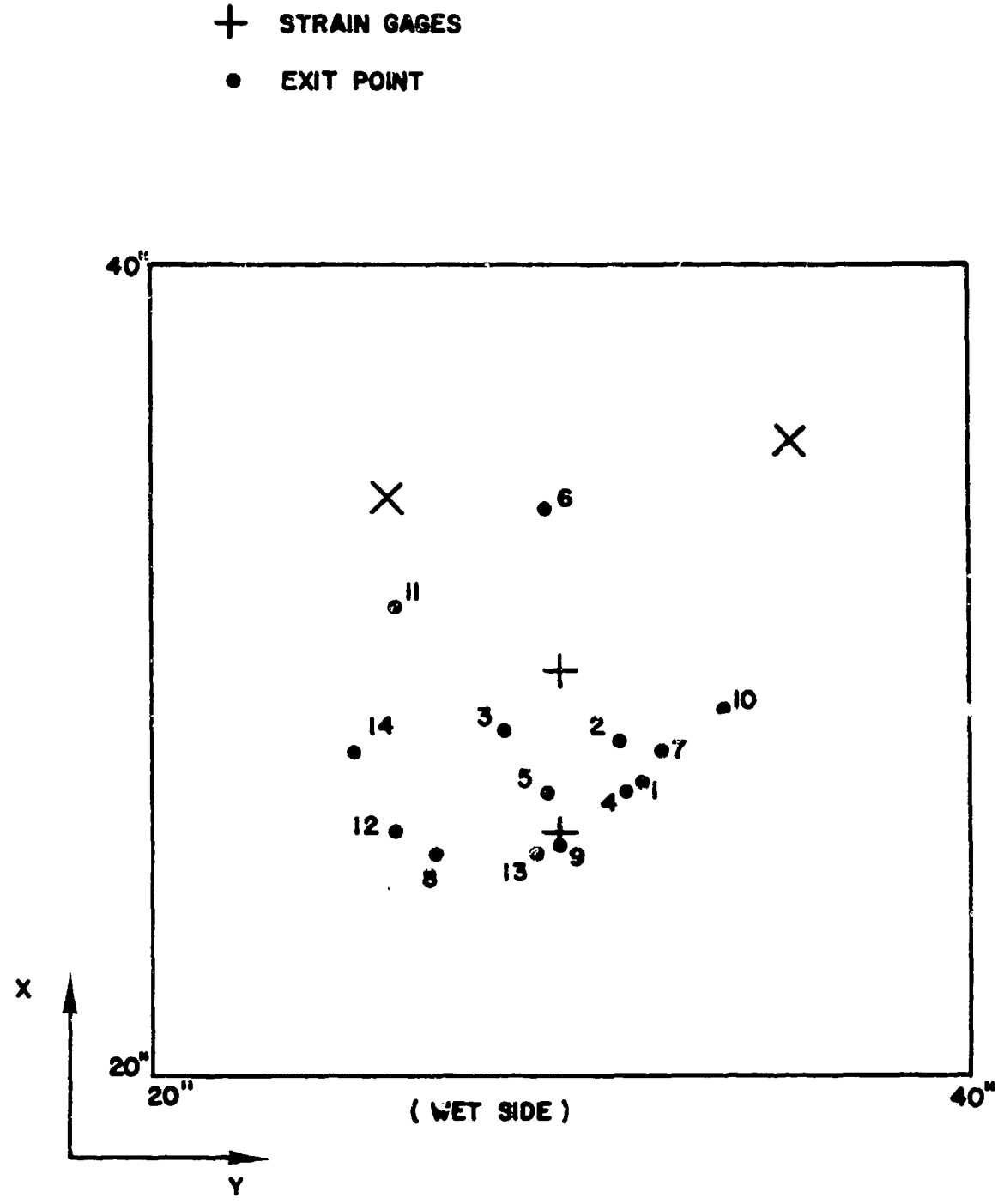

FIG. 2 Location of the Exit Points and the Strain Gages on the NWC Exit Wall

TABLE 1. - Projectile Velocity and

Extent of Exit Wall Damage

Shot	Velocity (fps)	Damage
1	2,200	Cigar-shaped hole 3 in. long
2	2,217	Small circular hole 2 in. in dia.
3	2,254	Cigar-shaped hole with one 19 in. crack
4	2,198	Cigar-shaped hole 2 in. long
5	2,113	" " " " " "
6	2,763	Circular hole 3 in. in dia with two 10 in. cracks
7	2,673	5 in. hole with several 5 in. cracks and petaling
8	2,643	5 in. hole with several 5 in. cracks and petaling
9	2,718	Bulged plate with 3 in. cigar-shaped hole
10	1,347	Cigar-shaped hole 3 in. long
11	1,386	" " " " " "
12	1,366	" " " " " "
13	1,396	Not available
14	1,389	Very small hole with two 2 in. cracks

running from the exit hole to the edges of the plate. Figure 3, taken from Ref. 6, shows the test panel from shot 14. A more detailed description of the experimental set-up, a presentation of all of the exit wall strain data, and photographs of each of the damaged plates are given in Ref. 6. Selected results from the NWC tests will be presented in Section VI where the comparison between the experimental results and the analytical results is made.

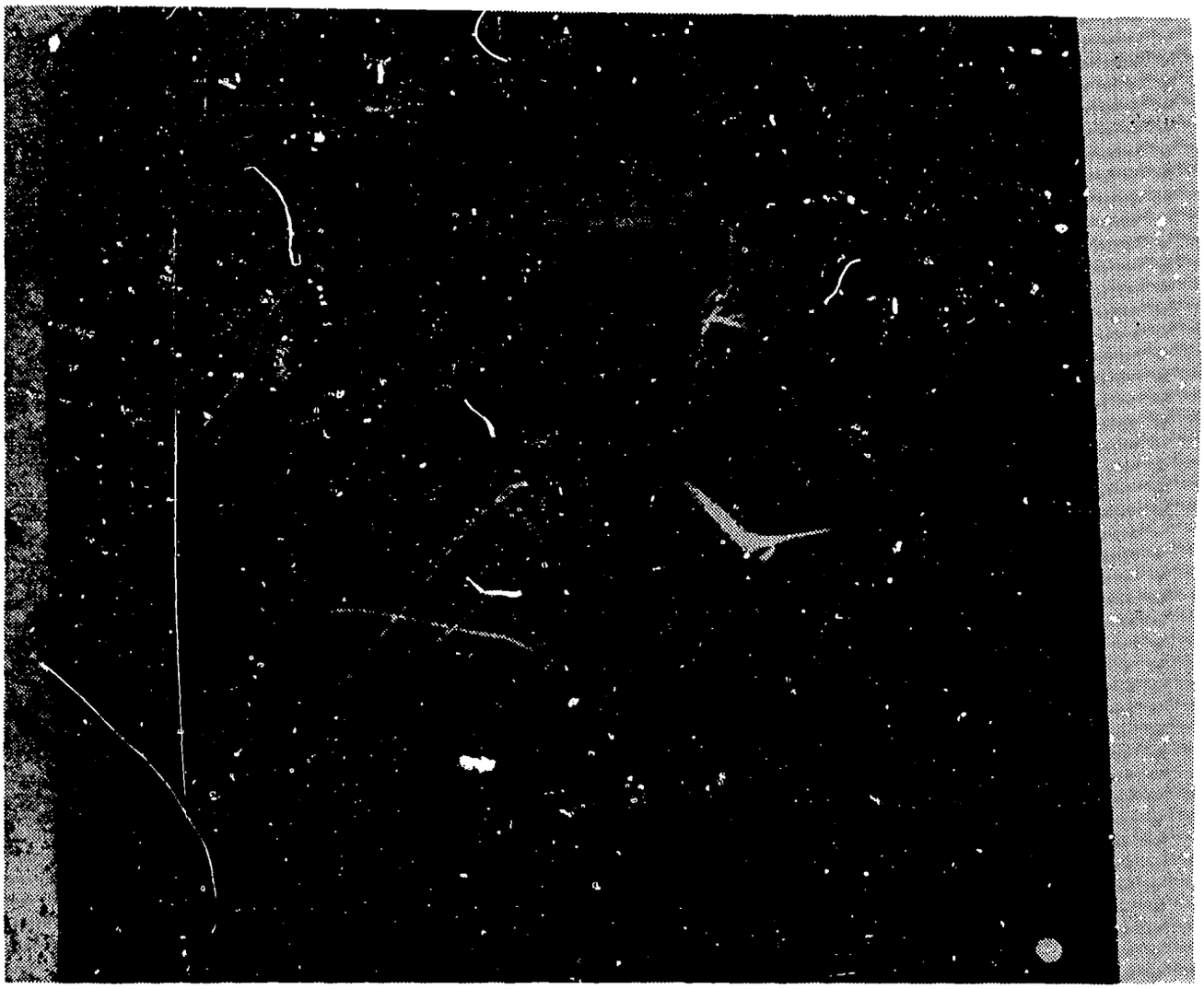

Fig. 3 Exit Wall Test Panel From Shot 14

B. Naval Postgraduate School Entry Wall Test Program

A series of experiments have been conducted at NPS using a simple tank configuration to determine hydraulic ram pressure loadings near the entry wall for several .222 caliber energy levels. The test fuel cell is cubical, with inside dimensions of 17 inches on a side, and was constructed by welding one quarter inch by three inch aluminum angle sections to form a frame. Side and bottom walls are one inch thick plexiglass and the entry and exit walls were bolted to the frame so that various thicknesses and materials could be tested. The top is open and bullet entry into the tank was accomplished by providing a one inch diameter hole in the center of the entry wall. A .222 caliber rifle was used to fire copper-jacketed lead projectiles whose mass and impact velocity were adjusted to obtain the various impact energy levels tested. Spark shadowgraphs were taken to determine shock phase wave shape, shock position and projectile location as a function of time, Ref. 13. Kistler 603H quartz pressure transducers were mounted in the tank to measure internal pressure at a given spatial position verses time. Pressures were measured along a line inclined 50° from the vertical at radii varying from two to eight inches from the impact point. The internal pressures were measured using both 0.5 inch and 0.05 inch thick steel plates at the entry wall in order to stimulate the case of a rigid entry wall and a flexible entry wall respectively. The pressure measurements are compared with the pressure predicted by the NWC hydraulic ram pressure code in Ref. 17. The projectile position data given in Ref. 13 was used to determine the drag coefficients used in the NWC code.

A series of experiments to determine the entry wall structural response to the shock and drag phase loadings for two energy levels (7,493 in.-lb and 12,323 in.-lb) have also been conducted. The entry wall was a circular plate with a fifteen inch diameter and a one inch diameter hole at the center*. The test plate was bolted to a one inch thick aluminum plate with a fifteen inch circular cutout. 7075-T6 Aluminum plates 0.05, 0.09, and 0.16 inches thick were tested. Each entry wall had four EA-13 type 175 ohm strain gages mounted 2 inches from the impact point. One pair of gages measured radial strain with one gage on the inside and the other on the outside of the plate. A second pair of gages was oriented circumferentially. Figure 4 shows the test tank set-up. A simple constant current strain gage circuit was used to measure the dynamic response of the entry wall. The recording system consisted of a dual-beam oscilloscope with two 1A7 pre-amp plug-in units with differential input capability and a Polaroid scope camera. The details of the test and the oscilloscope pictures of the strain traces are given in Refs. 15 and 17. The shots at the high energy level caused considerable tank leakage, strain gage bond failure and permanent deformation of the 0.05 in. plate. The low energy shots did not cause any apparent damage. A preliminary comparison of the measured strains with the strains predicted by SATANS is made in Refs. 15 and 17. A more detailed comparison, including the effects of cavitation, is made in Section VI of this report.

*A circular plate was tested so that the results from SATANS are directly applicable.

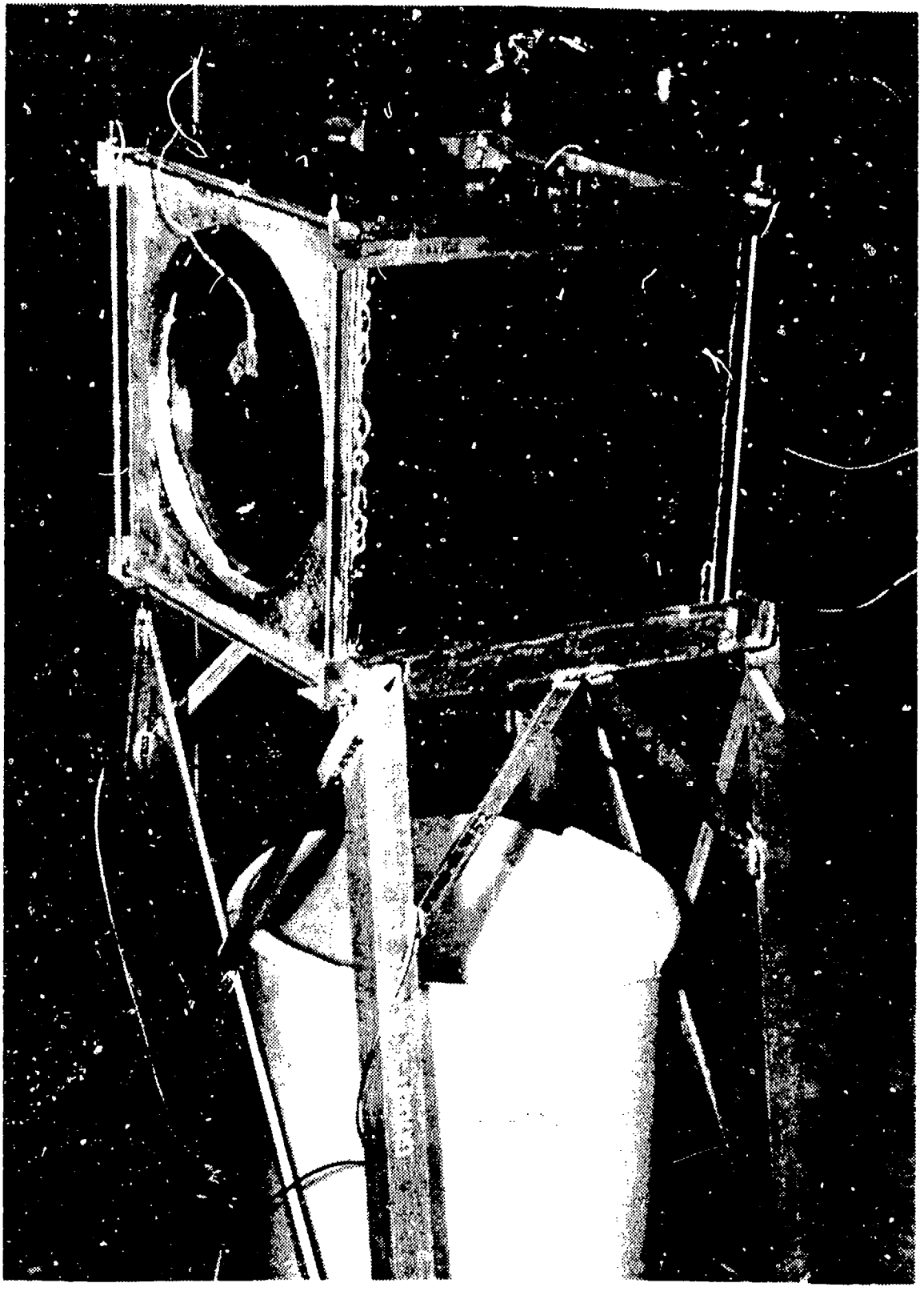

Fig. 4. NPS Entry Wall Test Tank

III FLUID-STRUCTURE INTERACTION

A. Governing Equations

Consider the fluid-structure interface at a typical portion of the entrance and exit walls of a fuel tank shown in Fig. 5. The linear differential equation representing unsteady, low velocity, irrotational, frictionless, compressible fluid flow can be given in terms of a velocity potential Φ in the form

$$\phi_{xx} + \phi_{yy} + \phi_{zz} = \frac{1}{c^2} \ddot{\phi} \tag{1}$$

where c is the sonic velocity of the fluid (assumed to be constant), subscripts denote partial derivatives, and ϕ_x, ϕ_y and ϕ_z are the velocities in the x, y and z directions respectively. The pressure in the fluid p can be obtained using Bernoulli's equation

$$p - p_a = - \rho\dot{\phi} - \frac{\rho}{2} V^2 \tag{2}$$

where ρ is the fluid density, assumed constant,

$$V^2 = \phi_x^{\,2} + \phi_y^{\,2} + \phi_z^{\,2} \tag{3}$$

and p_a is the ambient pressure. p is positive in compression. For low velocity flow the V^2 term in Eq. (2) is usually neglected, giving

$$p - p_a = - \rho\dot{\phi} \tag{4}$$

At the wall, the interface conditions are

$$\begin{aligned} p &= \pm q \\ \phi_z &= \dot{w} \end{aligned} \tag{5}$$

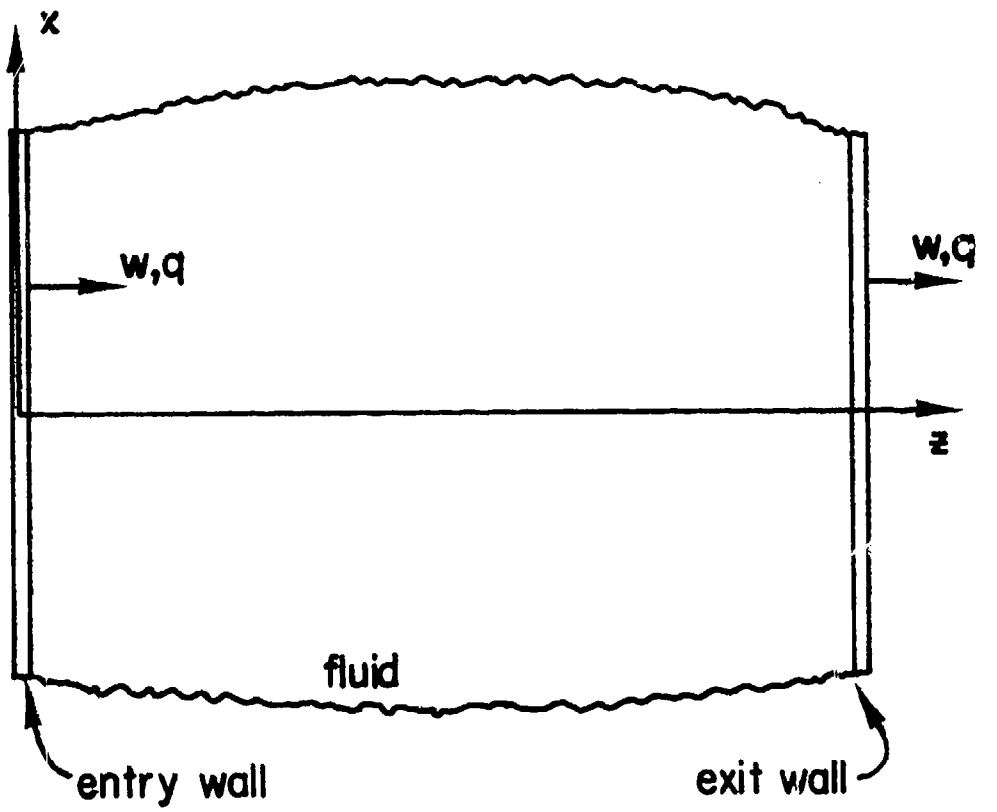

FIG. 5 Typical portion of Entrance and Exit Walls

where q is the normal pressure acting on the wall, and w is the wall deflection normal to the plane of the wall. The minus sign on q applies at the entry wall and the plus sign applies at the exit wall. These interface conditions are based upon the assumption that both compression and tension pressures can exist at the fluid-structure interface. In reality, cavitation may occur and the wall velocity and fluid velocity may not be the same.

A procedure for determining the pressure on the tank walls due to transient wall motion, based upon the above theory, was presented in Ref. 3. This procedure used Kirchoff's relation for the pressure at any point within the fluid due to motion of the surface of the fluid volume. The method requires simultaneous solution for the fluid pressures and wall deflections. It was emphasized in Ref. 3 that the proposed method, although simple in concept, is extremely difficult to carry out in practice, due mainly to computer storage space and running time.

B. One - Dimensional Interaction (Piston Theory)

Due to the considerable difficulties in treating the fully coupled fluid-structure interaction problem, the use of simplified procedures is appealing. One such procedure is the piston theory. This theory has been in use since the early 1940's when it was applied to the study of the effect of underwater explosions on ship plates, Ref. 27. It provides the correct interaction solution to the one-dimensional propagation of plane stress waves in an acoustic medium due to a moving plane boundary. Several recent studies have been made to determine its accuracy when applied to two-dimensional fluid-structure interaction problems, such as the propagation of plane waves over circular cylindrical shells and the vibration of spherical shells, Refs. 28 and 29.

A derivation of the piston theory is given in Ref. 10. The essential feature of piston theory is that the normal pressure at the wall is given by

$$q = p_o + \rho c(v_i - \dot{w}) \tag{6}$$

where p_o and v_i are the incident pressure and normal velocity of the fluid at the wall respectively, and $\dot{w}$ is the wall velocity*. The pressure p_o and velocity v_i are the pressure and velocity that would exist in the fluid if the wall was not there, i.e. p_o and v_i do not contain any reflection effects due to the presence of the wall. However, effects on p_o and v_i due to reflections from other surfaces should be included.

*The derivation in Ref. 10 used the relationship $p = -\rho\dot{\phi}$. If Eq. (2) is used, Eq. (6) becomes $q = p_o + \rho c(v_i - \dot{w}) - \frac{1}{2}\rho\dot{w}^2$. However, since $\dot{w} << c$, the velocity squared term can be neglected.

The pressure given by Eq. (6) can be interpreted as being composed of two parts, p_o, the incident pressure in the fluid, and $\rho c(v_i - \dot{w})$, the reflected pressure. Note that the reflected pressure is directly proportional to $(v_i - \dot{w})$, the mismatch between the fluid velocity and the wall velocity. The $\rho c v_i$ term is the reflected pressure in a plane wave at a rigid, non-moving wall ($\dot{w} = 0$) and can be shown to be equal to p_o, the incident pressure. Thus, Eq. (6) can also be given in the form

$$q = 2p_o - \rho c\dot{w} \tag{7}$$

If the plane wave front is moving normal to a rigid, non-moving wall, as is the case for a hemispherically expanding shock wave at the entry wall, then there is no mismatch between the normal fluid velocity and the wall velocity, and the incident pressure p_o should be used in place of the $2p_o$ term in Eq. (7).

C. Sprerical Wave Propagation and Interaction with a Planar Wall

The NWC hydraulic ram pressure code does not assume plane wave stress propagation in the fluid, but instead treats the problem of the penetrating projectile as a sequence of spherical stress waves in an acoustic medium whose centers of disturbance lie along the bullet path. Thus, spherical waves strike the planar tank wall, not planar waves. The pressure at a rigid wall, corresponding to the $2p_o$ pressure in the one-dimensional interaction, can be determined using the method of images. If the image source is of the same sign as the actual source, then the normal velocity at the wall is zero, and the pressure at the wall is the net result of the two sources. Thus, if Eq. (4) is used for the pressure, the pressure doubles at the rigid wall, just as in the one-dimensional planar wave case, and $2p_o$ is the pressure at the rigid wall. If the image source is of the opposite sign, the pressure is zero at the wall and the wall is like a free surface.

D. Cavitation

The assumption has been made in the discussion above that there is continuity between the fluid and the wall at the interface. This assumption becomes questionable when tension exists at the interface, i.e., when

$$p = 2p_o - \rho c \dot{w} < 0 \qquad (8)$$

Experiments have shown that cavitation occurs in the water in front of thin, circular, air-backed plates when they are subjected to underwater explosive-type shock waves, Ref. 27. Two values obtained for the maximum tension in seawater are 70 and 40 psi, Ref. 30. Cole has suggested that it usually is a good approximation to assume that cavitation begins at the surface of a free plate, neglecting diffraction effects from the plate edge, when the interface pressure becomes zero, Ref. 30.

IV STRUCTURAL RESPONSE COMPUTER CODES AND MODELS

A. BR-1HR

The Northrup Corporation, under Air Force funding, has developed a finite element digital computer code, called BR-1, for predicting the inelastic, large deflection, transient response of combat aircraft skin-rib-stringer structures when subjected to internal air blast loadings. The finite elements used are flat, isotropic, rectangular plates and beam stiffeners. The input pressure is assumed constant over each element. The output consists of all of the input data, the stable time increment, the stress-strain data for the panels and bars, and the deflections at the node points. The stresses and strains are tensor quantities at the cross-section at the center of the element. Two versions of the code were developed; one for IBM computers and one for CDC computers. The theory, user's manual and code listing of the CDC version are given in Ref. 23. The IBM version of the BR-1 code was modified by the author so that it could be used to predict the response of aircraft fuel tanks when subjected to the hydraulic ram pressure loading due to ballistic penetrators. The modification was based upon the piston theory described in Section III. The modified code is called BR-1HR. A description of the theory, the modifications, and the additional instructions required to operate BR-1HR are given in Ref. 24. The code is operational on the IBM 360/67 in FORTRAN IV, Level H.

The BR-1HR code can be used to compute the response of the NWC exit wall to the hydraulic ram pressure loading. One finite element model selected to represent the 20 inch x 20 inch exit wall shown in Fig. 2 is illustrated in Fig. 6. This model has 49 elements and 64 nodes. The reasons for selecting

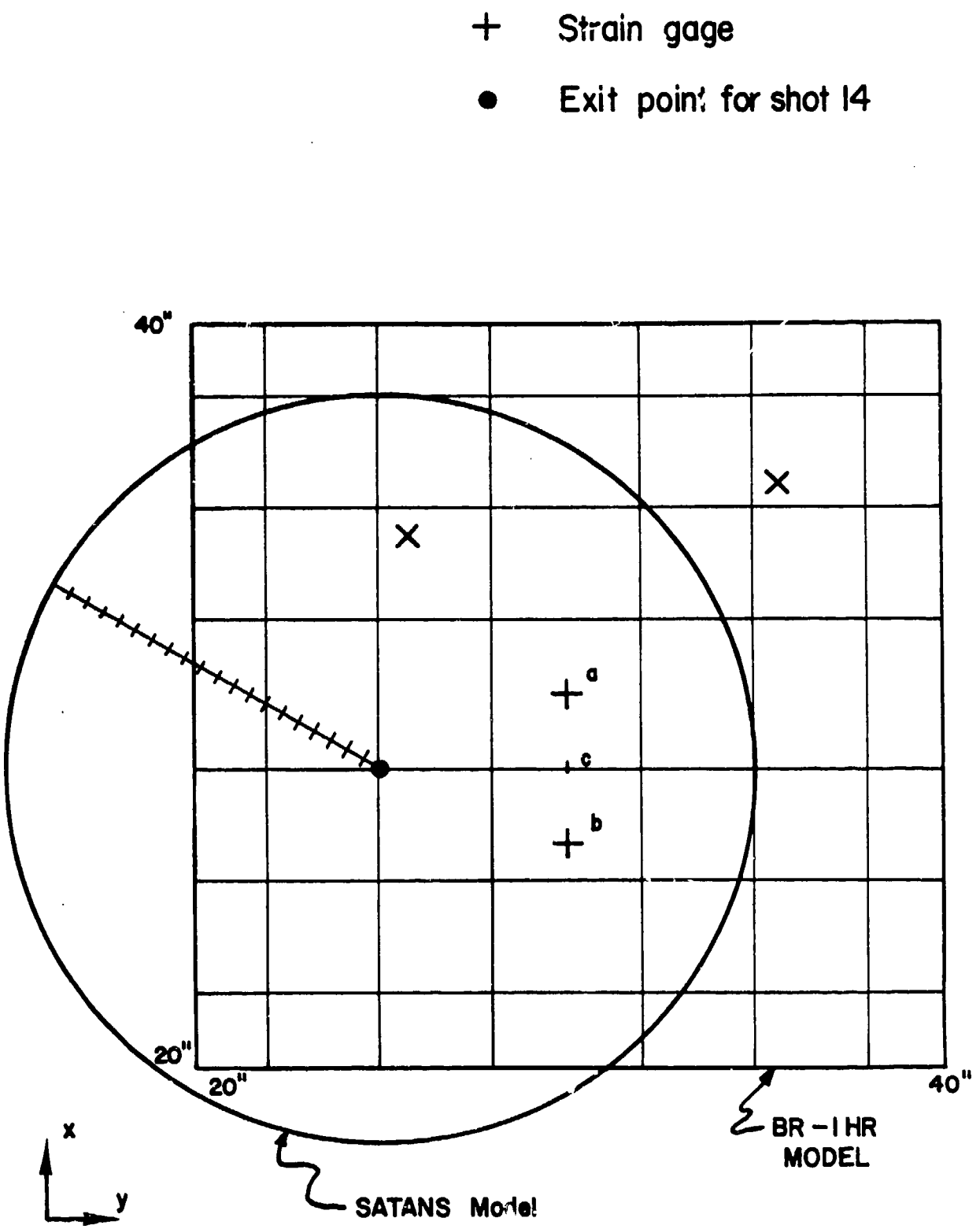

Fig. 6 Square and Circular Plate Models of Exit Wall

this model were:

1. The number of nodes must be small in order to keep the execution time to a reasonable figure.
2. The strain gage locations should be close to the center of the element since thats where the strains are printed.
3. The edge and corner elements should be small since considerable edge effects are anticipated.
4. This model can be further refined by subdividing the large element that contains the exit point into smaller elements in order to allow a more localized pressure loading.

The accuracy of this model for linear, elastic response is evaluated in the appendix, where the exact solution and the BR-1HR solution are compared for a simply supported plate subjected to a uniform step pressure. The response is obtained for both free and fluid backed plates. The essential result of the accuracy study is that the displacements are accurately predicted by the finite element model but the strains are not. In particular, the strains at the center portion of the plate are inaccurate. However, it should be noted that these strains are much smaller than the maximum strains in the plate. The solution for a 144 node model was also obtained in order to determine if a smaller grid size would yield more accurate results. The 144 node model provides somewhat more accurate strains, but they are still quite inaccurate in the center portion of the plate.

The BR-1 and BR-1HR codes are extremely computer-time consuming codes*. Execution times on the IBM 360/67 for small to moderate size problems (9-144 nodes) vary from 0.4 sec/node/time step to 0.6 sec/node/time step, depending to some extent upon the amount of output. Because of numerical stability requirements, the maximum time step for stable results is very small - of the order of microseconds.

The maximum time step for numerical stability for the 64 node model of the NWC exit wall shown in Fig. 6 is approximately 13.5 μsec. Furthermore, when the elements of the model are made smaller for better solution accuracy the maximum stable time step decreases. Thus, due to the very small allowable time step, the large number of nodes required for accuracy, and the large amount of time required per node at each time step, the total execution time can be considerable. For example, the total execution time required to compute the response of the 64 node model for 4 msec at 12 μsec/time step is estimated to be approximately 10,000 secs or about 3 hours on the IBM 360/67.

*The modifications made to BR-1 did not significantly effect the execution time required for a solution. Computer execution time for a problem run using BR-1HR is essentially the same as the execution time using BR-1.

B. SATANS

SATANS (Static And Transient Analysis, Nonlinear, Shells) is a digital computer code that computes the geometrically nonlinear static and dynamic response of arbitrarily loaded, elastic shells of revolution. SATANS has been in existence since 1967, and has undergone several significant modifications since the static version was first described in Ref. 31. The latest public version, available through COSMIC (LAR-11109) can be used to analyze any shell of revolution for which the following conditions hold:

(1) The geometric and material properties of the shell are axisymmetric, but may vary along the shell meridian.

(2) The shell material is isotropic, but the modulus of elasticity E may vary through the thickness.

(3) The applied pressure and temperature distributions can be expressed in a Fourier sine or cosine series in the circumferential coordinate.

(4) The boundaries of the shell may be closed, free, fixed or elastically restrained.

The governing partial differential equations are based upon Sanders' nonlinear thin shell theory for the condition of small strains and moderately small rotations. The inplane and normal inertial forces are accounted for, but the rotary inertial terms are neglected. The set of governing nonlinear partial differential equations is reduced to an infinite number of sets of four second-order partial differential equations in the meridional and time coordinates by expanding all dependent variables in a sine or cosine series in terms of the circumferential coordinate θ. The four state variables are

the three displacements and the meridional bending moment. The sets are uncoupled by utilizing appropriate trigonometric identities and by treating the nonlinear coupling terms as pseudo loads. The meridional derivatives are replaced by the conventional central finite difference approximations, and the displacement accelerations are approximated by the implicit Houbolt backward differencing scheme. This leads to sets of algebraic equations in terms of the dependent variables z and the Fourier index n. Each set is tridiagonal in the matrix sense with 4 x 4 matrices on each of the diagonals. Each set of algebraic equations is solved using Potters' form of Gaussian elimination. For considerably more detail concerning SATANS and its use the interested reader is referred to Refs. 25 and 26.

In SATANS, the applied pressure is defined at each finite difference station for each circumferential harmonic, and the output consists of the stress resultants and displacements at each station for each circumferential harmonic at each time step. For this study SATANS was modified to account for the piston theory radiation damping $\rho c\dot{w}$ in the transverse equation of motion. The output was also changed to print the strains at each station.

SATANS is a very fast code compared to BR-1HR. For example, an analysis of the axisymmetric response of a flat circular plate requires approximately 0.01 sec/station/time step. Thus, in this instance its approximately 50 times faster than BR-1HR*. However, it cannot account for inelastic effects, as BR-1HR can.

*The axisymmetric analysis uses only the n = 0 mode. An asymmetric analysis requires additional modes and hence more computational time. A reasonable comparison for asymmetric response would be a 60 node model for BR-1HR, requiring 30 sec/time step, verses a 15 station, 6 mode model for SATANS, requiring .9 sec/time step.

Since the NPS entry wall is a flat circular plate with a central hole and is subjected to an essentially axisymmetric hydraulic ram pressure loading, SATANS provides the appropriate analysis for purposes of comparison, provided the stresses in the plate remain elastic. However, for the exit wall study SATANS provides only an estimate of response, since the plate is square, the loading is not symmetric, and the plate stresses exceed the elastic limit near the exit point. Nevertheless, due to the considerable savings in computer execution time, SATANS is used for purposes of comparison. A typical 21 station model of the exit wall is shown in Fig. 6, where the plate has been centered at the exit point of shot 14.

C. Cavitation

If cavitation takes place in the fluid near the wall, negative interface pressures cannot exist, and the net pressure q drops to zero. SATANS has been further modified to account for cavitation by computing the net interface pressure $2p_o - \rho c\dot{w}$ at each station, at each time step, and at each iteration. If the net pressure at any station is found to be less than zero, then the net pressure at that station is set to zero and another iteration is taken. This in effect separates the wall from the fluid at those stations where cavitation occurs. If the net pressure later returns to positive values then the positive pressure is applied to the wall. This procedure takes advantage of the iterative solution procedure used by SATANS since the net pressure depends upon the velocity, which in turn depends upon the pressure. It's not possible to incorporate cavitation in BR-1HR exactly since an explicit time integration method is used without iteration.

V HYDRAULIC RAM PRESSURE PREDICTIONS AND COMPARISONS

A. The NWC HYDRAULIC RAM PRESSURE CODE

The NWC hydraulic ram pressure code is a digital computer code developed to predict the pressure and velocity throughout a rectangular volume of fluid due to a ballistic penetrator. The theory of the code and instructions for its use are described in detail in Ref. 5. This code provides the values of the hydraulic ram pressure to be used in the structural response codes as the incident pressure at the tank wall.

A simplified model of the complex bullet behavior is used for the pressure computation. The bullet is assumed to travel in a straight line. The rate of kinetic energy loss of the bullet is taken to be

$$\frac{dE}{dx_b} = m\beta V^2$$

where E is the kinetic energy of the bullet, x_b is the bullet position, m is the bullet mass, V is the bullet velocity, and β is a velocity decay coefficient that is a function of x_b for tumbling bullets. In the code the bullet is assumed to enter the test cell with 0-degree yaw and to continue in this attitude until the distance XTUM is reached where it begins to tumble. The bullet is assumed to be fully tumbled at a distance XTUM plus DXTUM Stripping of bullet jackets from the armor piercing core of API ammunition is also accounted for, albeit in a crude manner.

The wave equation is used to calculate the flow field resulting from the bullet and cavity motion. The projectile and cavity are approximated by the action of a line of sources along the bullet path. The stress waves are

assumed to propagate in a spherical manner from each source. The source strength distribution is estimated by equating the energy loss of the bullet to the sum of the work done by the difference in ambient and cavity pressure and the kinetic energy of the fluid. The pressure in the fluid is computed using Bernoulli's equation, Eq. (2). Although the action of the cavity is accounted for in the fluid model, the absence of fluid within the cavity is ignored. Thus, the code pressures for locations within the cavity are of dubious value. This aspect is discussed in the following section.

An important feature of the code is its ability to account for reflections from each of the six surfaces of the fluid volume using the method of images. Two options are available; either reflections from free surfaces, or reflections from rigid walls*. Since the piston theory requires either twice the incident hydraulic ram pressure ($2p_o$) or the pressure at a rigid wall (the two being the same when the velocity squared term is neglected in Bernoulli's equation), either option can be used to obtain the pressure at the wall. However, since the other walls of the tank are not rigid, only reflections from the wall being considered should be accounted for if the rigid wall approach is used**. Examples and users instructions on the image feature are given in Ref. 5.

*The free surface boundary condition $p = 0$ is satisfied for the potential term $\rho\dot{\phi}$ only. In order to have the rigid wall refelctions, the statement ASSIGN (I) = 1.0 must be inserted after 530 in SUBROUTINE IMAGE.
**Most aircraft fuel tank walls probably reflect more like free surfaces than rigid walls, Refs. 3 and 18.

The input parameters to the code include the dimensions of the rectangular volume of fluid into which the penetrator is fired, XC(1) - XC(3), and the entrance and exit points of the projectile, X(1) - X(6). In order to obtain the hydraulic ram pressure at the wall being considered the user must specify the locations of the points at which these variables are to be computed and the time increment for which the pressure is to be computed. Thus, in the BR-1HR code the center of each element is the location for the pressure computation, whereas in SATANS the location of the finite difference stations defines the points for the pressure computation*.

Additional input data to the NWC code is given below:

XMASS(1) - bullet mass, lb.

XMASS(2) - penetrator mass, lb.

XMASS(3) - jacket mass, lb.

AREA(1) - bullet presented area, normal attitude, in^2

AREA(2) - bullet presented area tumbled attitude, in^2

AREA(3) - penetrator presented area, normal attitude, in^2

AREA(4) - penetrator presented area, tumbled attitude, in^2

AREA(5) - jacket presented area, tumbled attitude, in^2

AREA(6) - bullet stern-first presented area, in^2

DRAG(1) - coefficient of drag for bullet, normal attitude

DRAG(2) - coefficient of drag for bullet, tumbled attitude

DRAG(3) - coefficient of drag for penetrator, normal attitude

DRAG(4) - coefficient of drag for penetrator, tumbled attitude

*The hydraulic ram pressure is either $2p_0$ or the reflected pressure at a rigid wall. Since the NWC code does not provide an option to punch the pressure, the code was modified by the author to punch these data in the format required by BR-1HR. This required changes to the subroutine MIRROR in the procedure for computing a minimum initial time. These changes established a common minimum initial time to be used at all points. The punch routine provides the pressure over the wall at each time increment, starting with the minimum initial time.

DRAG(5) - coefficient of drag for jacket, tumbled attitude

DRAG(6) - coefficient of drag for bullet stern-first, normal attitude

DENS - fluid density, lb/in^3

PO - ambient pressure, psi

PC - cavity pressure, psi, normally taken to be zero

C - sound speed in fluid, ft/sec

BC - constant, normally taken to be 0.434

VEL - initial bullet velocity, ft/sec

DX - distance increment along trajectory, in.

NT - a variable such that NT = 0/1 means that the bullet does not tumble/does tumble

XSTRIP - distance along the trajectory that the bullet begins to strip

XTUM - distance along the trajectory that the bullet begins to tumble, in.

DXTUM - distance required for the bullet to become fully tumbled, in. if NT = 0, XTUM and DXTUM can be arbitrary

NE - is a variable such that NE = 0/1 means bullet does not exit tank/does exit tank

XE - distance along the trajectory where the bullet exits the volume, in. If NE = 0, XE can be arbitrary

XMAX - maximum length of trajectory through volume, in. Dimension statements limit XMAX to 300*DX.

EN - exponent which specifies power law followed by the drag function (EN = 3.0 in general)

EFRACT - a factor related to bullet stripping (EFRACT = 3.0 in general)

NCTUM - a variable such that NCTUM = 0,1,2 - means bullet does not continuously tumble/bullet continuously tumbles/bullet continuously tumbles for one cycle

BS,ØMEG - parameters not used for this version, set equal to 1

NSTRIP - a variable such that NSTRIP = 0,1 means bullet does not strip/bullet does strip

The code is programmed such that the computation of the trajectory parameter is automatically stopped when the bullet reaches the exit wall (XMAX). However, its possible to compute pressures for times longer than the time the bullet takes to penetrate the tank. Since the theoretical model assumes spherical propagation from a line of sources, the source strength theoretically drops to zero when the bullet exits the tank. The program indicates this fact, when no reflections are considered, by printing a constant value for $\dot{\phi}$ (PPHI) at all times later than the time required for the zero source disturbance to reach the point in question. However, the pressure (P) printed at these times (Eq. 2) changes due to the change in V^2, which is based upon the invalid trajectory parameters. When reflections are considered, $\dot{\phi}$ also changes due to the image sources.

B. The Cavity

In the series of ballistic tests conducted by NWC to obtain the detailed pressure measurements (Ref. 4), highspeed motion pictures were taken through a one inch plexiglass window at the side of the tank. This provided a 30 inch high by 36 inch long field of view*. The opposite plexiglass wall was sandblasted and thus acted as a diffusing screen for backlighted photography. The films vividly show the bullet penetrating the entry wall and passing through the fluid, the resulting cavity caused by the bullet, and the entry wall deflection. Fig. 7 presents several frames of the film showing the penetration by a 30 caliber projectile**. Several features regarding the cavity can be seen from these pictures. First, the cavity does not touch the entry wall anywhere except in the immediate vicinity of the entry hole. Second, there does not appear to

*The tank was a five foot cube.
**The pipes extending into the tank from the top contain the pressure transducers. The first pipe is 6 inches from the entry wall and the pipes are spaced 6 inches apart.

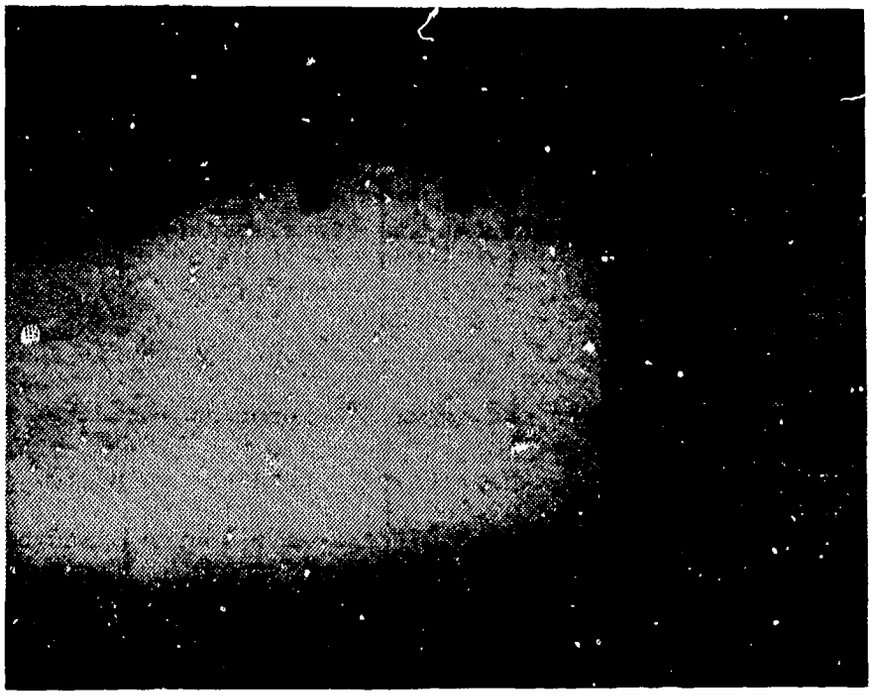

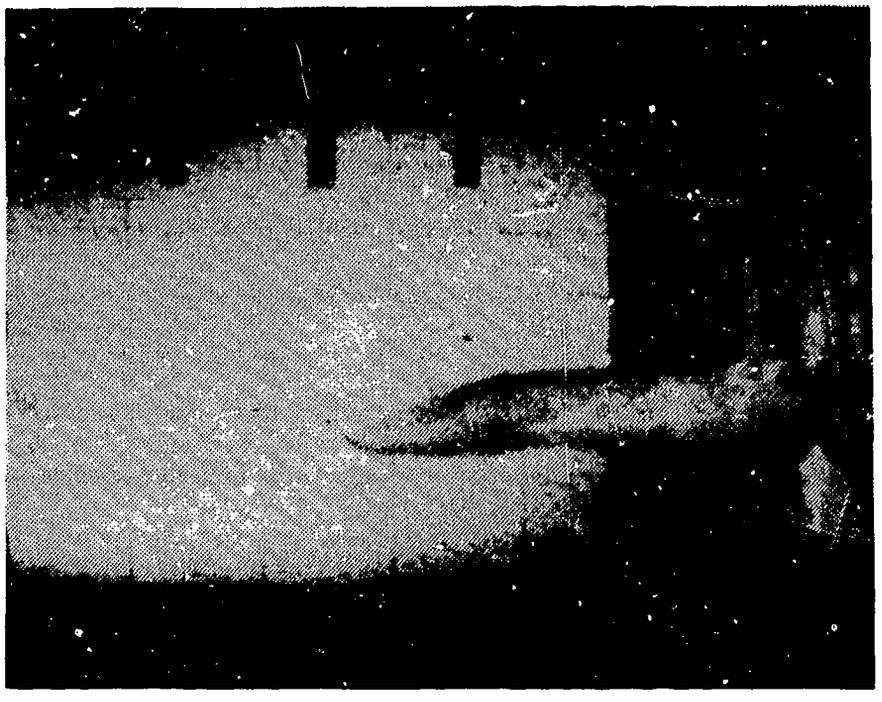

Fig. 7 High Speed Photographs of Bullet Penetration

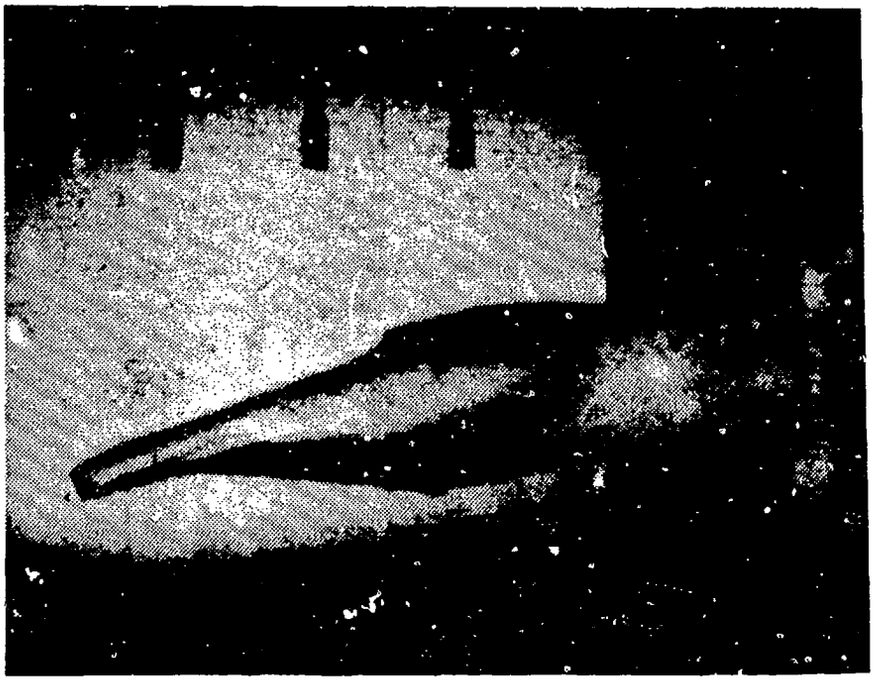

Fig. 7 Continued

be any cavitation in the fluid at the entry wall due to negative interface pressures caused either by the wall deflection (away from the fluid) or by tension waves in the fluid. However, pictures of later times definitely show cavitation on the side walls. Third, when the bullet has traveled approximately 24 inches into the tank the cavity is conical for about 12 inches, followed by a larger, more cylindrical cavity. The diameter of the cylindrical part of the cavity is approximately six inches. When the bullet has progressed approximately 30 inches, the cylindrical cavity has grown to about eight inches. The size of the cavity is important when attempting to determine the net pressure on the exit wall after the bullet exits the tank, i.e. where is there contact between the fluid and the wall?

C. Entry Wall Pressure

The loading on the entry wall of the fuel tank due to the ballistic penetrator can be divided into four successive phases:

1. a penetration phase where the projectile punches a hole in the entry wall,
2. a shock phase where the projectile protusion into the fluid causes a hemispherical shock wave,
3. a drag phase during which the kinetic energy of the projectile is dissipated by form drag and a cavity behind the projectile is formed,
4. a cavity oscillation phase which results from the growth and collapse of the cavity.

The penetration phase was not included in the NPS tests since the entry plate had a one inch diameter hole at the center through which the projectile passed. This was done to eliminate the first phase from the problem.

The NPS prediction of the fluid pressure during the shock phase uses the Yurkovich theory which is based upon the assumptions of a point energy source release, a rigid entry wall, and a shock radius that is proportional to a constant power of time. A typical predicted wave front pressure distribution resulting from the impact of a 45 grain .222 caliber bullet into a water filled tank is shown in Fig. 8. Note that this phase is much less than one msec in duration. The magnitude of this phase relative to the drag phase is heavily dependant upon the relative amount of kinetic energy lost by the projectile during the shock phase, which in turn is heavily dependant upon the projectile Mach number with respect to the fluid. Projectiles with high Mach numbers (>2) lose considerably more energy in the shock phase than those with low Mach numbers. Detailed shock phase results from the NPS experiments and comparisons with the results from the Yurkovich theory are given in Refs. 9, 12, and 13.

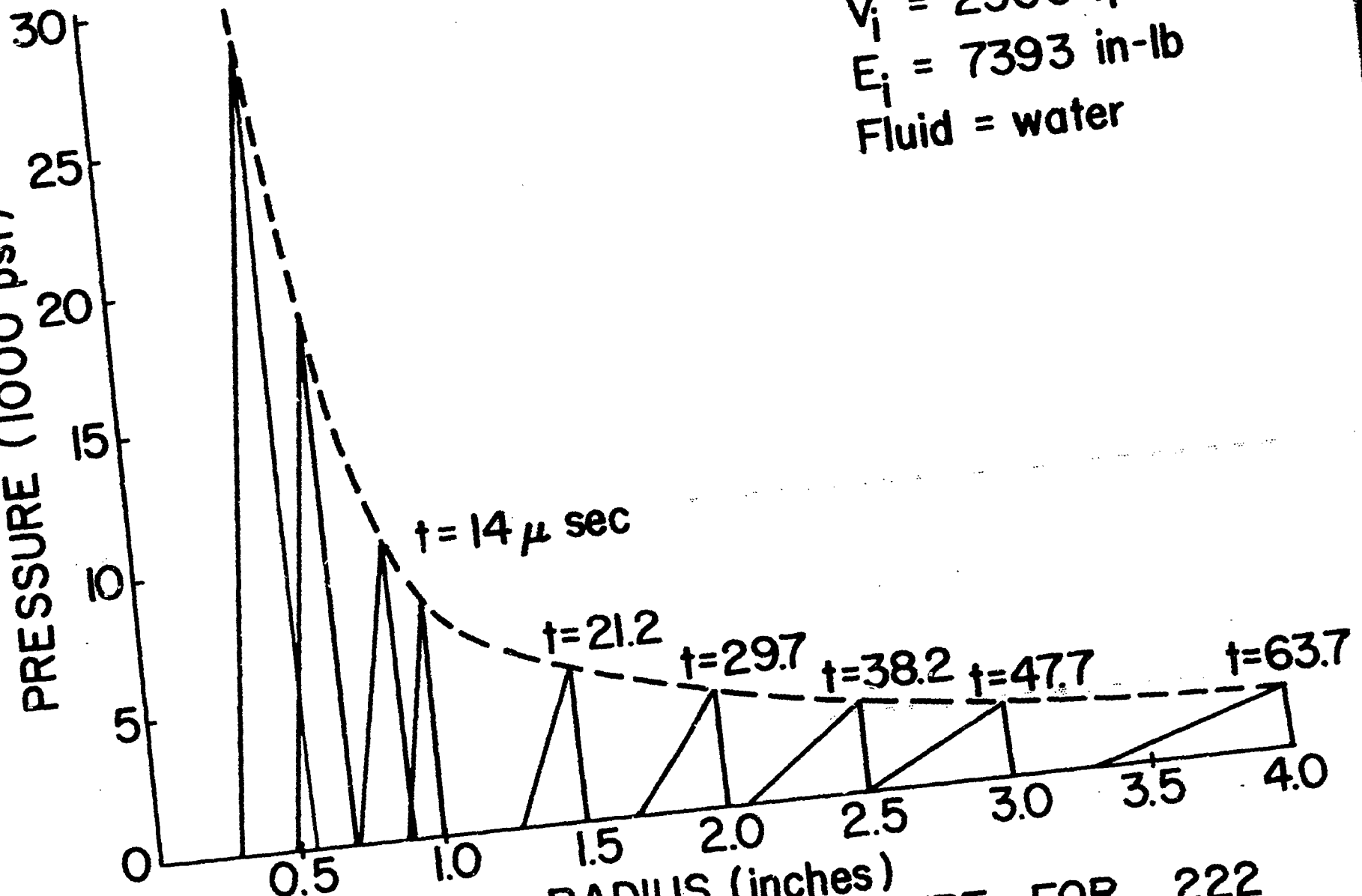

FIG. 8 SHOCK PHASE PRESSURE FOR .222 CALIBER PROJECTILE, (REF. 17)

Since the shock phase does not dissipate all of the available projectile kinetic energy, the projectile travels through the tank until either all of the energy is dissipated or it strikes and/or penetrates the exit wall. No projectiles penetrated the exit wall in the NPS tests. The predicted fluid pressures on the entry wall during the drag phase can be obtained from the NWC hydraulic ram pressure code.

Values of the input data used in the NWC hydraulic ram pressure code are given below:

EN	= 3.00000						
BS	= 1.00000						
EFRACT	= 3.00000						
NCTUM	= 0						
NSTRIP	= 0						
NT	= 0						
XTUM	= 20.00000						
DXTUM	= 25.00000						
XSTRIP	= 20.00000						
XMASS(3)	= 0.00640	0.00010	0.00010				
AREA(6)	= 0.03800	0.03800	0.03800	0.03800	0.03800	0.03800	
DRAG(6)	= 3.00000	3.00000	3.00000	3.00000	3.00000	3.00000	
BETA(7)	= 0.32063	0.32063	20.51999	20.51999	20.51999	0.32063	20.51999
VEL	=2500.00000						
DENS	= 0.03600						
PO	= 14.70000						
PC	= 0.0						
C	=4900.00000						
BC	= 0.43400						

Note that tumbling of the bullet was not considered since no data on tumbling behavior was available. Instead, a constant drag coefficient for the bullet was determined from the projectile position data. Neglect of the tumbling behavior strongly influences the shape of the pressure curves. Figure 9 shows comparisons of the measured and predicted fluid pressure 2 in., 3 in., and 4 in. from the entry point along a radius 50° from the vertical and in the direction of the projectile trajectory. The energy level was 7,493 in.-lb and the entry wall

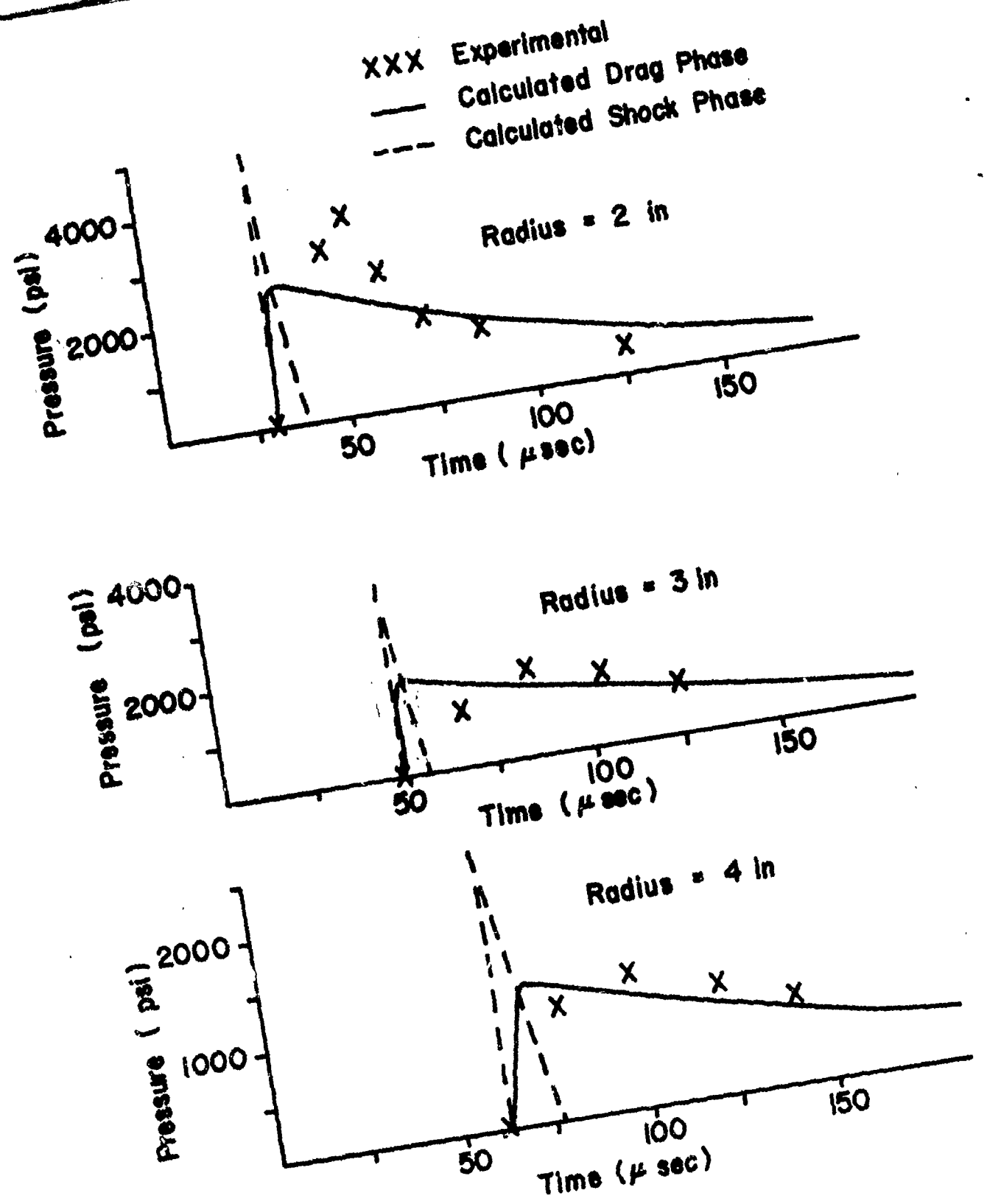

FIG. 9 FLUID PRESSURE COMPARISON, RIGID WALLS (REF. 17)

was 0.5 in. thick. Rigid wall reflections from all surfaces, including the front wall, were assumed. The predicted shock pressures are included in the comparison. The shock pressures were obtained based upon the assumption of a 10% loss of projectile energy during the shock phase. The measured and predicted fluid pressure at 2 in., 4 in. and 6 in. for the condition of free surface everywhere is shown in Fig. 10. The shock phase pressures are not included in this figure. Examination of Figs. 9 and 10 reveals that the predicted drag phase pressure at the larger radii have essentially the same peak pressure as the measured pressure but the wave form is different. The difference in form may be due to the fact that the tumbling behavior is not properly accounted for. Furthermore, note that the measured pressure trace does not indicate a shock phase. This may be due to the limitations on the time rise of the charge amplifier used*. Much more detailed information concerning the fluid pressure measurements near the entry wall is given in Refs. 8, 9, 11, 12, 13, 14, 16, and 17.

The predicted hydraulic ram pressure on the entry wall for the 7,493 in.-lb energy level shot is shown in Fig. 11 at 50μsec, 100μsec, and 150μsec after impact. The hydraulic ram pressure is taken as the sum of twice the incident drag pressure and the shock pressure. Free surface reflections from every surface except the entry wall were included**. This transient pressure field is the one selected for use with SATANS.

*Shadowgraphs show the existence of a hemispherical shock front, Ref. 13.
**The choice was made to use twice the incident drag phase pressure rather than the reflected pressure at a rigid wall since this allows the use of free surface at the other walls. A comparison of the two pressures on one shot revealed a difference of less than 4%.

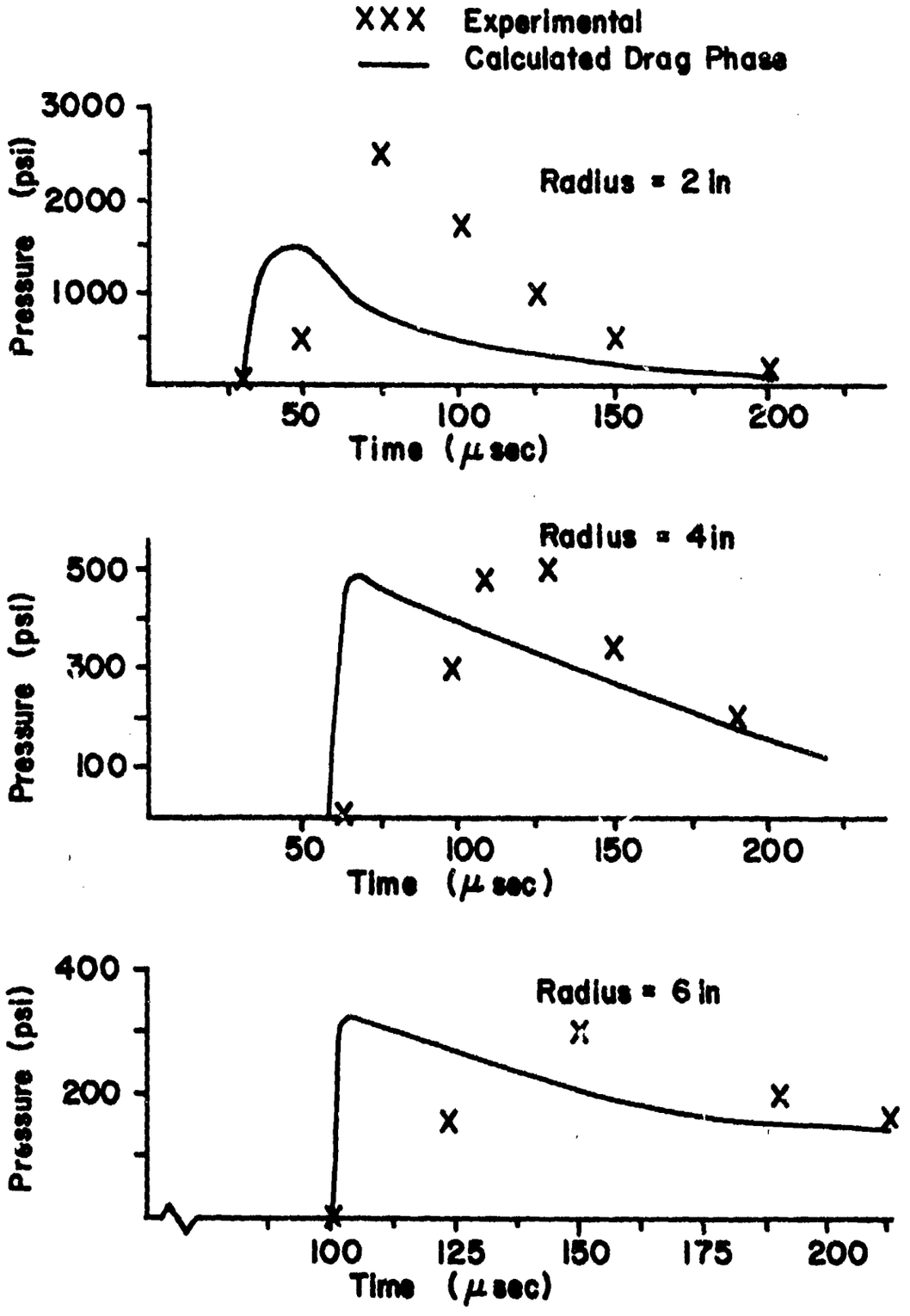

FIG. 10. FLUID PRESSURE COMPARISON, FREE SURFACES, (REF. 17)

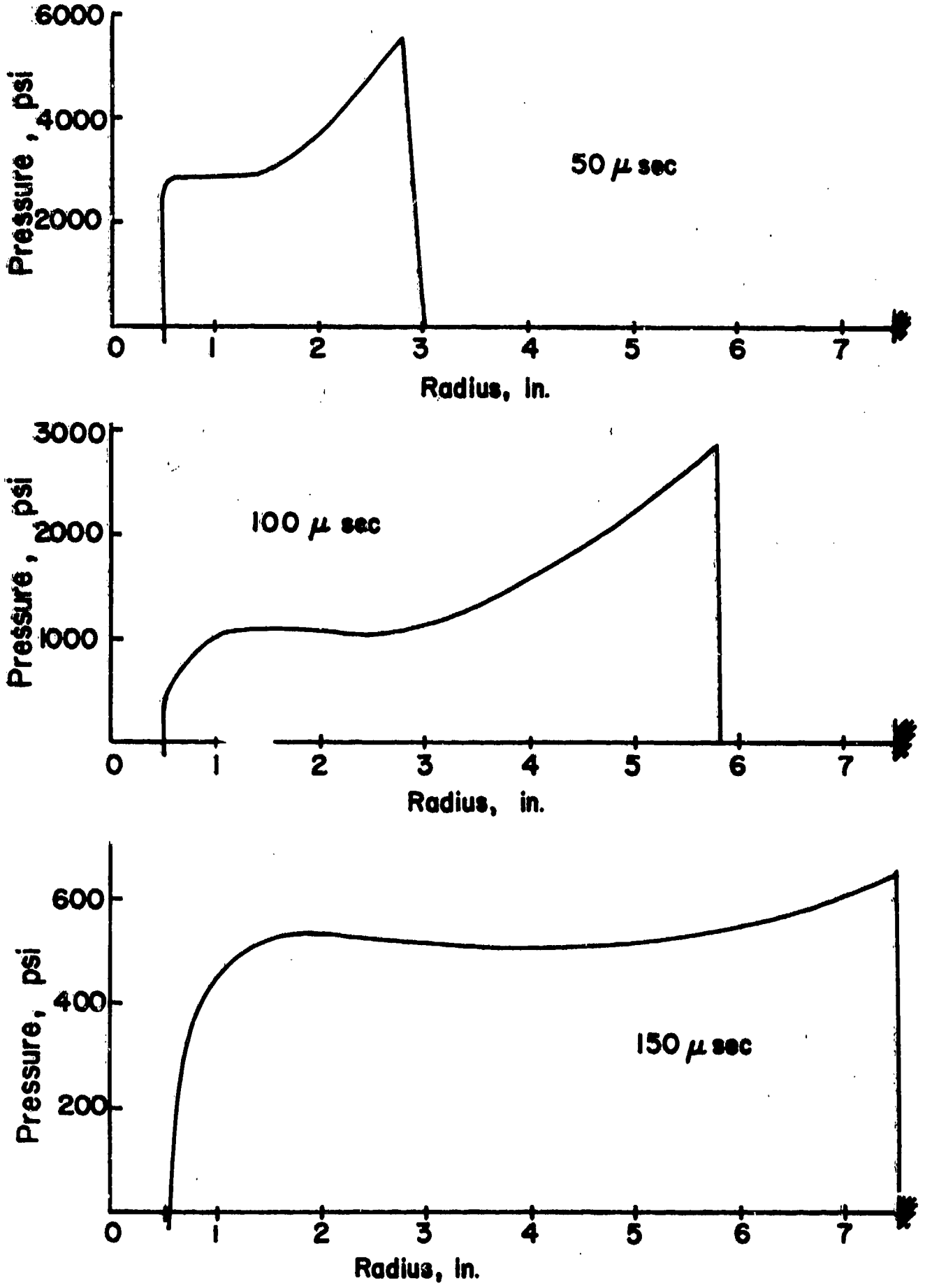

FIG. II ENTRY WALL PRESSURE $2p_o$ (drag) + p_o (shock) AT 50, 100 AND 150 μsec AFTER IMPACT

D. Exit Wall Pressure

The hydraulic ram pressure on the exit wall can also be predicted using the NWC code.

Values of the input data for shot 14 of the NWC test program are given below:

EN	=	3.00000						
BS	=	1.00000						
EFRACT	=	3.00000						
NCTUM	=	1						
NSTRIP	=	0						
NT	=	1						
XTUM	=	0.67929						
DXTUM	=	11.35918						
XSTRIP	=	35.00000						
XMASS(3)	=	0.10660	0.06410	0.04250				
AREA(6)	=	0.20460	1.03780	0.14320	0.70020	1.03780	0.08550	
DRAG(6)	=	0.05000	0.30000	0.05000	0.30000	1.00000	0.82000	
BETA(7)	=	0.00173	0.05272	0.00202	0.05915	0.44076	0.01187	0.01974

The tumbling parameters XTUM and DXTUM were obtained by determining the best fit of the predicted pressure to the measured pressure at one point in the fluid. The entry point of the projectile was 30 in., 30 in., and 0 in. in the x, y, and z directions respectively. The exit point was 28 in., 25 in. and 22 in. The projectile was predicted by the code to strike the exit wall at 1.63 msec after entering the tank. The pressure build up started at 0.35 msec. This time is taken as the zero time for the structural response computations.

Two different image conditions are considered for shot 14 in order to illustrate the effect of reflections from the other walls of the tank; that of no image and that of free surface reflections from every wall except the exit wall. The predicted pressure $2p_o$ at the center of the exit wall, at $x = y = 26.5$ in., and at the exit point is given in Fig. 12 as a function of time for the condition of no images and in Fig. 13 for the condition with free

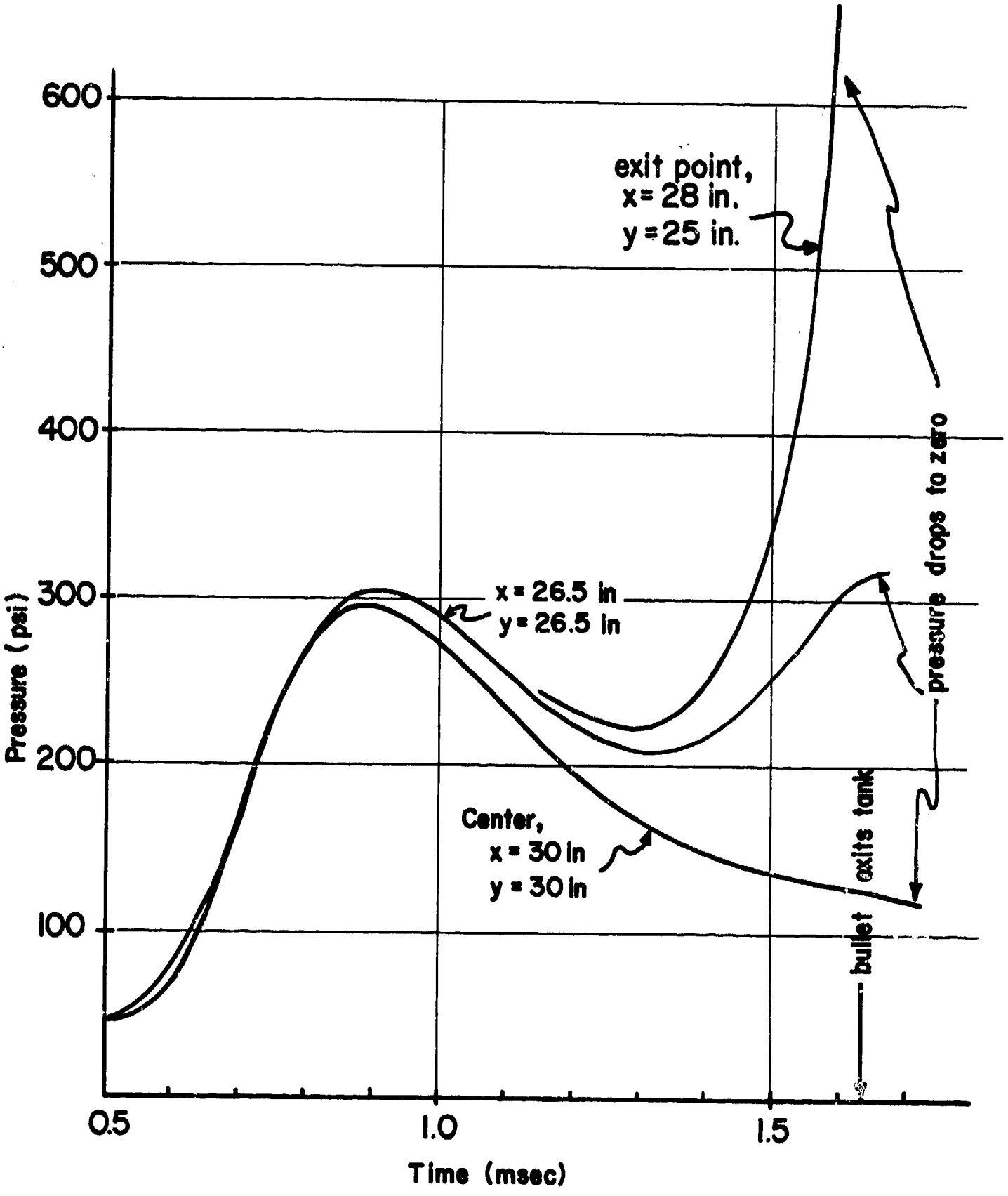

FIG. 12 EXIT WALL PRESSURE $2p_o$, NO IMAGES, SHOT 14

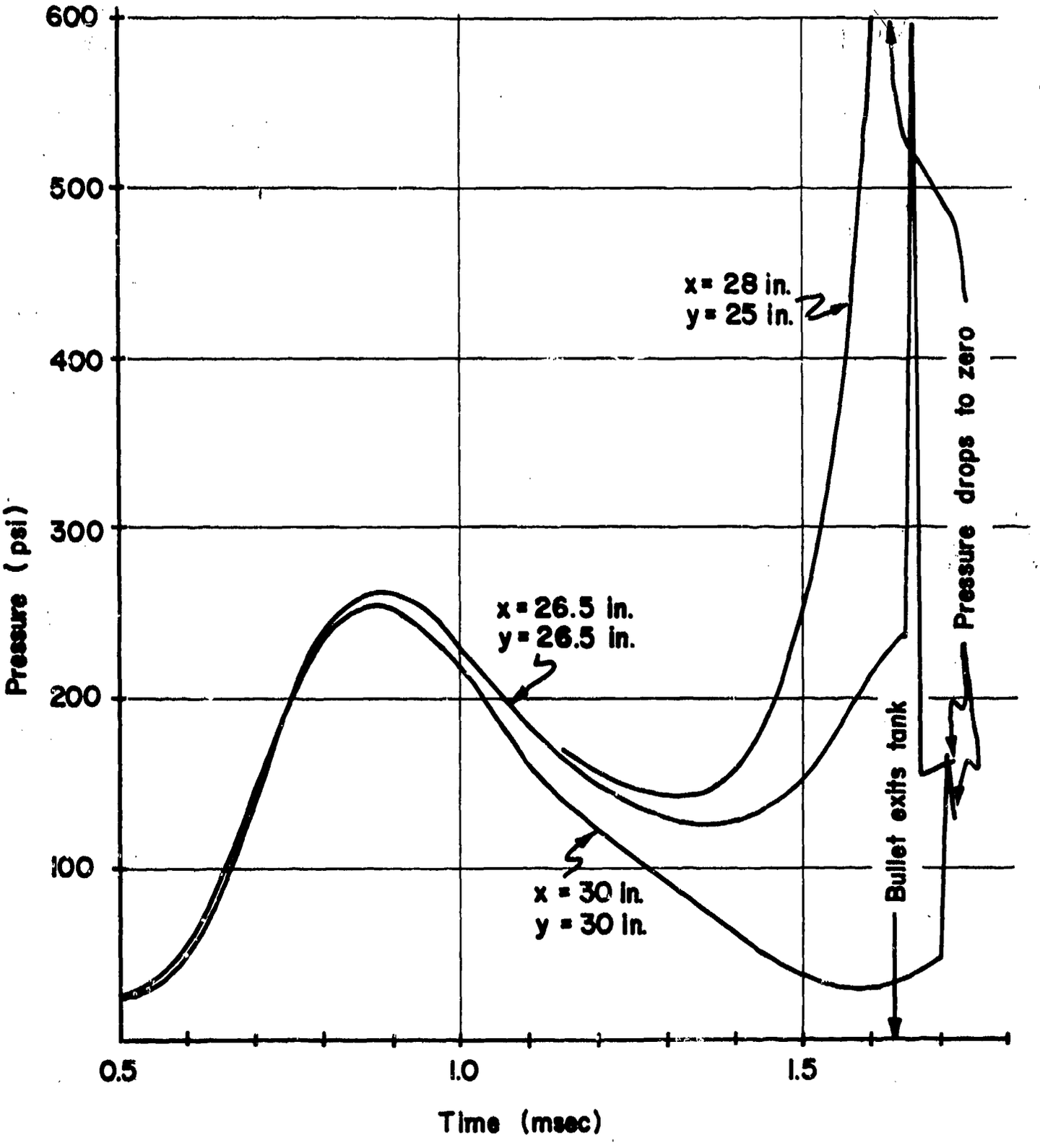

FIG. 13 EXIT WALL PRESSURE $2p_0$, FREE SURFACE REFLECTIONS

surface reflections. The pressures given in Figs. 12 and 13 are assumed to drop to zero shortly after the bullet exits the tank, for the reasons given in Section V.A. The pressure field $2p_o$ on the exit wall at $t = 0.9$ msec, 1.6 msec, and 1.75 msec is shown in Figs. 14-16 for the conditions of no images, and in Figs. 17-19 for the condition of free surface images. The region around the exit point where the pressure is assumed to be zero. The zero pressure there is due to the fact that the energy source has exited the tank; it is not related to the cavity that follows the bullet. However, the presence of the cavity will also cause the pressure to drop to zero.

A comparison of the pressures on the exit wall without reflections with the pressures with reflections reveals a considerable difference between the two pressure fields, particularly at times later than 1.5 msec. In general, the no image pressures are higher than those with images. Figure 18 shows negative pressures over a considerable portion of the plate at 1.6 msec. In addition, Fig. 13 shows some strong pressure spikes just after the bullet exits the tank. Its not clear where these spikes come from.

As a consequence of both the doubtful validity of the predicted fluid pressure on the wall after the bullet exits the tank and the presence of the cavity, the assumption is made in the analysis for the exit wall response that the pressure field $2p_o$ drops to zero when the bullet exits the tank. This assumption of course neglects the incoming pressures that have been reflected from the other surfaces, but the presence of the cavity makes it questionable whether or not the fluid is in contact with the wall. High-speed films of the exit wall show that the water does not immediately pour out of the exit hole

192	204	211	206	189	168	149
217	234	243	235	213	187	165
245	267	280	269	238	206	180
265	293 306	310	295	256	218	189
261	294 306 312 288 299 305		290	253	216	187
240	262	274	264	234	203	177
216	233	242	235	212	186	164

FIG. 14 EXIT WALL PRESSURE $2p_o$, NO IMAGES, t = 0.9 msec

60	62	62	58	51	46	43
73	79	79	70	58	50	45
98	118	119	92	68	55	48
144	249	273	128	78	59	50
148	271	303	131	79	60	51
108	137	140	101	71	57	49
83	93	94	79	63	53	47

398

348 690 427

367

FIG. 15 EXIT WALL PRESSURE $2p_o$, NO IMAGES, t= 1.6 msec

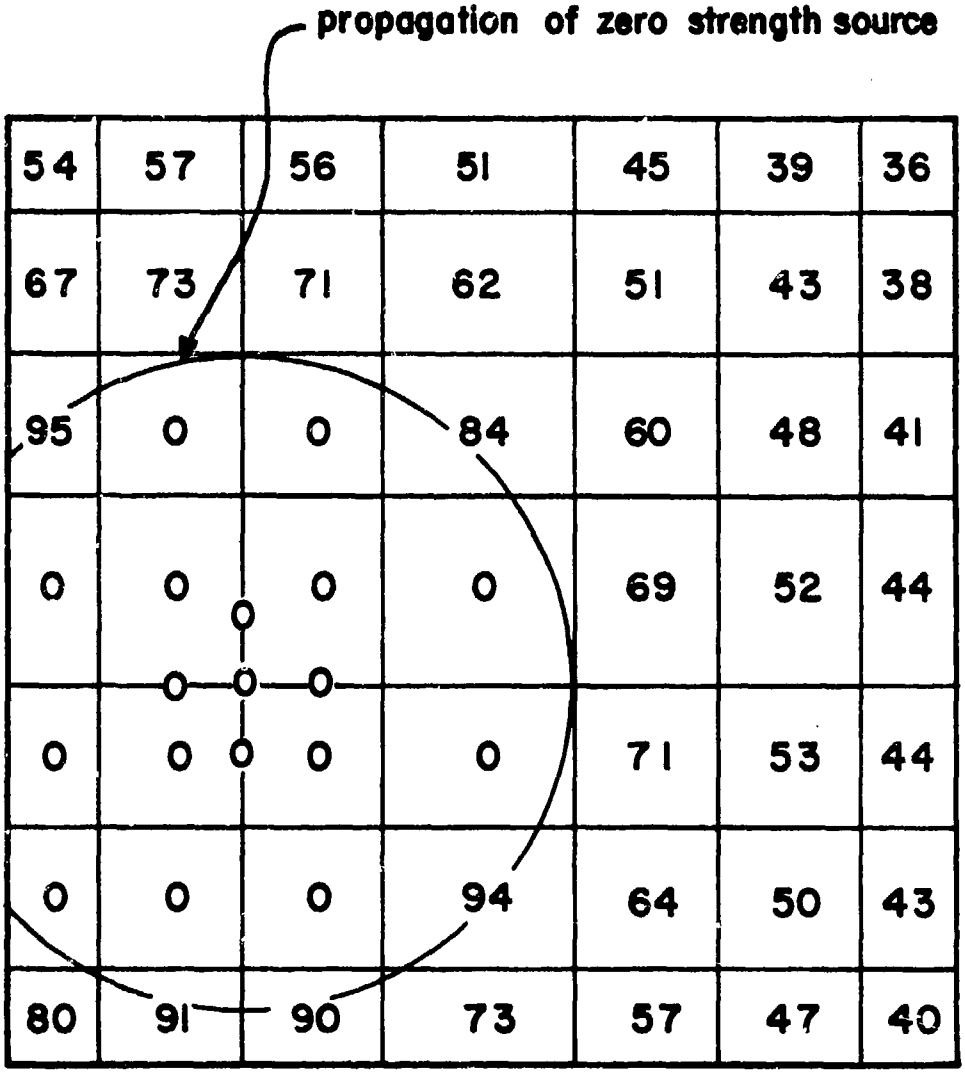

FIG. 16. EXIT WALL PRESSURE $2p_o$, NO IMAGES, t = 1.75 msec

156	168	173	168	152	134	117
180	194	202	195	174	151	131
205	226	238	227	197	168	144
224	250 263 267		252	214	179	153
221	252 263 269 246 256 261		248	211	177	151
201	221	233	220	194	166	142
180	195	203	196	174	151	130

FIG. 17 EXIT WALL PRESSURE $2p_o$, FREE SURFACE REFLECTIONS, $t = 0.9$ msec

-11	-14	-21	-29	-36	-37	-35
-4	-4	-9	-22	-34	-38	-38
17	30	27	-4	-27	-38	-40
62	162 308 180		31	-18	-34	-38
	-262-601-336-					
69	186 280 213		37	-15	-32	-36
35	57	54	11	-19	-30	-32
16	20	14	-5	-22	-28	-29

FIG. 18 EXIT WALL PRESSURE $2p_o$, FREE SURFACE REFLECTIONS, t = 1.6 msec

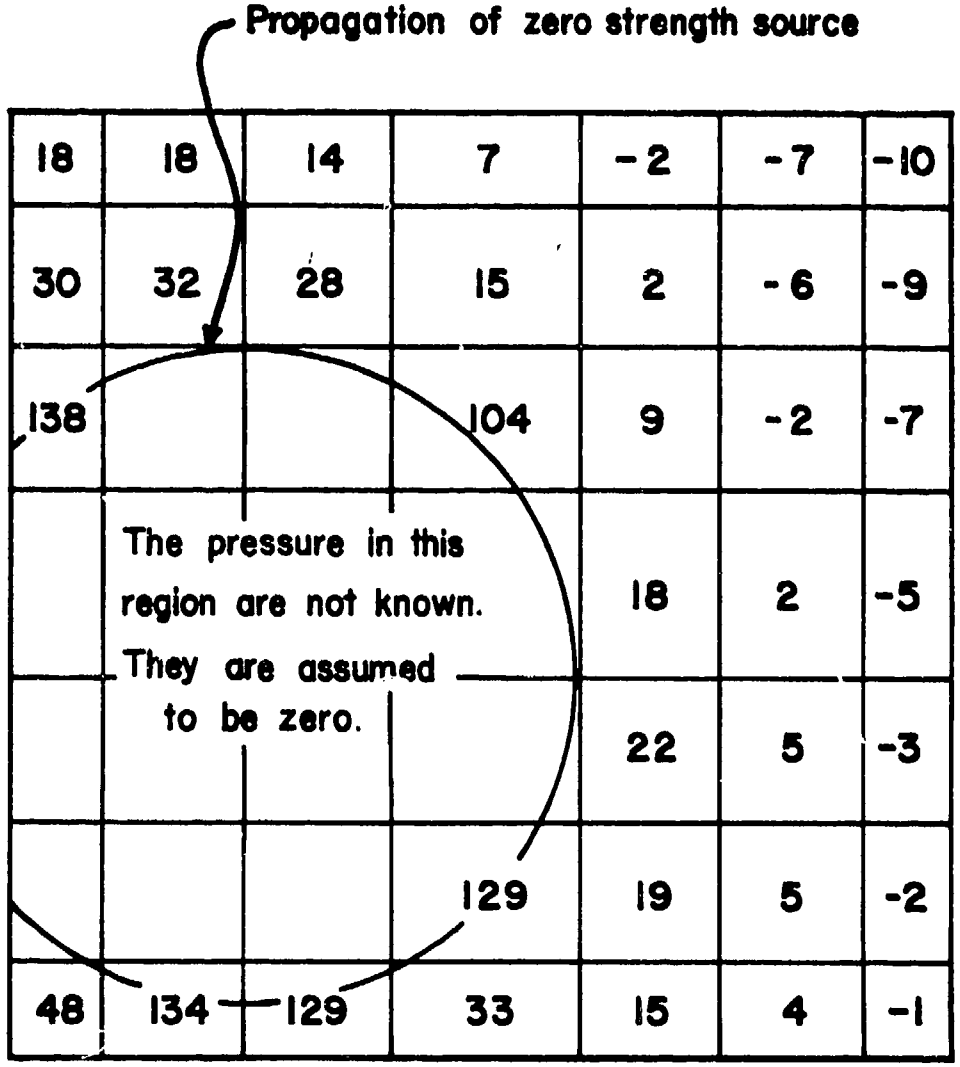

FIG. 19 EXIT WALL PRESSURE $2p_e$, FREE SURFACE REFLECTIONS

$t = 1.75$ msec

after the bullet penetrates the wall. There appears to be some delay, indicating the presence of the cavity in the vicinity of the hole. Later, however, the water is periodically pumped out in large quantities during the oscillating cavity phase.

VI WALL STRAIN COMPARISONS

A. Entry Wall Strains

Figure 20 shows typical experimental entry wall strains for a 0.16 inch thick aluminum wall. Additional data are contained in Refs. 15 and 17. The upper photograph shows that the radial strain is essentially due to pure bending because of the relatively symmetrical traces. The lower photograph shows that circumferential strains are also primarily due to pure bending of the plate for the first 400 μseconds. However, after 400 μseconds the circumferential strains are not as symmetric, which is indicative of stretching of the middle surface of the plate. The traces for the 0.09 in. plate are similar to those shown in Fig. 20, but they reveal more stretching of the middle surface.

Strains in the 0.09 in. entry wall have been computed using SATANS. The applied transient pressure field on the wall was the shock and cavity pressure shown in Fig. 11. The 7.5 in. radius plate was modeled with 71 equally spaced nodes, starting at the inner radius of 0.5 in. and continuing outward, 0.1 in. apart. The boundary conditions at the inner hole were those of a free edge; fully clamped conditions were assumed at the outer edge. The time increment was 5 μsec. Poisson's ratio was taken as 0.33.

Several cases of fluid-structure interaction were considered. When the effect of the fluid on the wall motion, i.e. the $-\rho c\dot{w}$ term in Eq. (7), was ignored, the computed strains caused by the sum of the shock and drag pressures were very large compared to the measured strains. When the piston theory is

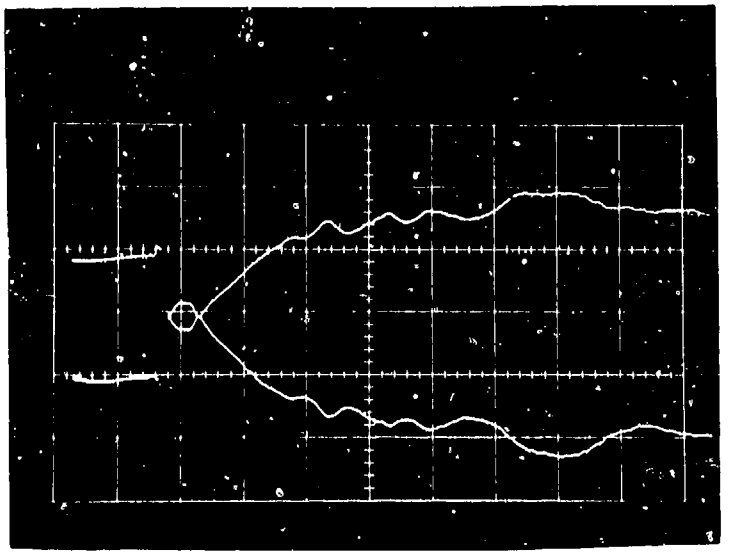

Radial Gages
100μsec/cm 2 mvolts/cm

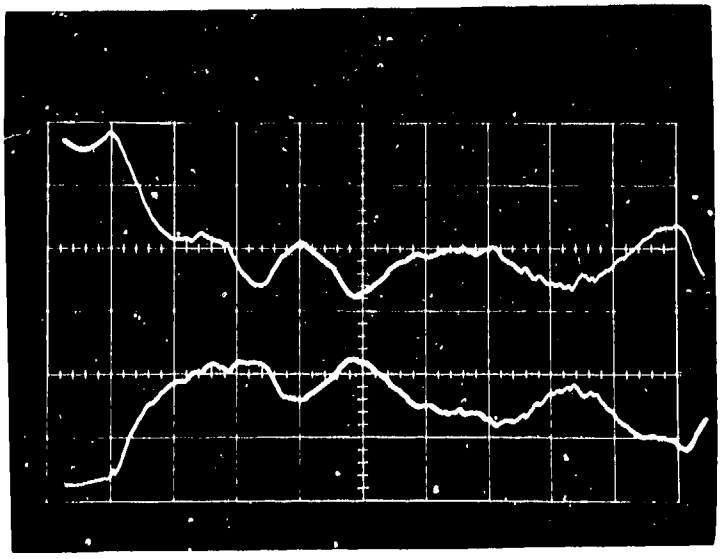

Circumferential Gages
200μsec/cm 2 mvolts/cm

h (thickness) = .16 in.

Fig. 20. Measured Entry Wall Strain, (Ref. 17)

used, the predicted strains are reduced by a considerable amount. Figure 21 presents the predicted and the measured radial strains on both sides of the wall at 2 in. from the entry point as a function of time. Figure 22 shows the corresponding circumferential strains*.

The sharp rise and fall of the predicted radial strain around 50 μsec in Fig. 21 is probably due to the passage of the shock pressure front. Note that the the early strains indicate compression on the dry side and tension on the wet side. The reason for this can be seen by examining a plot of the predicted wall deflection at 50 μsec shown in Fig. 23.

In general, the form of the predicted strains in Figs. 21 and 22 is the same as the form of the measured strains. However, except for the radial strains due to the shock pressure, the predicted strains are considerably smaller than the measured strains. One possible explanation for this difference is that cavitation takes place in regions where the net interface pressure is negative (tension)*. The predicted net interface pressure, $2p_o$ (drag) $+p_o$ (shock) $-\rho c\dot{w}$, is plotted in Fig. 24 at 50,100 and 150 μsec after impact. This figure can be compared with Fig. 11 to illustrate the effect of the wall motion on the interface pressure. Note the presence of large negative pressures in Fig. 24 The response of the entry wall assuming cavitation takes place has been computed using the modified version of SATANS discussed in Section IV. C.

*A similar comparison of strains is presented in Ref. 17. However, in Ref. 17 the sign of the strain appears to be reversed from normal convention, i.e. tension strain is called negative and compression strain is called positive. This conclusion is based upon the assumption that in general the plate will stretch, not compress, after the initial wavefront passes. In addition, the shock pressure used in Ref. 17 was multiplied by a factor of two.
**Recall that the photographs of the entry plate presented in Fig. 7 do not appear to indicate any cavitation.

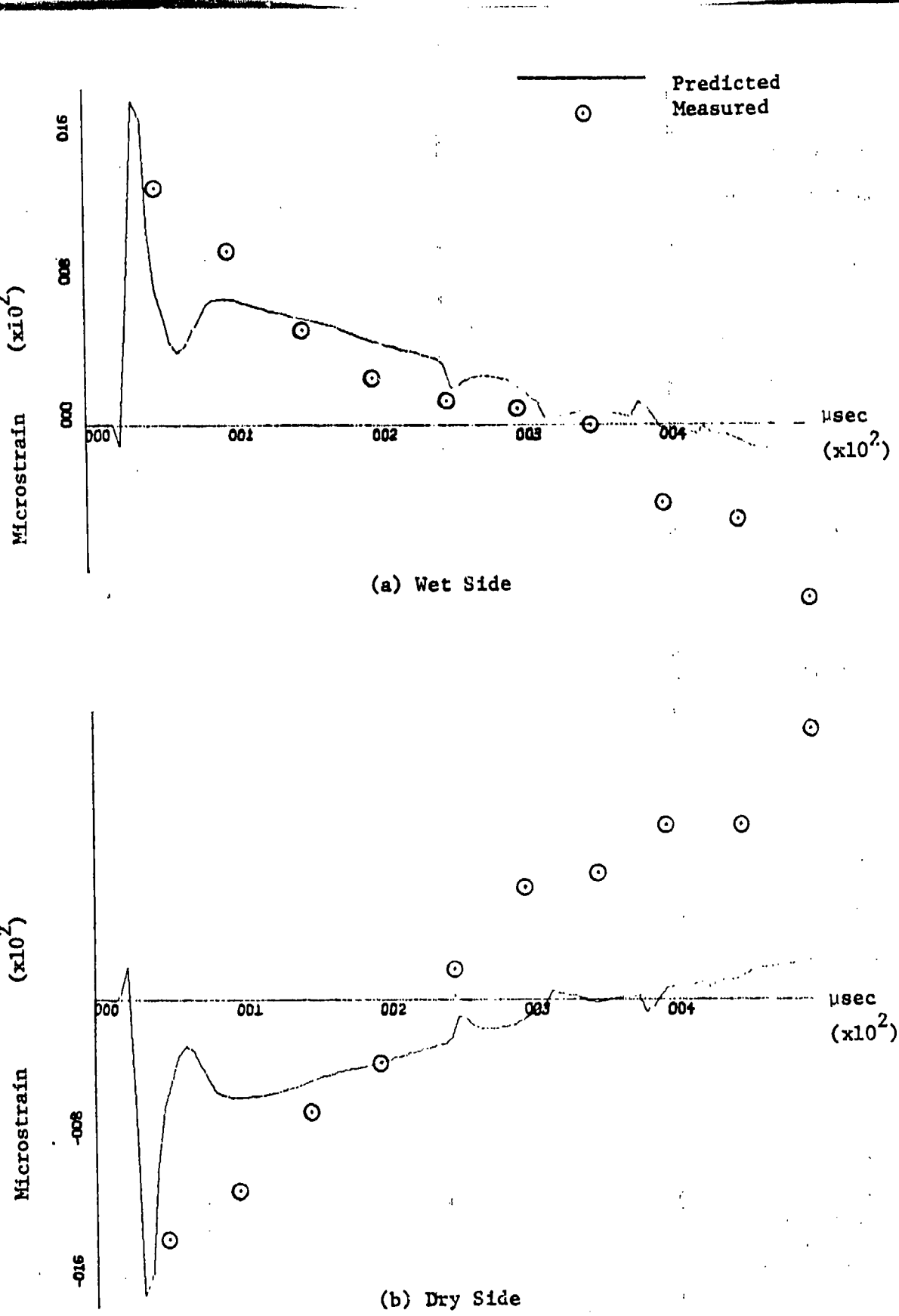

Fig. 21. Entry Wall Radial Strains 2 in. From Center of Plate

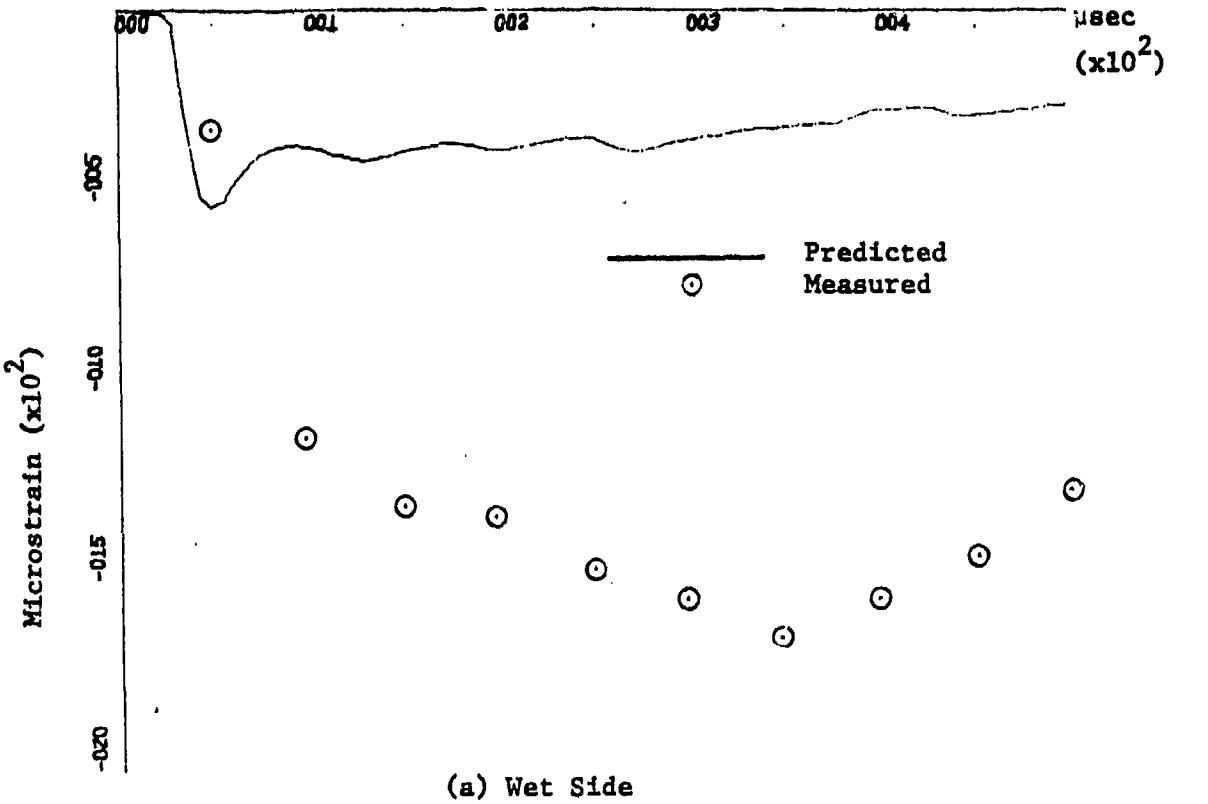

(a) Wet Side

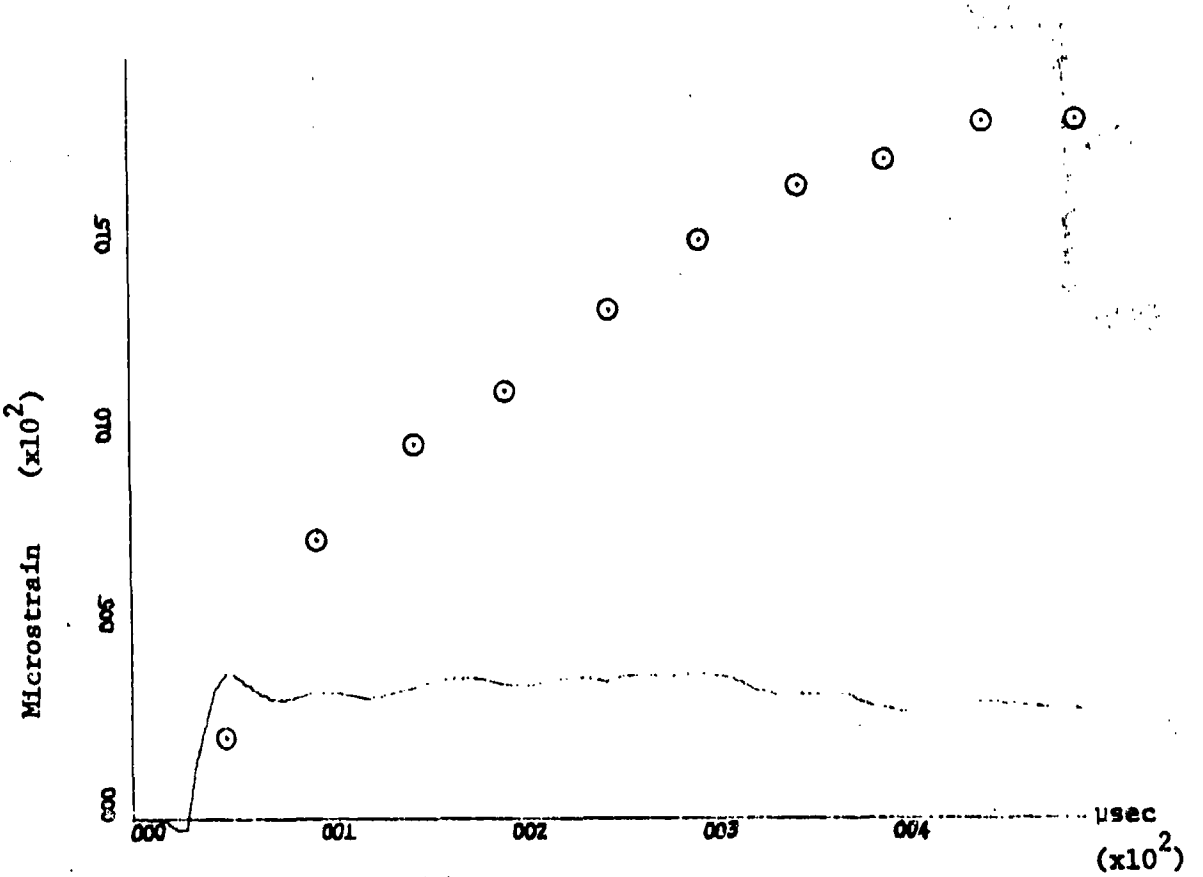

(b) Dry Side

Fig. 22. Entry Wall Circumferential Strains 2 in. From Center of Plate

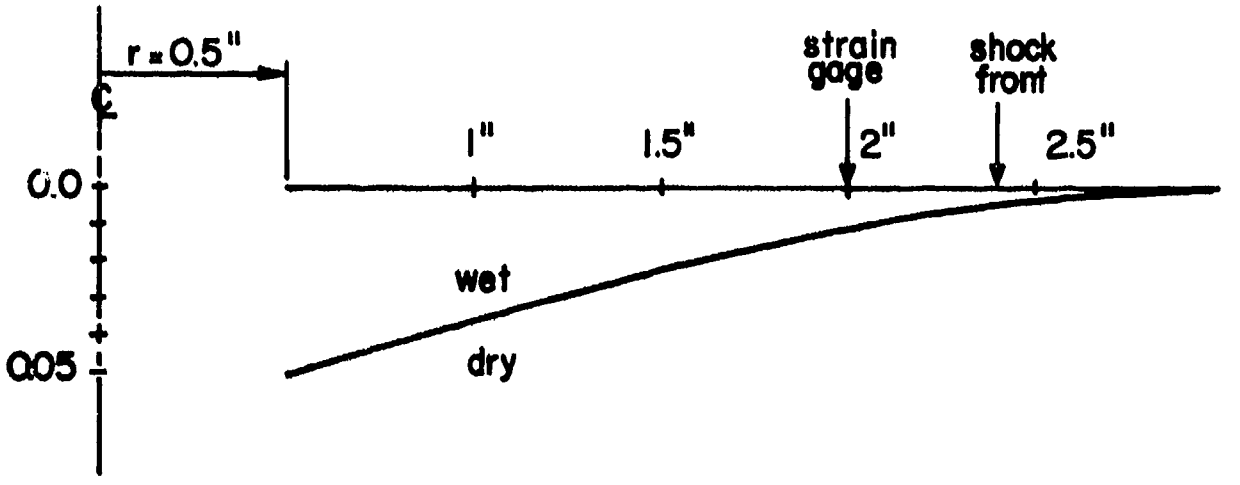

FIG. 23 ENTRY WALL PREDICTED DEFLECTION AT 50μsec

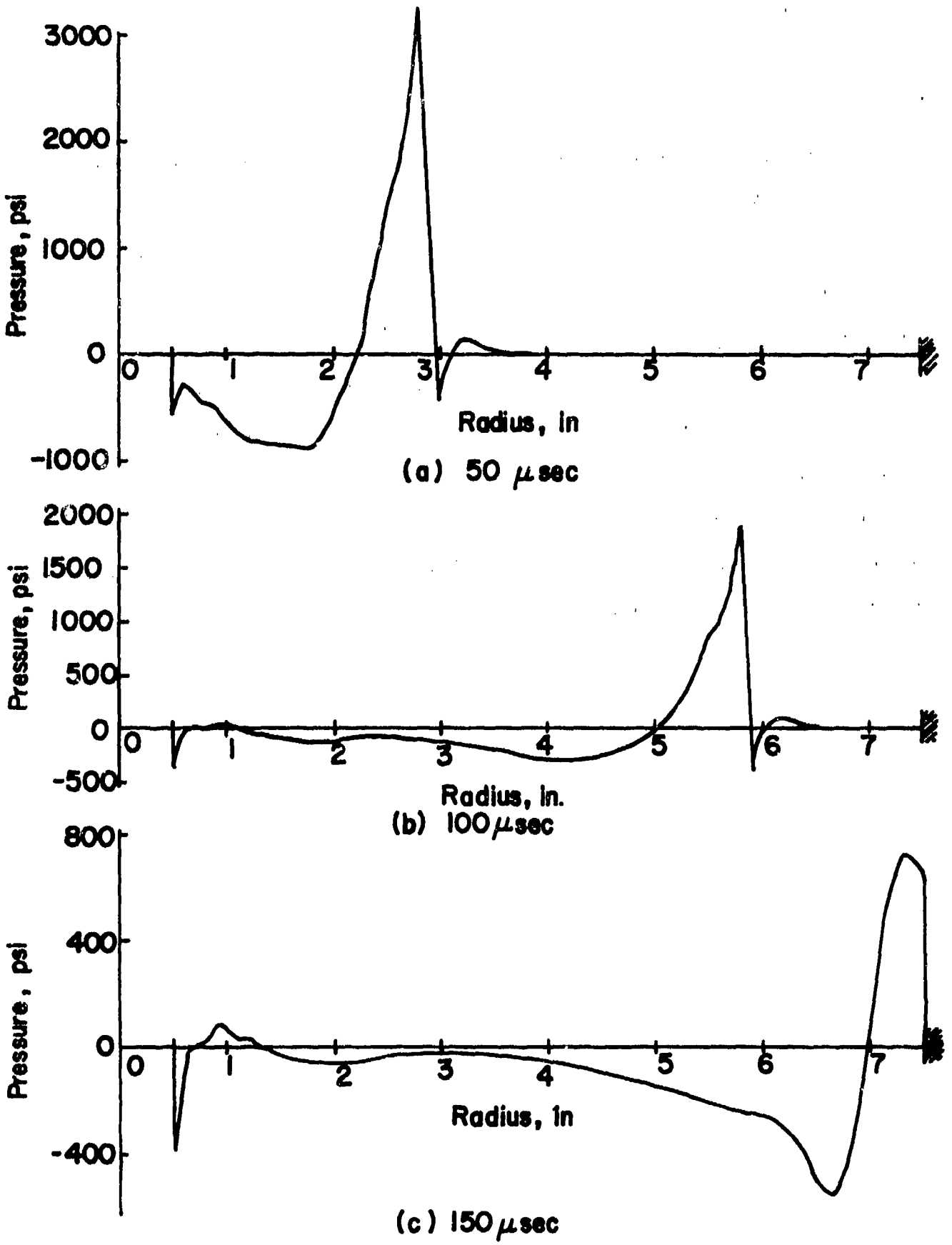

FIG. 24 ENTRY WALL NET PRESSURE $2p_o$ (DRAG) + p_o (SHOCK) $-\rho c\dot{w}$ AT 50, 100 AND 150 μsec

The predicted and measured results for the radial and circumferential strains on both sides of the wall at 2 in. from the entry point are presented in Figs. 25 and 26. Examination of these results reveals that the strains with cavitation included are significantly larger than those computed without cavitation. However, except for the circumferential strain on the dry side, the general form of the predicted strains with cavitation differs from that of the measured strains. There is considerably more oscillation in the predicted strains. This is because the damping effect of the fluid has been removed in those areas where cavitation occurs. Thus, perhaps cavitation is not occurring at the entry wall. Recall that the NWC high-speed motion pictures did not reveal any cavitation at an entry wall.

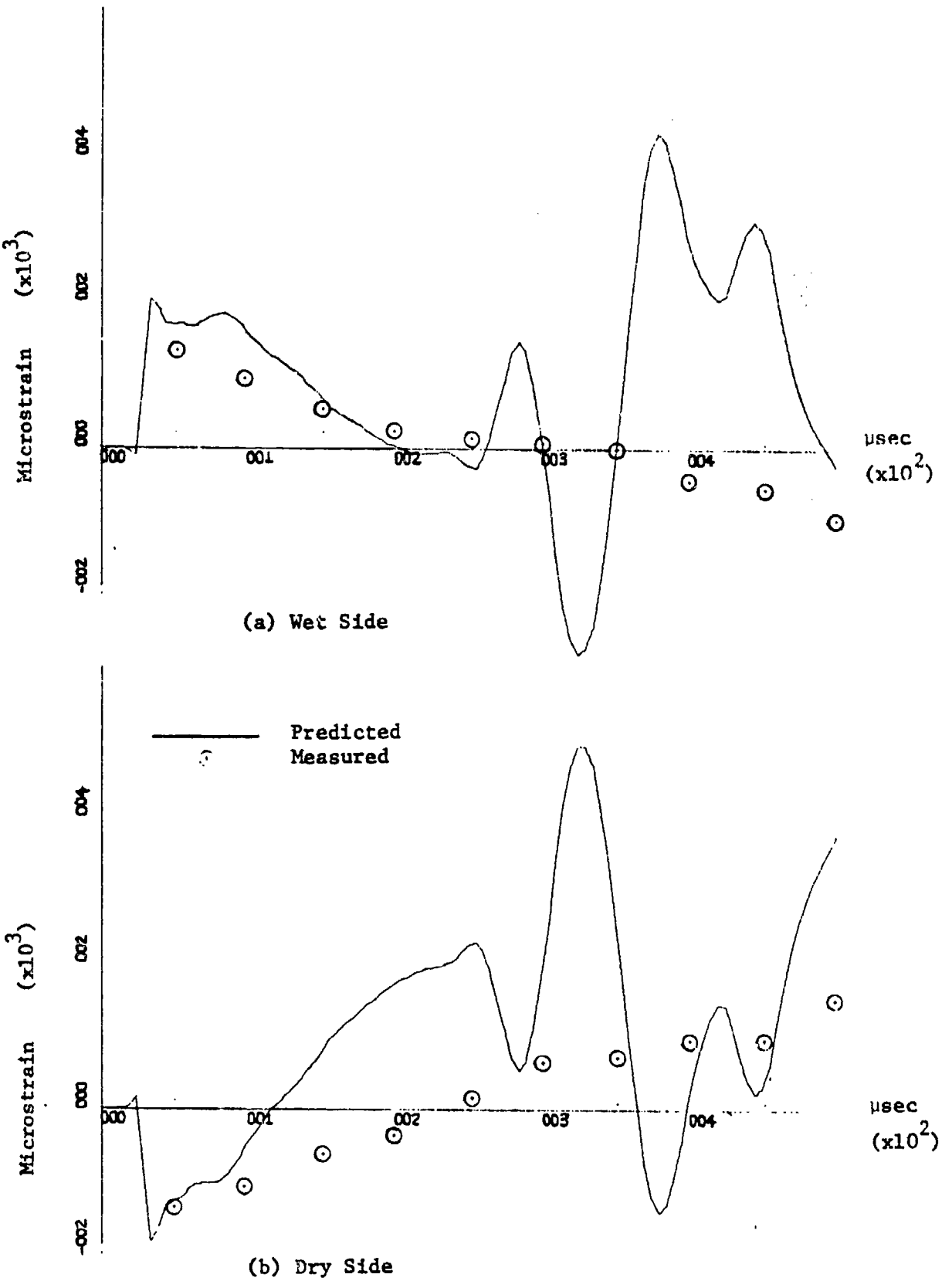

Fig. 25. Entry Wall Radial Strains 2 in. From Center of Plate (with Cavitation)

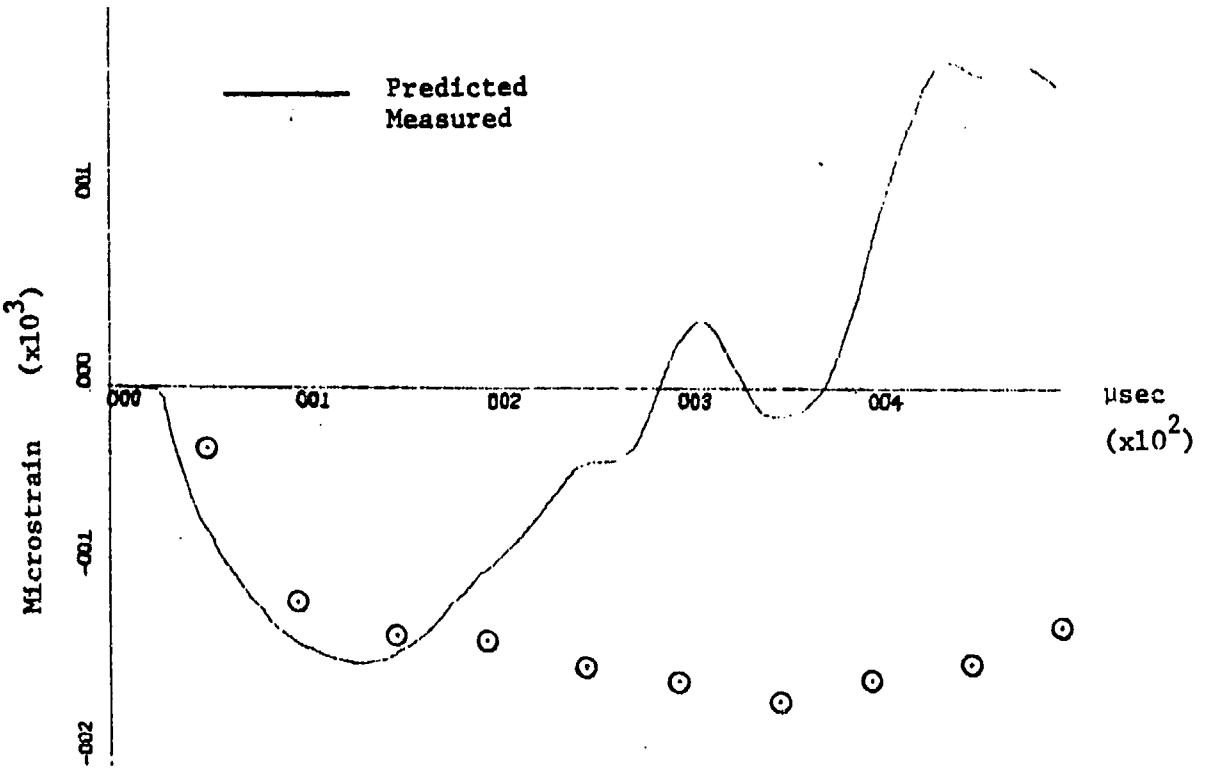

(a) Wet Side

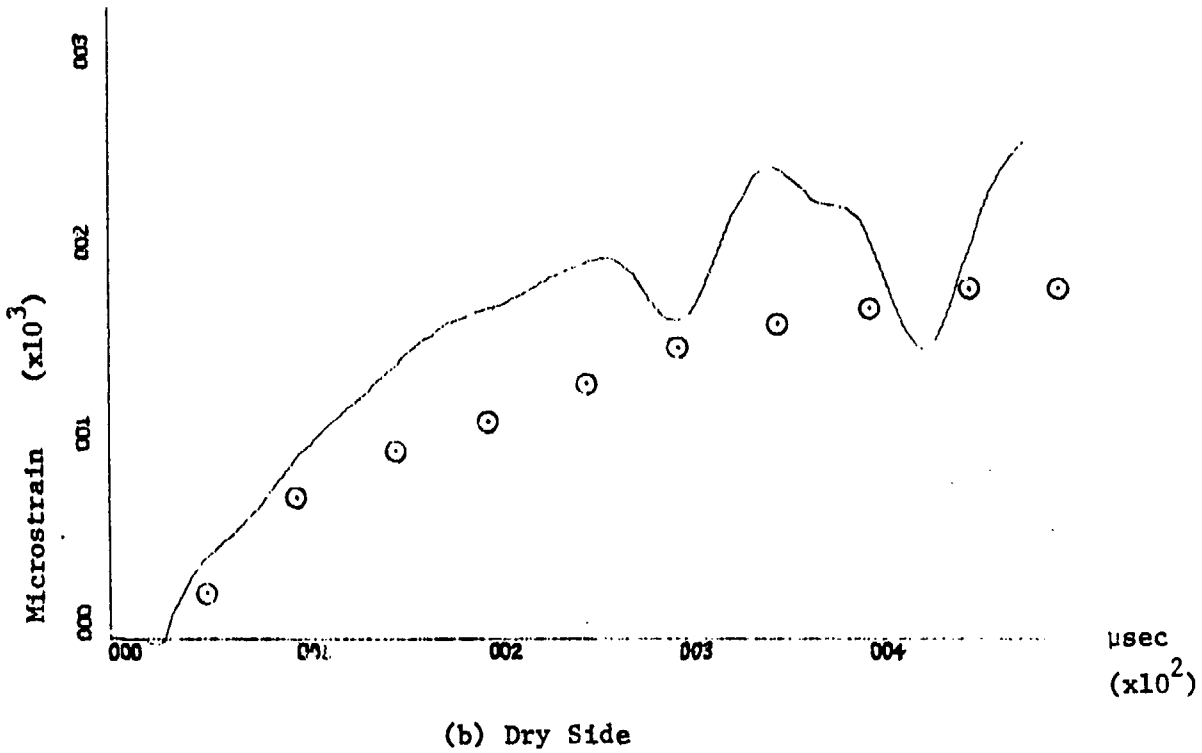

(b) Dry Side

Fig. 26. Entry Wall Circumferential Strains 2 in. From Center of Plate (with Cavitation)

B. Exit Wall Strains

As an example of the strain data obtained by NWC in their exit wall tests, the strains measured at the 16 gages are presented for shot 14 in Fig. 27. Figure 28 shows the correspondence between the gage number and the location and direction of strain measurement. The gage locations are also indicated in Figs. 2 and 6. The locations defined as a and b in Fig. 27 at gages 9-12 and 13-16 respectively are also indicated in Figs. 6 and 28. Note in Fig. 27 that only gage 6 appears to be clearly inoperative. However, the results from gage 16 are also suspect since they are of a different nature than those from the other gages. On most of the other shots many more gage readings were lost because the wires leading from the gages to the recording device were broken by the exiting bullet, the large wall motion, and the spewing water.

As a consequence of the experimental set-up, the time coordinate on each strain trace has a different origin with respect to universal time; hence, the strain traces cannot be compared using the printed time as a reference. In addition, there is no precise indication or data on the exact time when the bullet strikes the exit wall*. Thus, its difficult to directly compare predicted strains with the measured strains on a timewise basis. Nevertheless, some indication of the applicability of the analysis can be obtained by comparing the general form of the predicted and measured strains and the maximum strains.

*An examination of the strain at gage 14 in Fig. 27 reveals a significant change in behavior between 10.2 and 10.7 msec. That could be an indication that the bullet exited the tank at that time. Furthermore, a study of the high-speed films of shot 12 revealed that two of the wires from gages 9 through 12 were cut by the bullet about four frames after the bullet exited the tank. Thus, the signals from these gages were probably lost approximately 0.5 msec after penetration. The strain trace for gage 9 was definitely lost at about 5.7 msec. Prior to that time the strain was less than 1000 μstrain. Since the maximum strain of shot 12 was approximately 4500 μstrain, and since gage 9 was as close to the exit point as any of the other gages, it appears that the large strains in the wall occur after penetration, except of course, in the immediate vicinity of the exit point.

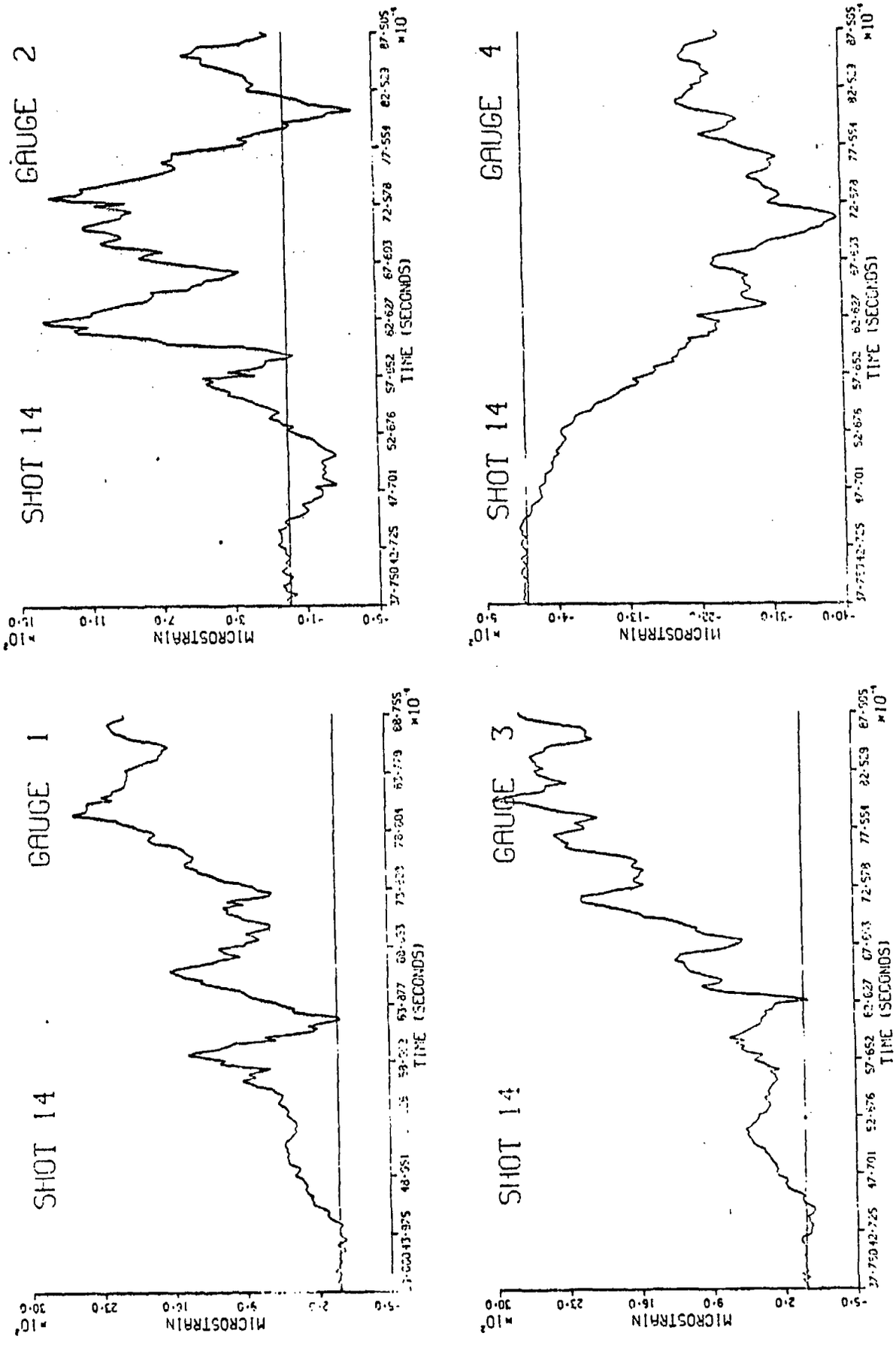

Fig. 27. Measured Exit Wall Strains, Shot 14 (Ref. 6)

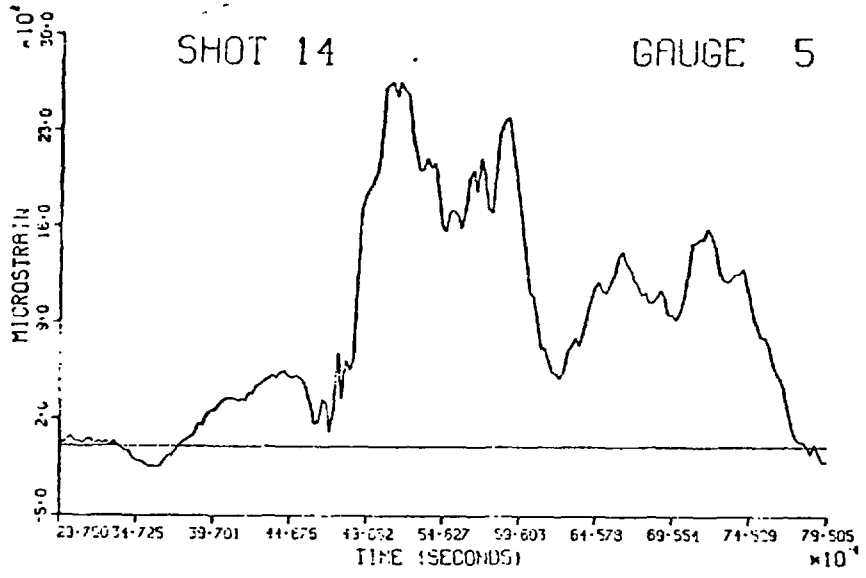
SHOT 14
GAUGE 5
MICROSTRAIN
TIME (SECONDS)

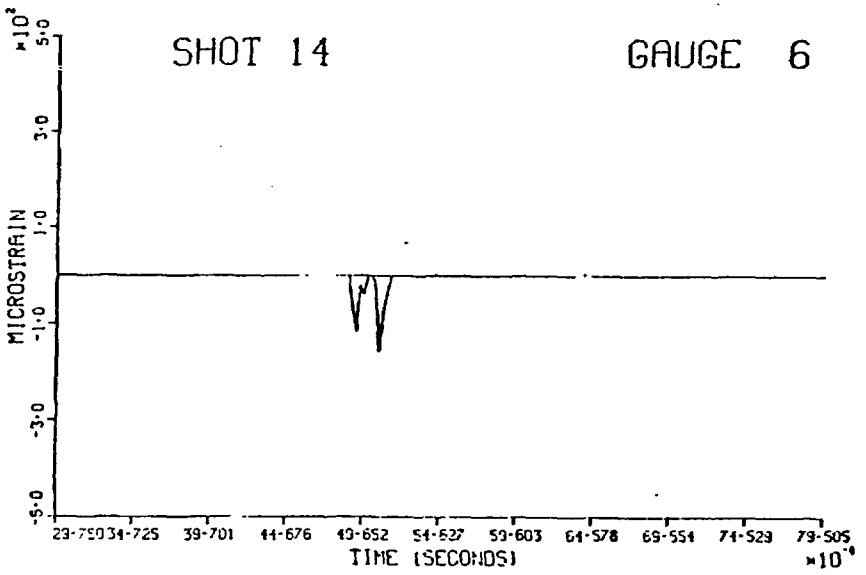
SHOT 14
GAUGE 6
MICROSTRAIN
TIME (SECONDS)

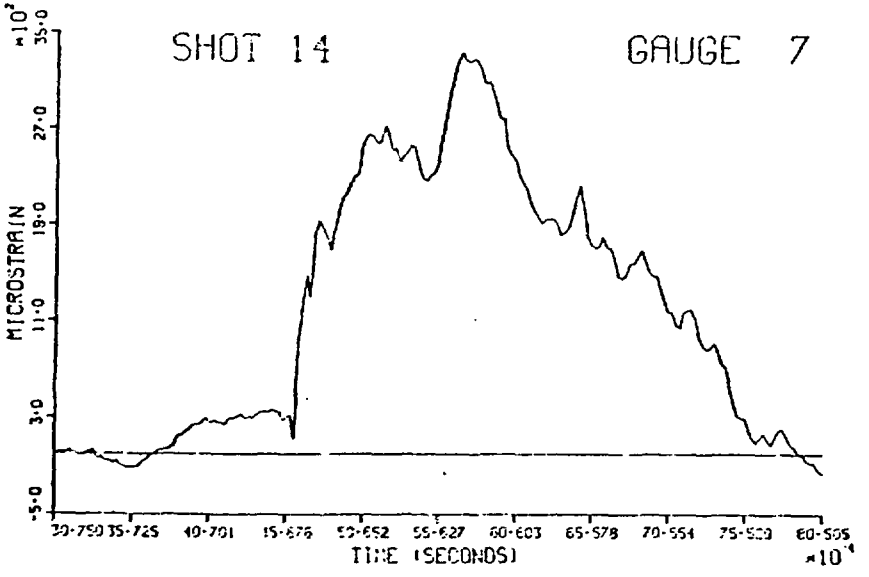
SHOT 14
GAUGE 7
MICROSTRAIN
TIME (SECONDS)

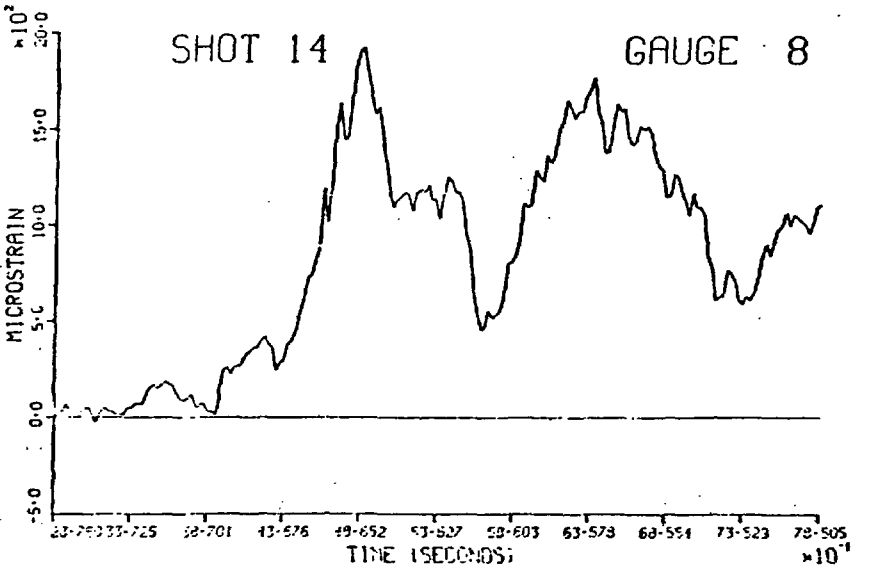
SHOT 14
GAUGE 8
MICROSTRAIN
TIME (SECONDS)

Fig. 27 Cont.

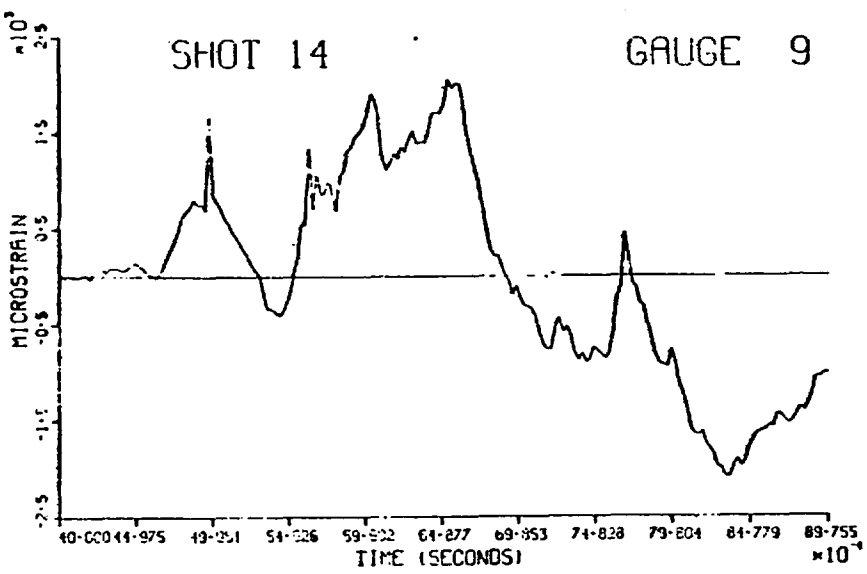
SHOT 14
GAUGE 9
MICROSTRAIN
TIME (SECONDS)

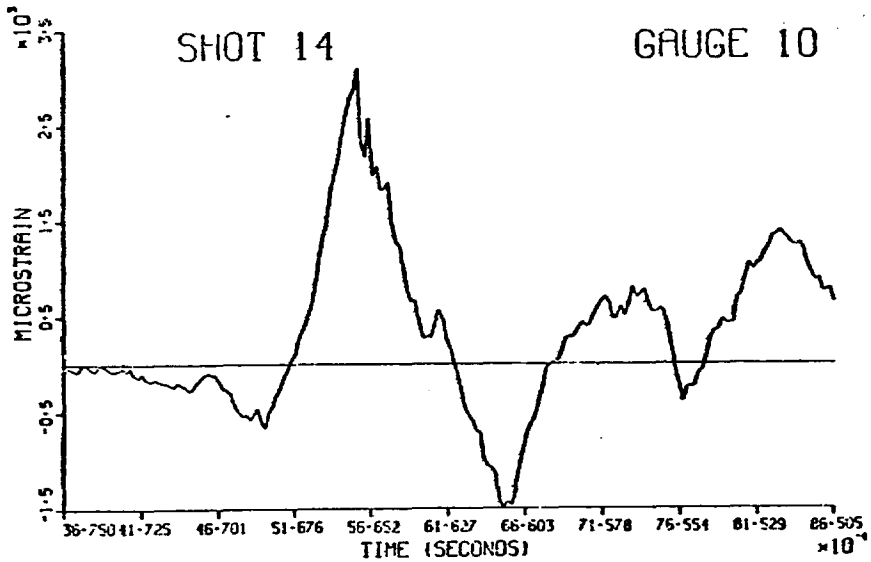
SHOT 14
GAUGE 10
MICROSTRAIN
TIME (SECONDS)

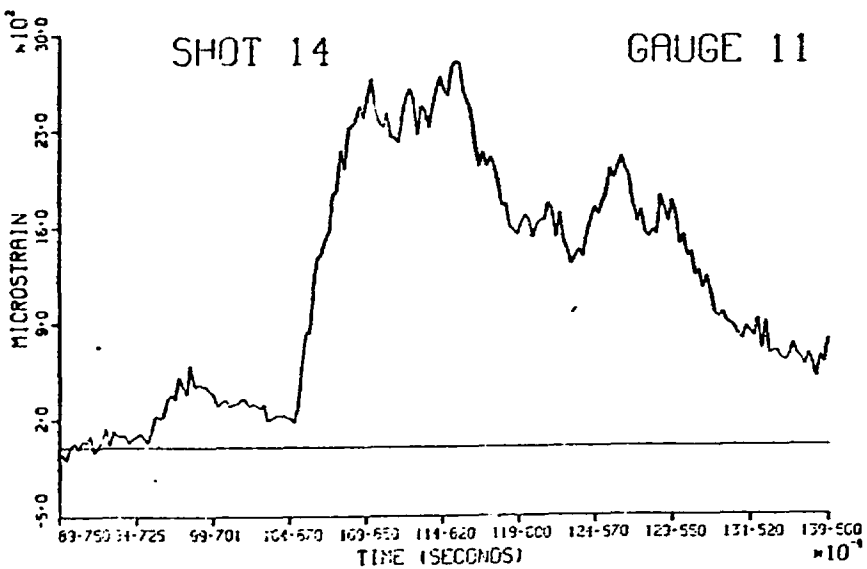
SHOT 14
GAUGE 11
MICROSTRAIN
TIME (SECONDS)

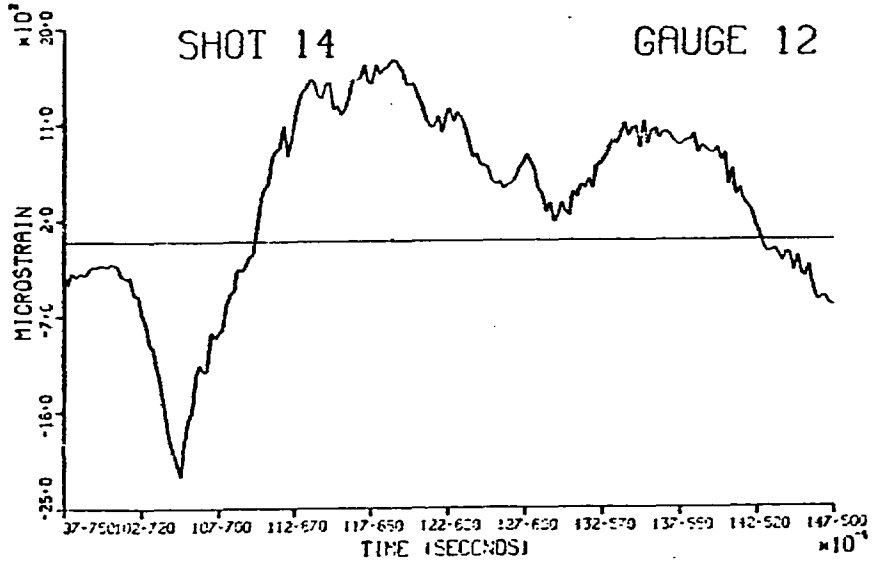
SHOT 14
GAUGE 12
MICROSTRAIN
TIME (SECONDS)

Fig. 27 Cont.

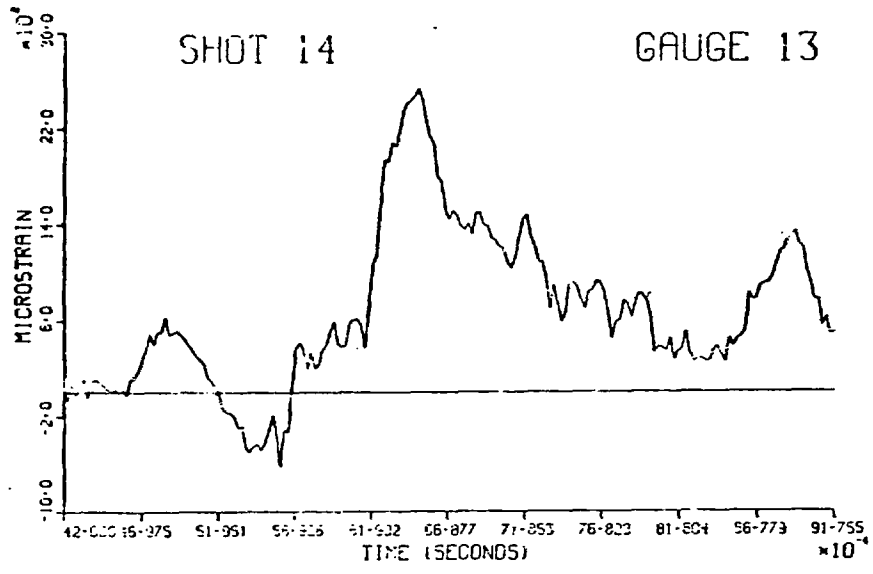
SHOT 14
GAUGE 13
MICROSTRAIN
TIME (SECONDS)

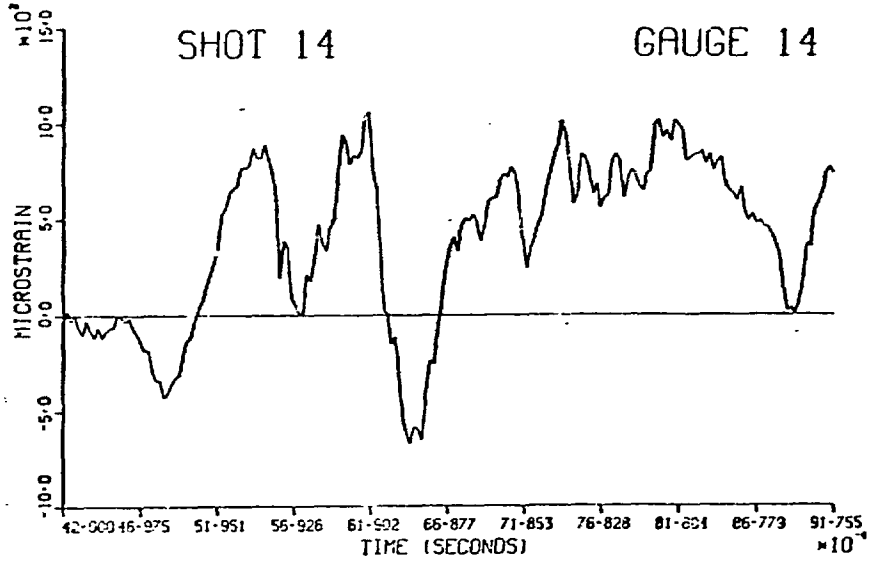
SHOT 14
GAUGE 14
MICROSTRAIN
TIME (SECONDS)

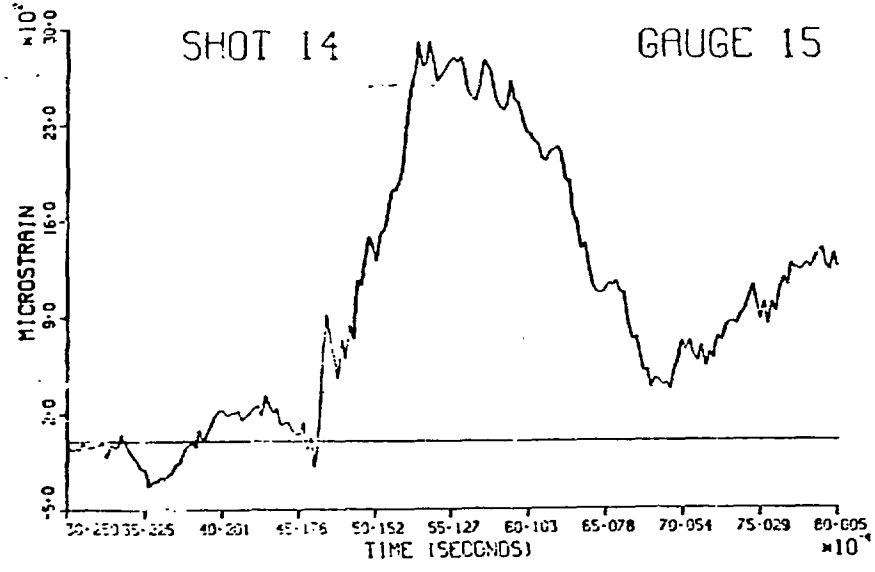
SHOT 14
GAUGE 15
MICROSTRAIN
TIME (SECONDS)

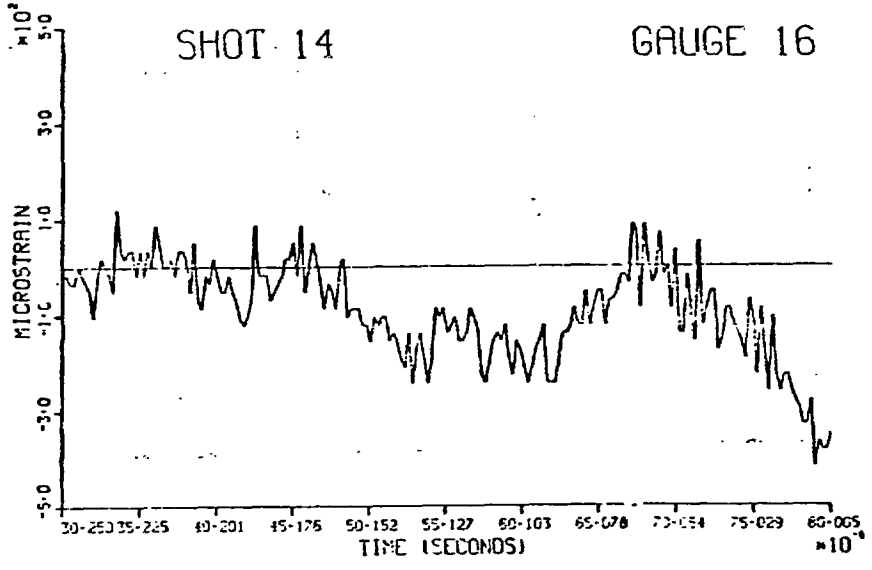
SHOT 14
GAUGE 16
MICROSTRAIN
TIME (SECONDS)

Fig. 27 Cont.

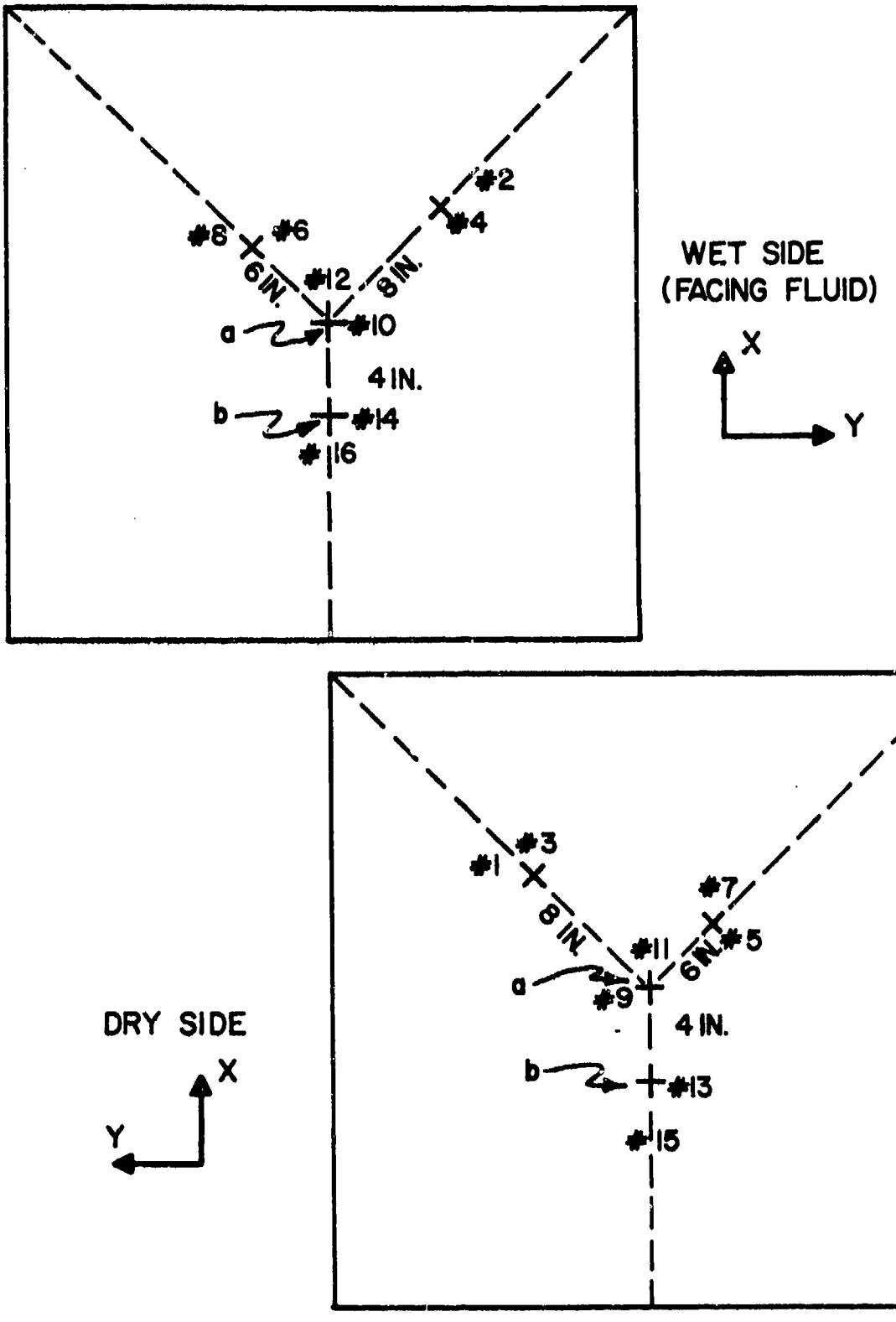

FIG. 28 STRAIN GAGE LOCATIONS AND DIRECTIONS

The response of the exit wall to shot 14 has been computed using SATANS with the 21 station model shown in Fig. 6. The stations are 0.5 in. apart. The plate is assumed to be continuous at the center (the exit point), and the outer edge is assumed to be fully clamped. The pressure $2p_o$ from the NWC hydraulic ram pressure code for shot 14 along the line $x = 28$ in. and centered at the exit point was applied for the interval $t = 0.35$ msec to $t = 1.625$ msec (fluid time) or $t = 0$ to $t = 1.275$ msec (structure time) in increments of 25 μsec*. The pressure was assumed to be zero after 1.275 msec for the reasons given in Section V.D. The axisymmetric response of the circular plate was computed at intervals of 25μsec for the interval $t = 0$ to 4 msec. The results for the radial strain (ε_y) history and circumferential strain (ε_x) history on both sides of the wall at point c in Fig. 6 are presented in Fig. 29 for the condition of no pressure reflections from the other walls and in Fig. 30 for the condition of free surface reflections. A comparison of Figs. 29 and 30 reveals that the strains computed with the reflections are smaller than those without reflections. Only ε_x on the wet side shows any major change in the form of strains.

The predicted strain traces in Figs. 29 and 30 can reasonably be compared with those of gages 9 through 12 (point a in Fig. 6) or 13 through 16 (point b in Fig. 6) shown in Fig. 27. The time scale for the predicted strains has been made essentially the same as that for the measured strains for ease of comparison, but the exact times cannot be compared. The location of each strain in Figs. 29 and 30 corresponds to the strains as they are located in Fig. 27.

*The minimum time at which the fluid pressure starts to build up on the exit wall is 0.35 msec. This time is used as the zero time for the structural response computations.

Fig. 29. Predicted Wall Strains at 5 in. From Exit Point (No Reflections)

Fig. 30. Predicted Exit Wall Strains at 5 in. From Exit Point (Free Surface Reflections)

A comparison of the predicted and measured strains shows that the shape of the measured traces for ε_x on the dry side (gages 11 and 15), ε_x on the wet side (gage 12; gage 16 appears to be inoperative) and ε_y on the wet side (gage 10) is very similar to the predicted strain history for those three strains. In particular, note the build up of ε_x on the dry side and the rapid change of direction of ε_x on the wet side when the bullet exits the tank. However, the magnitude of the predicted strains is off by factors of 60, 200 and 30 respectively. Furthermore, the predicted strains do not show the high frequency content exhibited by the measured strains. This could be due in part to the fact that the analysis is axisymmetric and does not contain the high frequency asymmetric motion generated by the corners of the square plate, and in part to the fact that the piston theory without cavitation causes the plate to respond as a heavily damped oscillator. An examination of the net fluid pressure on the exit wall revealed that negative (tension) pressures of approximately 20 psi or less occurred over portions of the wall at various times. To illustrate this, Fig. 31 presents the net interface pressure over the wall at 1, 2 and 3 msec. When the assumption is made that cavitation occurs at any negative pressure, the modified version of SATANS predicts the strains shown in Fig. 32 for the condition of no reflections. A comparison of these strains with the measured strains (Fig. 27) and with the predicted strains without cavitation (Fig. 29) reveals that the predicted strains with cavitation are much closer in magnitude to the measured strains, but the similarity in form has been lost.

An analysis with cavitation using a 30 in. diameter plate centered at the exit point of shot 14 gave roughly the same results as the analysis of the 20 in. plate.

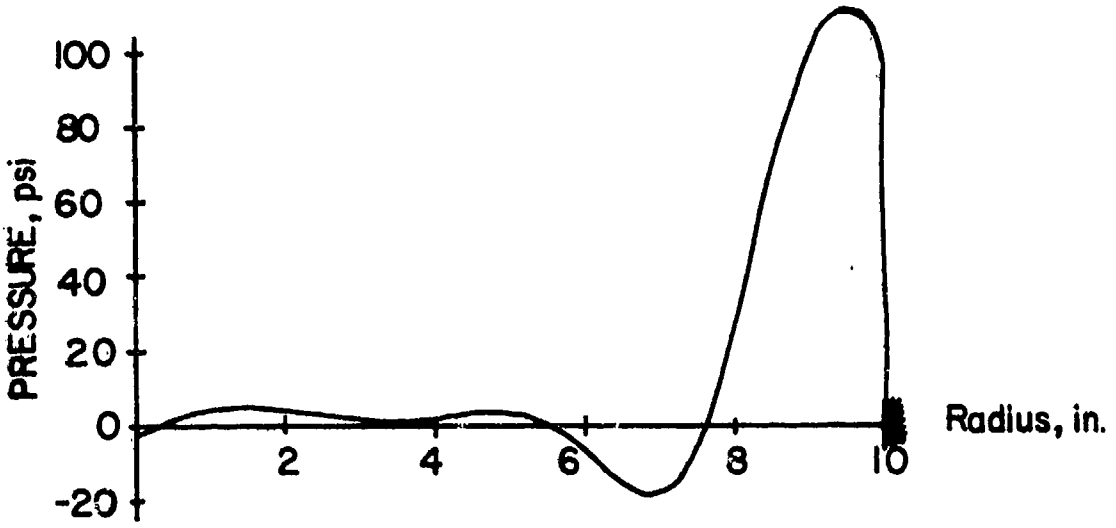

(a) 1 msec

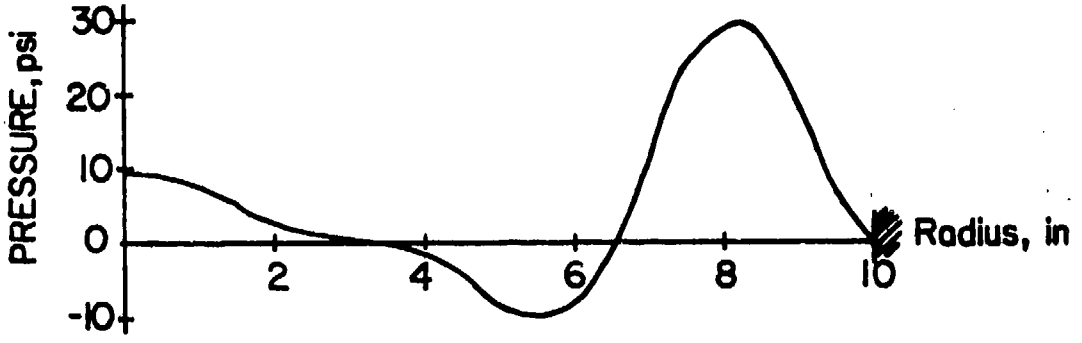

(b) 2 msec

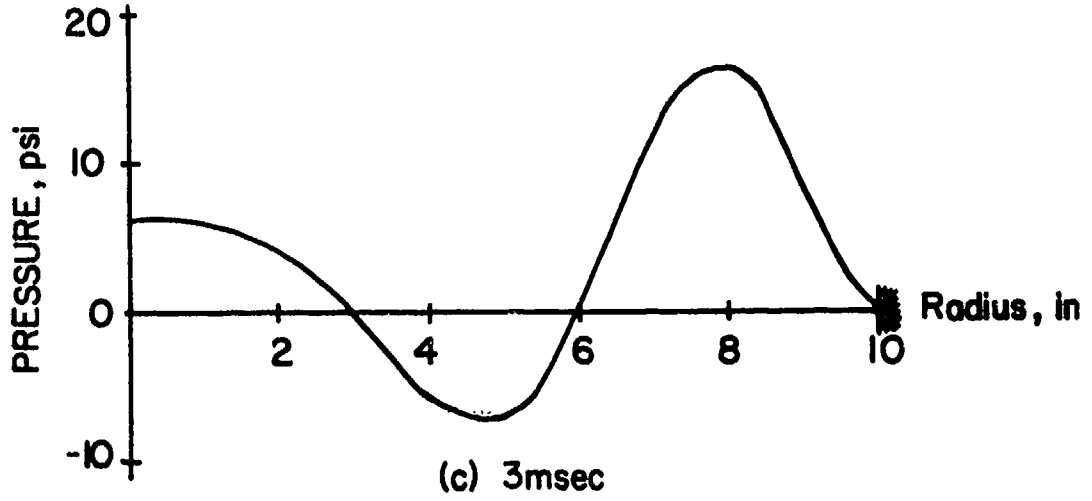

(c) 3msec

FIG. 31 EXIT WALL NET PRESSURE $2p_o - \rho c\dot{w}$ AT 1, 2, AND 3 msec

Fig. 32. Predicted Exit Wall Strains at 5 in. From Exit Point (No Reflections, with Cavitation)

A general comparison of maximum strains some distance removed from the exit point may also be helpful in determining the merit of the analysis. An examination of the exit points for the low velocity shots (10-14) shown in Fig. 2 reveals that they are approximately 4-6 inches away from gages 9-12 at the center of the plate. The maximum strain at the center gages for each shot is 2.5×10^3 (10), 2.6×10^3 (12), 3.3×10^3 (13), and 3.2×10^3 (14) microstrain*. The maximum strain from the SATANS results for shot 14 between 4 and 6 inches from the exit point is approximately 300 microstrain with no images and no cavitation, and approximately 1000 microstrain when cavitation is assumed. Thus, the maximum predicted strain at the center of the plate is underestimated.

An examination of all of the measured strain traces for shots 10-14 reveals that apparently the maximum strain for all five shots occurs at gage 4 and is approximately -4.0×10^3 to -4.5×10^3 microstrain**. Also noted is the fact that the only other gage that registers a large negative (compression) strain for these shots is gage 3. These two gages are on the wet side of the wall. The opposite gages on the dry side register tension strains, thus indicating large bending moments at these two gages. This behavior is probably due to the fact that these two gages are closest to the clamped edges of the plate where the bending effects would be pronounced. The maximum predicted strains near the edge are also larger than those at point c.

*The traces at gages 9-12 were lost for shot 14.
**The strain traces at gage 4 look essentially the same as that of Fig. 27 for almost every shot, including the high and medium velocity shots.

As a consequence of the rather poor comparison between the measured and predicted strains when cavitation is not included, and the extremely long computation time required, a full scale analysis using BR-1HR has not been made. The results from preliminary runs using BR-1HR for short periods of time indicate the same low estimates of strain that SATANS predicts.

VII SUMMARY AND CONCLUSIONS

The experimental and analytical hydraulic ram and structural response programs at NWC and NPS have been briefly described. Particular attention was given to the hydraulic ram pressure code developed by Lundstrom and Fung at NWC, the hydraulic ram tests conducted on exit walls by NWC, the computer study of the exit wall response by NPS, and the experimental and computer study of the hydraulic ram shock and drag phase pressures and circular entry wall response by NPS. The goals of this combined NWC-NPS effort have been the development of an understanding of the hydraulic ram-structural response phenomenon and the preparation of computer codes that can be used to accurately predict the fluid pressures and the subsequent wall response to the penetrating projectiles.

This report is particularly concerned with the comparison of measured wall strains and predicted wall strains at both the entry wall and the exit wall. The piston theory for approximating the fluid-structure interaction has been incorporated into the two computer codes, SATANS and BR-1, allowing the separation of the fluid and structural analyses. For the entry wall analysis, the Yurkovich shock pressure theory has been combined with the NWC hydraulic ram pressure code to give a predicted fluid pressure field on the the entry wall as a function of time. This predicted pressure field was applied to the circular entry wall and the response of the wall was computed using SATANS. A comparison of the measured and computed strain histories two in. from the center of the plate reveals that the predicted strains have the same general form as the measured strains, but the magnitudes of the predicted strains are smaller than the measured strains shortly after the

response begins. When cavitation at the wall is accounted for in SATANS (no net tension interface pressure), the magnitude of the predicted strains increases to the level of the measured strains. However, except for the circumferential strain on the dry side, the similarity in the form of the strain history is lost. In addition, the predicted radial strain with cavitation shows considerably more oscillation than the measured radial strain. Thus, its questionable whether or not cavitation occurs at the entry wall. The NWC high-speed motion pictures of the entry wall response do not reveal any cavitation there.

For the exit wall analysis, the predicted incident fluid pressure field on the exit wall was obtained from the NWC hydraulic ram pressure code. The incident pressure was assumed to drop to zero when the bullet exited the tank. The other walls were taken either as free surfaces or were not considered in two separate analyses. The response of the 20 inch square exit wall to the two pressure fields was computed using SATANS by idealizing the square plate as a 20 inch diameter circular plate centered at the exit point.

A comparison of the strains in the exit wall measured by NWC with the strains predicted by SATANS, without cavitation, reveals that three of the four predicted strain histories have essentially the same form as those of the corresponding measured strains. In particular, the predicted and measured strain behavior appear to be in very good qualitative agreement at the time when the bullet is estimated to exit the tank. However, the magnitude of the predicted strains is one to two orders of magnitude smaller than the measured strains. When cavitation is accounted for in the analysis, the magnitude of the predicted strains increases to less than an order of magnitude smaller

than the measured strains, but the similarity in the form of the strain histories is lost. Thus, it appears from both the entry wall strain comparison and the exit wall strain comparison that the cavitation assumption of no net tension pressure at the interface is probably not correct. A certain level of tension should be allowed.

No full scale analyses of the exit wall were conducted using the modified BR-1 code, BR-1HR, due to: 1) a projected minimum execution time of about 3 hours on the NPS IBM 360/67, 2) the fact t' ... rt preliminary runs using BR-1HR gave the same level of small strain as , and 3) the code in its present form cannot handle cavitation.

As a result of this study, the major conclusion can be made that the piston theory without cavitation yields good predictions of the form of the strains, but the magnitude of the predicted strains is often an order of magnitude or more too small. Addition of cavitation of the fluid-structure interface leads to larger predicted strains, but the similarity in the form of the strains is lost. Studies are currently underway to modify the piston theory to allow larger strains without changing the form of the strain history.

VIII REFERENCES

1. McKenzie, J. R., "Survey and Bibliography of Aircraft Survivability - Vulnerability Research with Emphasis on Hydraulic Ram," Master Thesis, Naval Postgraduate School, Dec. 1973.
2. Fry, P., "A Review of the Analyses of Hydraulic Ram," Air Force Flight Dynamics Laboratory Tech, Rpt. TR-pending.
3. Lundstrom, E. A., "Fluid Dynamic Analysis of Hydraulic Ram," Naval Weapons Center, NWC TP 5227.
4. Lundstrom, E. A., and Stull, E. W., "Fluid Dynamic Analysis of Hydraulic Ram II (Results of Experiments)," Joint Technical Coordinating Group/ Aircraft Survivability, JTCG/AS 73-T-291.
5. Lundstrom, E. A., and Fung, W. K., "Fluid Dynamic Analysis of Hydraulic Ram IV (Users Manual for Pressure Wave Generation Model)," Joint Technical Coordinating Group/Aircraft Survivability, JTCG/AS 74-T-018, Dec. 1974.
6. Fung, W. K., "Analysis of Hydraulic Ram - Structural Response I (Results of Experiment)," Joint Technical Coordinating Group/Aircraft Survivability, JTCG/AS-74-T-020 (I), Dec. 1974.
7. Bates, K. S. Jr., "Aircraft Fuel Tank Entry Wall-Projectile Interaction Studies," Master Thesis, NPS, June 1973.
8. Holm, D. P., "Hydraulic Ram Shock Wave and Cavitation Effects on Aircraft Fuel Cell Survivability," Master Thesis, NPS, Sept. 1973.
9. Soper, W. R., "Hydraulic Ram Studies," Master Thesis, NPS, Dec. 1973.

10. Fuhs, A. E., Ball, R. E., Power, H. L., "FY 73 Hydraulic Ram Studies," NPS-57Fu74021, Feb. 1974.

11. Mueller, L. S., "Experiments in Hydraulic Ram," Master Thesis, NPS, March 1974.

12. Kappel, L. C., "Hydraulic Ram Shock Phase Effects on Fuel Cell Survivability," Master Thesis, NPS, March 1974.

13. Power, H. L., "FY 74 Experimental Hydraulic Ram Studies," NPS-57Ph74081, Aug. 1974.

14. Holm, C. M., "Hydraulic Ram Pressure Measurements," Master Thesis, NPS, Dec. 1974.

15. Page, B., "Entry Wall Strain Measurements During Hydraulic Ram." Master Thesis, March 1975.

16. Patterson, J. W., "Fuel Cell Pressure Loading During Hydraulic Ram," Master Thesis, NPS, June 1975.

17. Power, H. L., "FY 75 Experimental Hydraulic Ram Studies," NPS-57PH75061, June 1975.

18. Ball, R. E., Power, H. L., and Fuhs, A. E., "Fuel Tank Wall Response to Hydraulic Ram During the Shock Phase," Journal of Aircraft, Vol. 10, No. 9, pp 571-572, Sept. 1973.

19. Ball, R. E., "Prediction of the Response of the Exit Wall of the NWC 50 Cubic Feet Tank to Hydraulic Ram," NPS-57Bp74031, March 1974.

20. Ball, R. E., "A Discussion of Dynamic Crack Propagation in Bent Plates," NPS-57Bp74041, April 1974.

21. Bitzburger, J. C., "Two-Dimensional Analysis of Fluid-Structural Interaction by Method of Finite Differences - Hydraulic Ram, The Fuel Tank Problem," Master Thesis, NPS, June 1974.

22. Yurkovich, R., "Hydraulic Ram: A Fuel Tank Vulnerability Study," McDonnell Aircraft Engineering Methods Authorization, F76-76-555, Sept. 1969.

23. Brass, J., Yamane, J. R., and Jacobson, M. J., "Effects of Internal Blast on Combat AircraftStructure; Volume I. Engineer's Manual, Volume II. User's and Programmer's Manual," Air Force Flight Dynamics Laboratory Tech. Rpt. AFFDL-TR-73-136, Jan. 1974.

24. Ball, R. E., "Aircraft Fuel Tank Vulnerability to Hydraulic Ram: Modification of the Northrup Finite Element Computer Code BR-1 to Include Fluid-Structure Interaction -- Theory and User's Manual for BR-1HR," NPS-57Bp74071, July 1974.

25. Ball, R. E., "A Program for the Nonlinear Static and Dynamic Analysis of Arbitrarily Loaded Shells of Revolution," J. Computers and Structures. Vol. 2, pp 141-162, 1972.

26. Ball, R. E., "A Computer Program for the Geometrically Nonlinear Static and Dynamic Analysis of Arbitrarily Loaded Shells of Revolution, Theory and User's Manual," NASA CR-1987, April 1972.

27. "Underwater Explosion Research, A Compendium of British and American Reports; Volume III - The Damage Process," Office of Naval Research, Dept. of the Navy, 1950.

28. Klosner, J. M., "Inadequacies of Piston Theory in Fluid-Shell Interactions," Journal of the Engineering Mechanics Division, ASCE, Vol. 96, No. EM2, pp 143-159, April 1970.

29. Bedrosian, B. and DiMaggio, F. L., "Acoustic Approximations in Fluid-Shell Interactions," Journal of the Engineering Mechanics Division, ASCE, Vol. 98, No. EM3, pp 731-742, June 1972.

30. Cole, R. H., Underwater Explosions, Princeton University Press, Princeton, NJ, 1948.

31. Ball, R. E., "A Geometrically Nonlinear Analysis of Arbitrarily Loaded Shells of Revolution," NASA CR-909, Jan. 1968.

IX. APPENDIX - EVALUATION OF THE BR-1HR MODEL

The accuracy of the BR-1HR model shown in Fig. 6 for linear response can be demonstrated by comparing the results from BR-1HR with the series solution to the problem of a simply supported, square, fluid-backed plate subjected to a uniform step pressure load P . The piston theory equation governing the motion of the plate can be given in the form

$$D\,\nabla^4 w + \frac{\gamma h}{g}\,\ddot{w} + \rho c\dot{w} = P \qquad t>0 \tag{A1}$$

where

$$D = \frac{Eh^3}{12(1-\nu^2)} \quad , \quad \nabla^4 = \frac{\partial^4}{\partial x^4} + \frac{\partial^4}{\partial x^2 \partial y^2} + \frac{\partial^4}{\partial y^4}$$

$E = 10.4 \times 10^6$ psi	- Young's modulus
$\gamma = 0.0965$ lb/in.^{3}	- Specific weight of the plate
$\nu = 1/3$	- Poisson's ratio
$h = 0.125$	- Thickness
$P^* = 1.0$ lb/in.^{2}	- Uniform pressure
$a = 20$ in.	- Plate length and width
$g = 386$ in./sec^2	- Acceleration due to gravity
$\rho = 7.64 \times 10^{-5}$ #-sec^2/in.^{4}	- Density of fuel
$c = 53{,}000$ in./sec	- Acoustic velocity of fuel

The solution to Eq. (A1) for the simply supported plate can be given in the series form

$$w = \sum_{m=1,3,5}^{\infty} \sum_{n=1,3,5}^{\infty} \eta_{mn} \sin \frac{m\pi x}{a} \sin \frac{n\pi y}{a} \tag{A2}$$

*When executing BR-1HR, P was taken as 0.01 lb/in.^{2} in order to keep the nonlinear effects small. The results were multiplied by 100 in the comparison with the series solution.

where

$$\eta_{mn} = \frac{gp}{\gamma h \omega^2} \left\{ 1 - \frac{e^{-\zeta\omega t}}{\sqrt{1-\zeta^2}} \cos\left(\sqrt{1-\zeta^2}\,\omega t - \psi\right) \right\}$$

when $\zeta < 1$, and

$$\eta_{mn} = \frac{gp}{\gamma h \omega^2} \left\{ 1 - \frac{e^{-\zeta w t}}{2\sqrt{\zeta^2-1}} \left[\left(\zeta + \sqrt{\zeta^2-1}\right) e^{\omega\sqrt{\zeta^2-1}\, t} - \left(\zeta - \sqrt{\zeta^2-1}\right) e^{-\omega\sqrt{\zeta^2-1}\, t} \right] \right\}$$

when $\zeta > 1$, where

$$p = \frac{16P}{\pi^2 mn}$$

$$\omega^2 = \frac{Dg\pi^4}{\gamma h a^4} \left(m^2 + n^2\right)^2$$

$$\zeta = \frac{\rho c g}{2\omega\gamma h}$$

$$\psi = \tan^{-1} \frac{\zeta}{\sqrt{1-\zeta^2}}$$

The outer surface strains ε_x, ε_y and γ_{xy} are given by

$$\varepsilon_x = \mp \frac{h}{2} \sum_{m=1,3}^{\infty} \sum_{n=1,3}^{\infty} \eta_{mn} \left(\frac{m\pi}{a}\right)^2 \sin\frac{m\pi x}{a} \sin\frac{n\pi y}{a}$$

$$\varepsilon_y = \mp \frac{h}{2} \sum_{m=1,3}^{\infty} \sum_{n=1,3}^{\infty} \eta_{mn} \left(\frac{n\pi}{a}\right)^2 \sin\frac{m\pi x}{a} \sin\frac{n\pi y}{a}$$

$$\gamma_{xy} = \pm\, h \sum_{m=1,3}^{\infty} \sum_{n=1,3}^{\infty} \eta_{mn} \left(\frac{m\pi}{a}\right) \left(\frac{n\pi}{a}\right) \cos\frac{m\pi x}{a} \cos\frac{n\pi y}{a}$$

where the top sign is used at the loaded (wet) surface and the bottom sign is for the unloaded (dry) surface. This problem is selected as a test case because it has a relatively simple series solution and it roughly approximates the actual loading condition on the exit wall.

The results from Eq. A2 for the displacement at the center of the plate are given in Fig. A1 as a function of time for $\rho c = 0$ (no fluid) and for $\rho c = 4.1 \frac{\#\text{-sec}}{\text{in}^3}$. Note the significant reduction in the response due to the presence of the fluid. The results from BR-1HR for the displacement at the center of the plate are given in Figs. A2 and A3, for $\rho c = 0$ and $4.1 \frac{\#\ \text{sec}}{\text{in}^3}$ respectively, for 50 time steps. The time increment used in BR-1HR was the maximum allowable for numerical stability. Also shown in Figs. A2 and A3 are the results from Eq. A2. Note the accurate displacement response from BR-1HR for both values of ρc.

Profiles of the plate displacement at 50 time steps with $\rho c = 0$ are given in Figs. A4a and A4b for $y = 5$ in. and $x = 8$ in. respectively. Profiles of the corresponding outer surface strain ε_x are given in Figs. A5a and A5b for $y = 6.5$ in. and $x = 10$ in. respectively. Examination of these figures reveals that the displacements are accurately predicted by the finite element model but the strains are not. In particular, the strains in the center portion of the plate are inaccurate. However, note that the strains at the center of the plate are relatively small. A plot of the outer surface strain ε_x at the center of the plate as a function of time is given in Fig. A6. Note the relative smoothness of the finite element strain compared to the strain from the series solution.

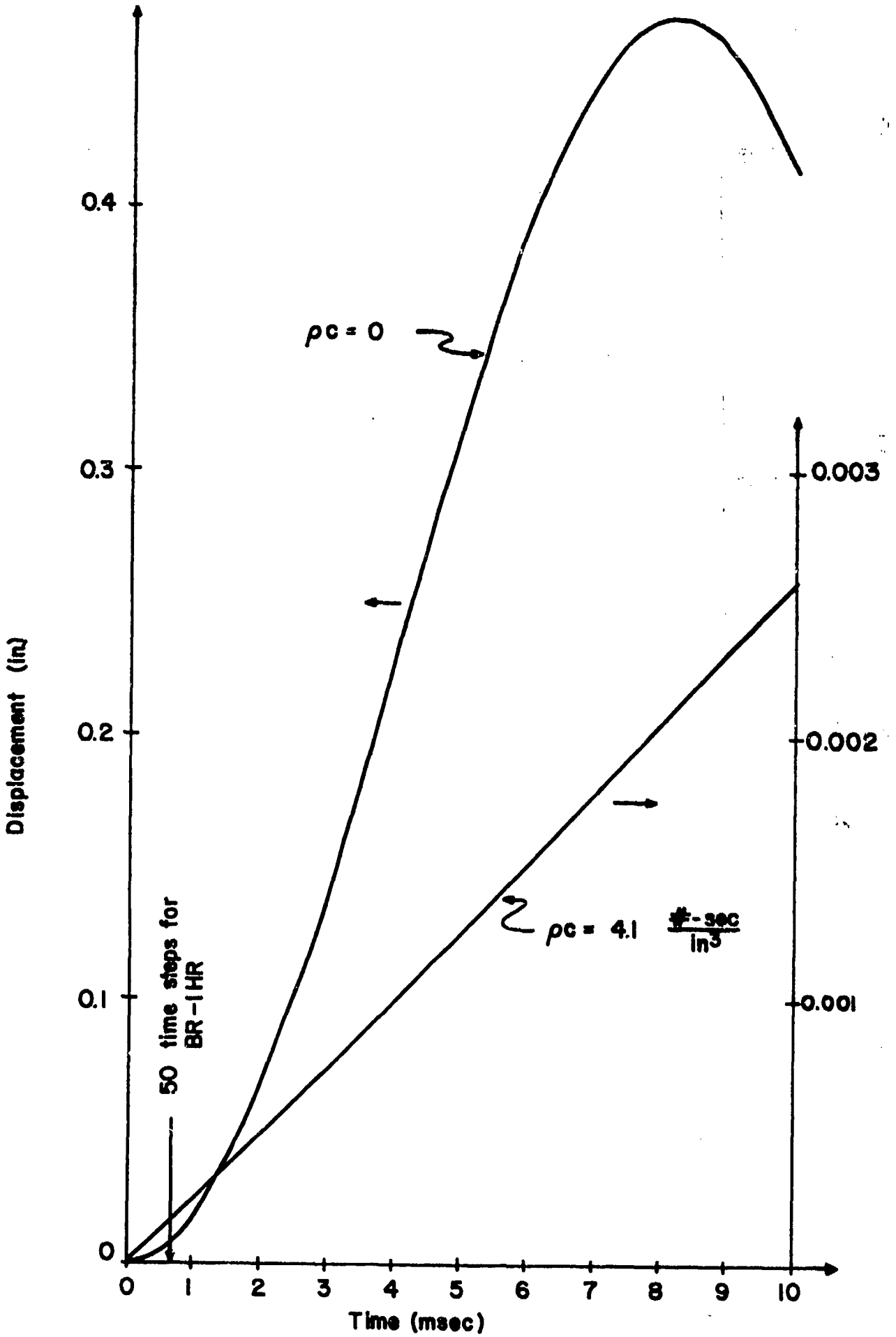

FIG. A1. SERIES SOLUTION FOR THE DISPLACEMENT AT THE PLATE CENTER

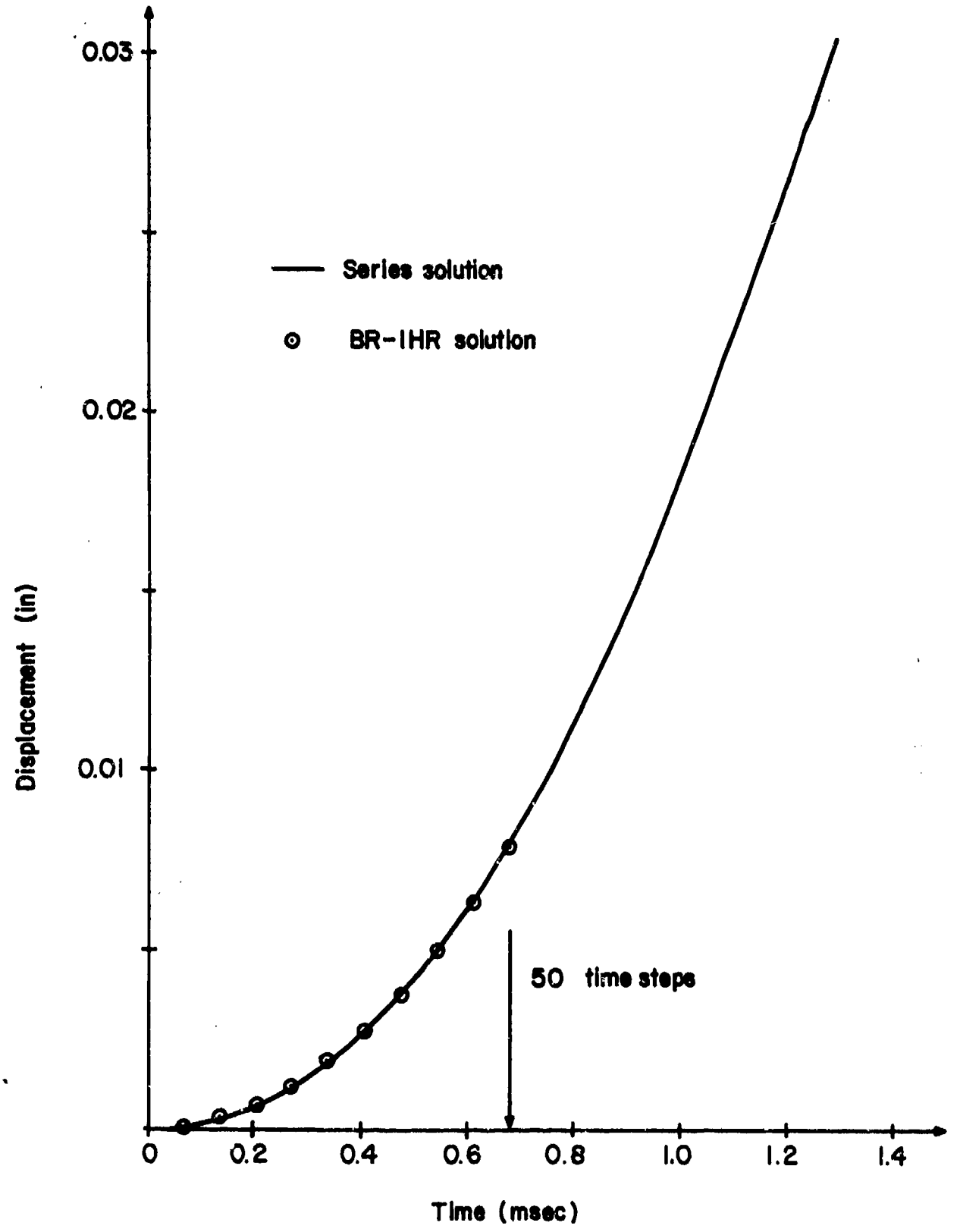

FIG. A2. COMPARISON OF DISPLACEMENT, NO FLUID

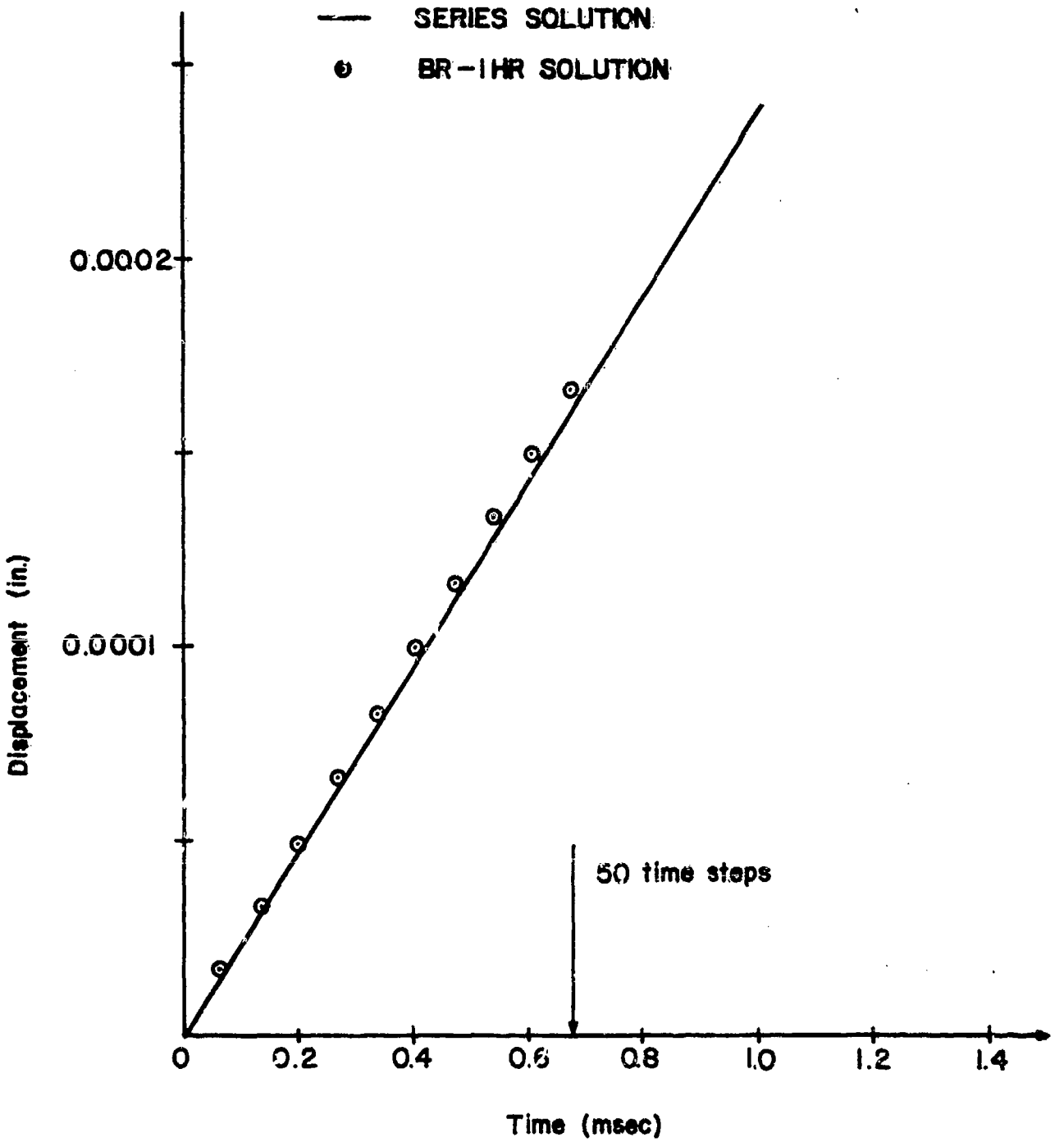

FIG. A3. COMPARISON OF DISPLACEMENTS, WITH FLUID

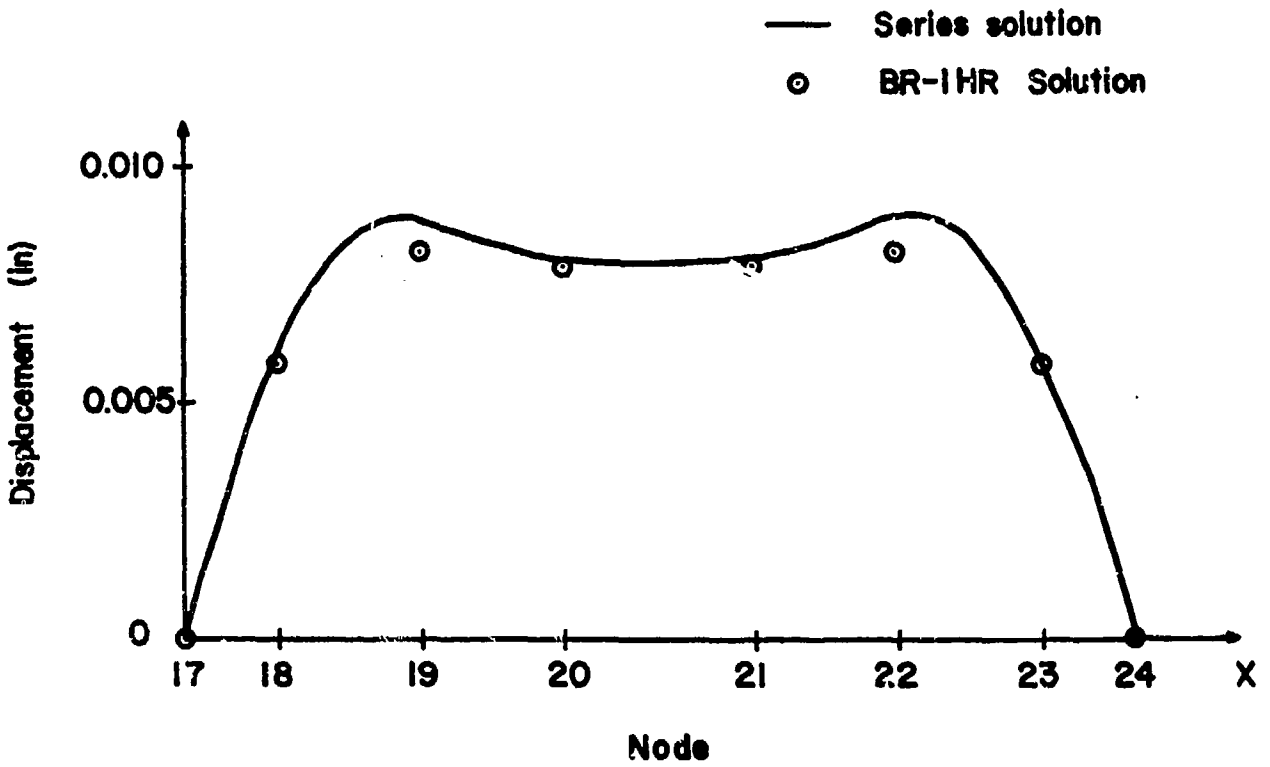

(A4a) y = 5 in

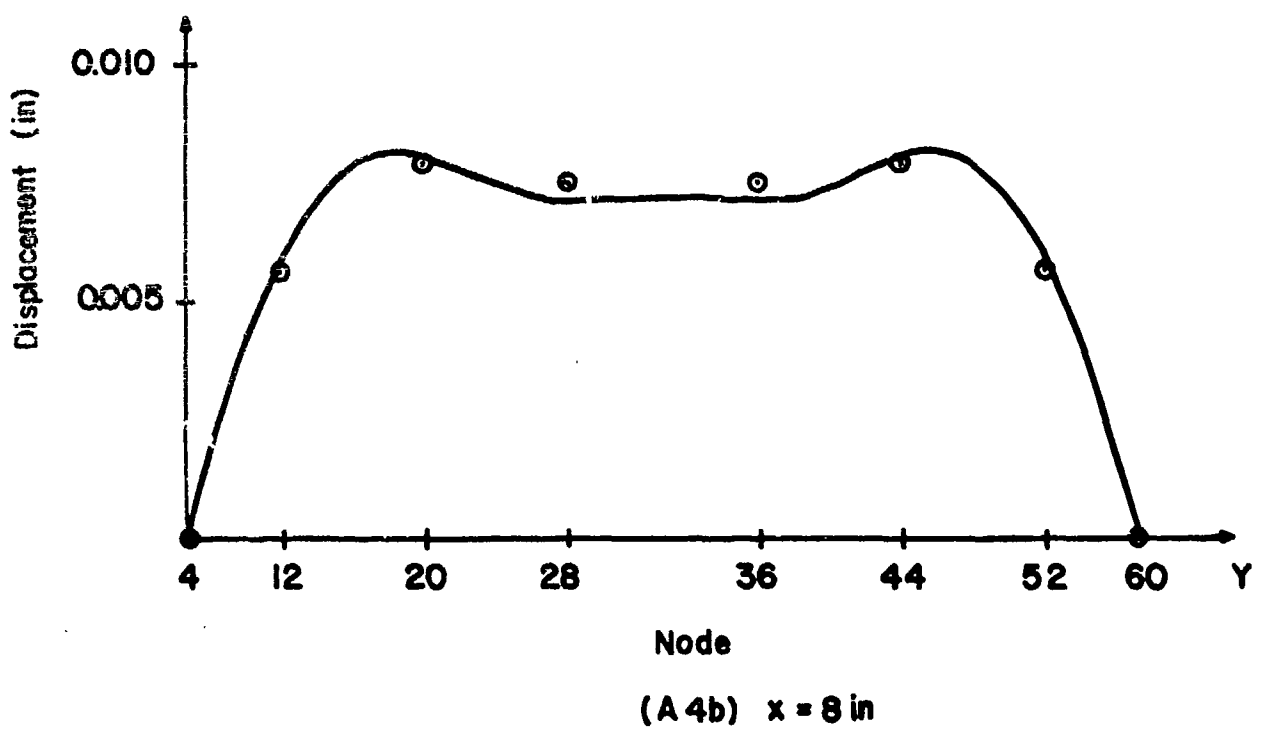

(A4b) x = 8 in

FIG. A4. PROFILE OF PLATE DISPLACEMENT

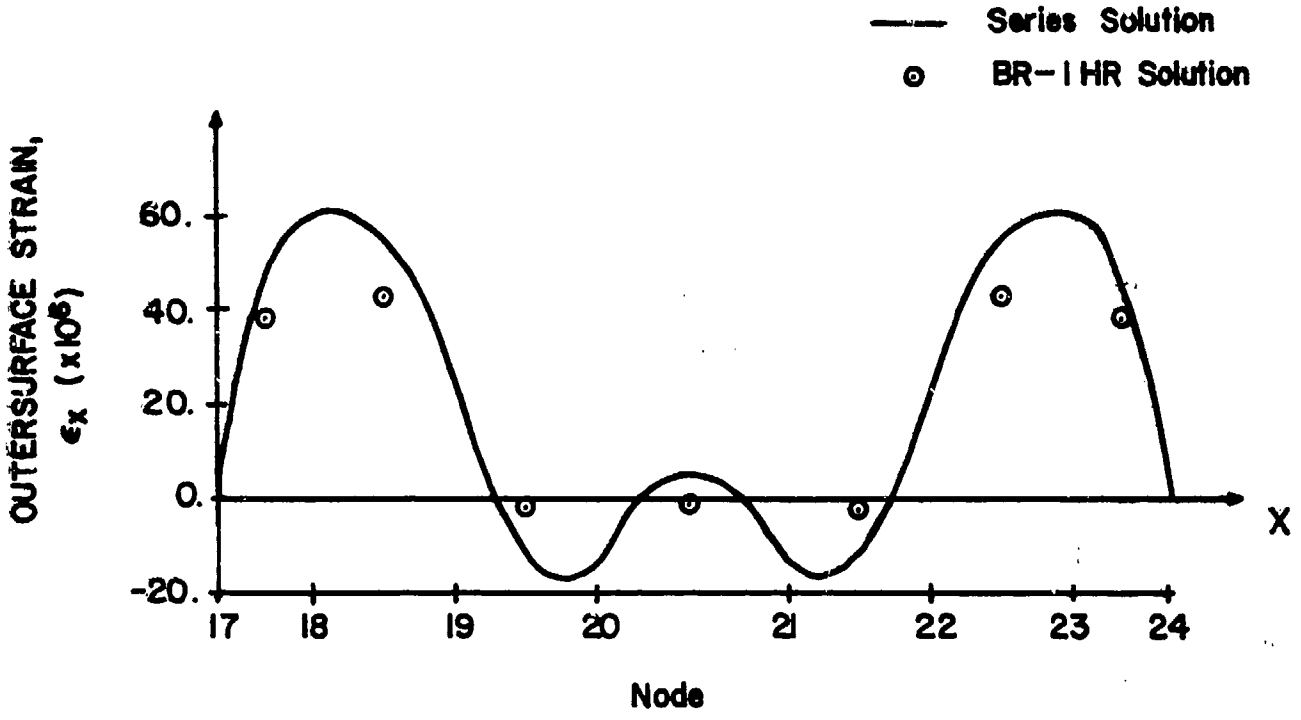

(A5a) y = 6.5 in.

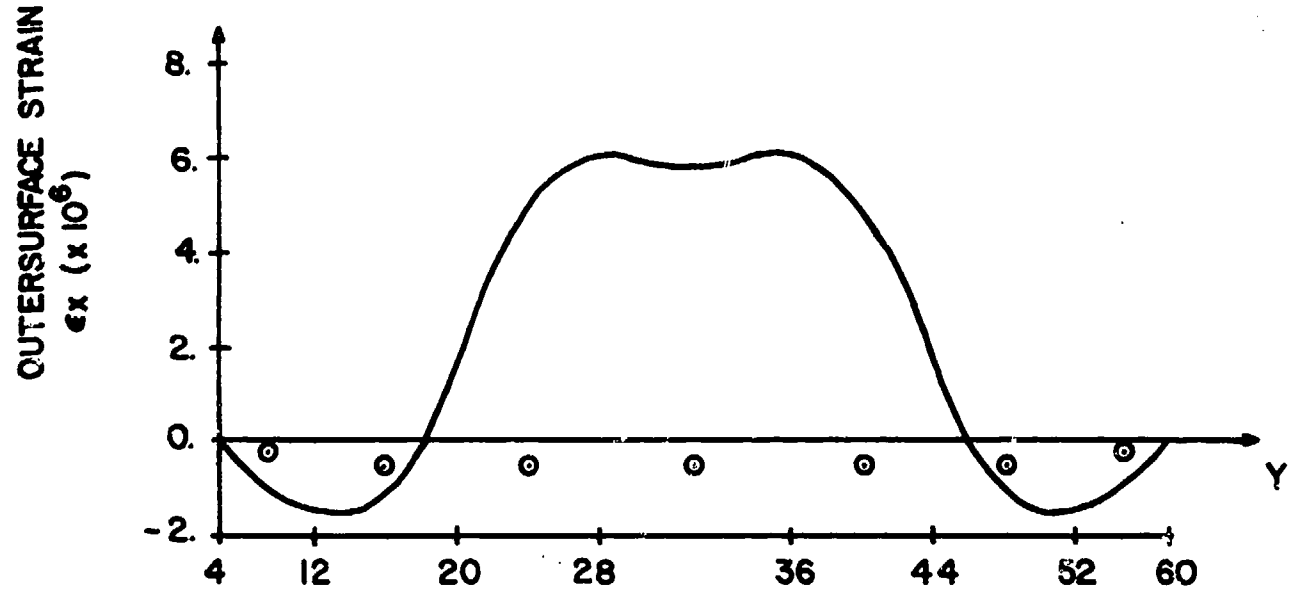

(A5b) x = 10 in.

FIG. A5. PROFILE OF PLATE OUTERSURFACE STRAIN ϵ_x

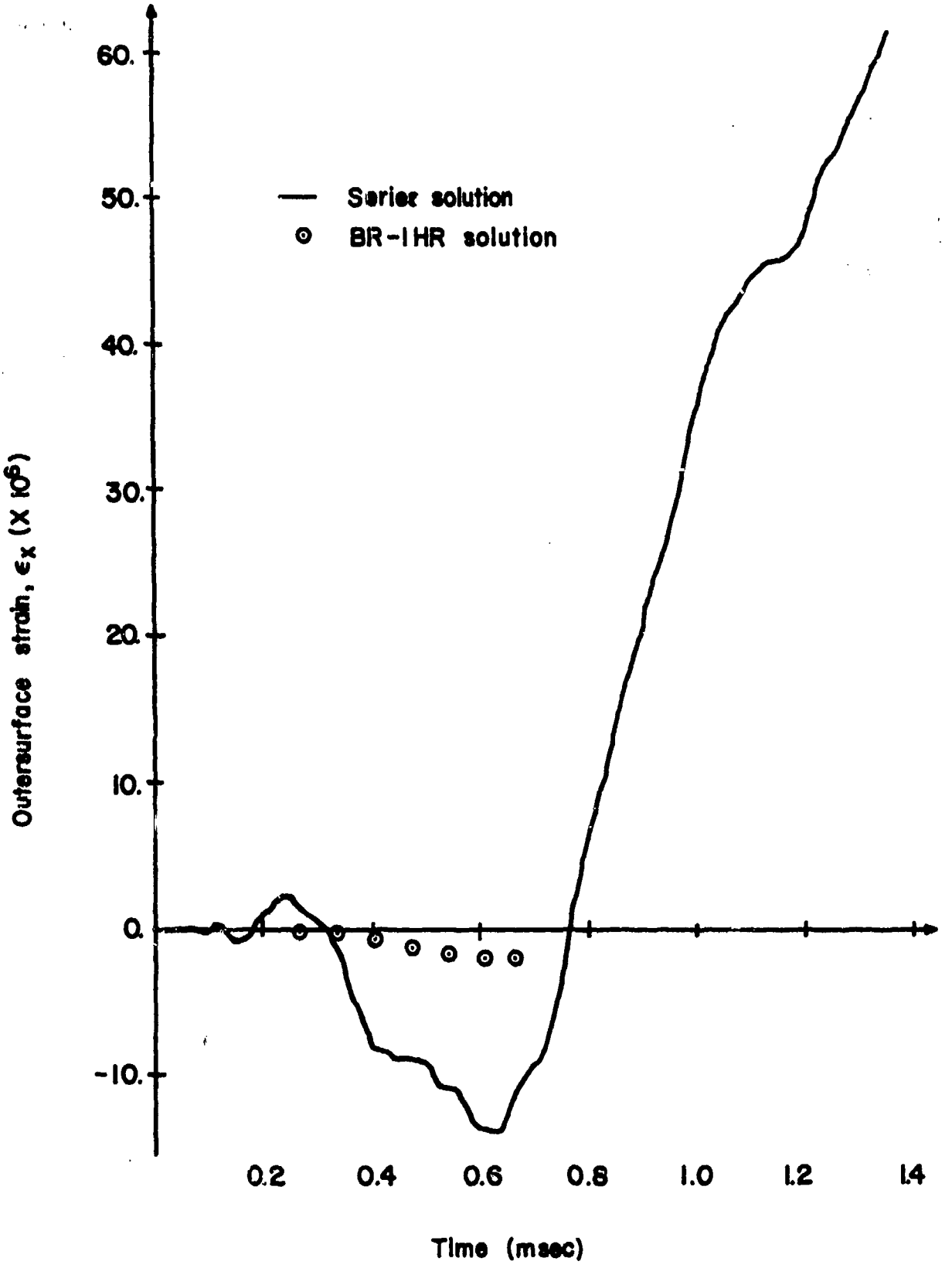

FIG. A6. COMPARISON OF THE STRAIN HISTORY AT THE CENTER OF THE PLATE

In order to determine the effect of the model upon the results, a 144 node model was also considered. A comparison of results showed that the 144 node model provided somewhat more accurate strains, but they were still inaccurate in the center portion of the plate.

X LIST OF FIGURES

XI. DISTRIBUTION LIST

	No. of Copies
1. Library Code 0212 Naval Postgraduate School Monterey, California 93940	2
2. Department of Aeronautics Code 67 Naval Postgraduate School Monterey, California 93940	
Prof. R. W. Bell, Chairman	1
Prof. R. E. Ball	5
3. Prof. R. R. Fossum Code 023 Dean of Research Administration Naval Postgraduate School Monterey, California 93940	1
4. Prof. A. E. Fuhs Code 59Fu Naval Postgraduate School Monterey, California 93940	1
5. Defense Documentation Center Cameron Station Alexandria, Virginia 22314	12
6. Commander Naval Weapons Center China Lake, CA 93555	1
Attn: George Moncsko, Code 408	2
D. P. Ankeney, Code 408	2
7. Mr. D. C. Ward (ASD/ENYW) Aeronautical Systems Division Wright-Patterson AFB, OH 45433	1
8. Mr. R. F. Jones, Jr. Code 1745, Structure Dept. Naval Ship Research & Development Center Bethesda, MD 20034	1
9. Commander (AIR-03PAF) Naval Air Systems Command Washington, DC 20361 Attn: CDR Gibson	1

		No. of Copies
10.	Commander (AIR0530XI) Naval Air Systems Command Washington, DC 20361 Attn: Alan DeGray	1
11.	Commander (AIR-320) Naval Air Systems Command Washington, DC 20361 Attn: Dr. Somoroff	1
12.	Commander (AIR-530313B) Naval Air Systems Command Washington, DC 20361 Attn: R. Hume	1
13.	Commander (AIR-5204) Naval Air Systems Command Washington, DC 20361 Attn: CAPT W. B. Rivers, USN	1
14.	Commander (AIR-530215) Naval Air Systems Command Washington, DC 20361 Attn: A. Cowles	1
15.	Marine Corps Dev. & Education Command Dev. Center Quantico, VA 22134 Attn: MAJ W. Waddell (D-042) Air Operations Div.	1
16.	Department of Transportation FAA Washington, DC 20591 Attn: Thomas G. Horeff (ARD-520)	1
17.	Commander (PE42) Naval Air Propulsion Test Center 1440 Parkway Ave. Trenton, NJ 09628 Attn: Russell Vizzini	1
18.	Commander (Code DG-10) Naval Surface Weapons Center Dahlgren, VA 22448 Attn: Thomas L. Wasmund	1

No. of Copies

19. Commander (Code 30P7) — 1
Naval Air Development Center
Warminster, PA 18974
Attn: Frank Borriello

20. Commander (Code 30C) — 1
Naval Air Development Center
Warminster, PA 18974
Attn: Robert A. Ritter

21. Commander (Code GAV) — 1
Naval Surface Weapons Center/DL
Dahlgren, VA 22448
Attn: Thomas McCants

22. Commander (AIR-5204) — 1
Naval Air Systems Command
Washington, DC 20361
Attn: MAJ William Allen

23. Roland Bernier (AMXBR-VL) — 1
Ballistic Research Labs
Aberdeen Proving Ground, MD 21005

24. US Army Aviation Sys Command — 1
P. O. Box 209
St. Louis, MO 63166
Attn: COL Jack Keaton, USA
(AMCPM-ASEO

25. C. Pedriani (SAVDL-EU-MOS) — 1
US Army Mobility R&D
Laboratories, Eustis Direct.
Fort Eustis, VA 23604

26. Albert A. Anctil (AMXMR-EM) — 1
Army Materials and Mechanics
Research Center
Watertown, MA 02172

27. Stuart V. Arnold (AMXMR-K) — 1
Army Materials and Mechanics
Research Center
Watertown, MA 02172

28. LTV Aerospace Corp. — 1
Vought Systems Division
P. O. Box 5907
Dallas, TX 75222
Attn: R. McGregor, U2-51773

No. of Copies

29. Ultrasystems, Inc. 1
1850 West Pinnacle Peak Road
Phoenix, AZ 85027
Attn: Mr. Patrick Zabel

30. Grumman Aerospace Corp. 1
South Oyster Bay Rd.
Bethpage, NY 11714
Attn: J. P. Archey (Dept 662)
Surv, Adv. Afc System

31. General Dynamics 1
Convair Aerospace Division
P. O. Box 80847
San Diego, CA 92138
Attn: V/STOL Fighter-Attack
Aircraft Group

32. Hughes Helicopter 1
Centinela Avenue
Culver City, CA 90230
Attn: A. C. Edwards

33. McDonnell Aircraft Company 1
P. O. Box 516
St. Louis, MO 63166
Attn: Jim Pousson, F-18

34. Sikorsky Aircraft 1
Stratford, CN 06602
Attn: Jim Foulk

35. The Boeing Company 1
P. O. Box 3999
Seattle, WA 98124
Attn: R. G. Blaisdell

36. Northrup Corporation 1
Aircraft Division
3901 Broadway
Hawthorne, CA 90250
Dr. R. Heitz, ORG 3772, Z-62

37. Armament Systems Inc. 1
712-F North Valley St.
Anaheim, CA 92801
Attn: Tom Gilbert

No. of Copies

38. McDonnell Aircraft Company — 1
P. O. Box 516
St. Louis, MO 63166
Attn: Ed Wiggins

39. Fairchild Industries Inc. — 1
Fairchild Republic Division
Farmingdale, NY 11735
Attn: J. A. Arrighi
A-10 Sur/Vul

40. Mr. Rodney F. Recht — 1
Denver Research Institute
University of Denver
2930 South University Blvd.
Denver, CO 80206

41. Dr. Frank Tiberi, Ft. Wth Div — 1
General Dynamics Corporation
P. O. Box 748
Fort Worth, TX 76101

42. Bell Helicopter Company — 1
P. O. Box 482
Ft. Worth, TX 76101
Attn: Jerry F. Joggers
Survivability Group

43. Falcon Research & Dev Corp — 1
1225 South Huron
Denver, CO 80223
Attn: Levelle Mahood

44. Rockwell International (Dept 421) — 1
Los Angeles Aircraft Division
International Airport
Los Angeles, CA 90009
Attn: Walt Dotseth/MS-AB75

45. Commander — 1
Naval Air Systems Command
Washington, DC 20361
Attn: COL R. Remers, USAF
(AIR-5204)

No. of Copies

46. R. G. Clodfelter (AFAPL/SFH) — 1
Air Force Aero Propulsion Laboratory
Wright-Patterson AFB, OH 45433

47. Jerry Wallick (ASD.ENYW) — 1
Aeronautical Systems Division
Wright-Patterson AFB, OH 45433

48. Commanding General — 1
Air Force Flight Dynamics Lab
Wright-Patterson AFB, OH 45433
Attn: MAJ John W. Mansur
(AFFDL/FES)

49. J. Rutland (AFATL/DLRV) — 1
Air Force Armament Test Lab
Eglin AFB, FL 32542

50. Gerald Bennett (ASD/XRHD) — 1
Air Force Aero Propulsion
Laboratory
Wright-Patterson AFB, OH 45433

51. Northrup Corp., Aircraft Div. — 1
3901 Broadway
Hawthorne, CA 90250
Attn: Don Wanlass, F-18
Code 2614/AH35

52. Columbus Aircraft Division — 1
Rockwell International
4300 East Fifth Avenue
Columbus, OH 43216
Attn: Robert J. Strohl

53. Andre Holten (AFFDL/FES) — 1
Air Force Flight Dynamics
Laboratory (AFSC)
Wright-Patterson AFB, OH 45433

54. Dr. M. J. Jacobson — 1
Orgn 3761/62
Northrop Corp.
Aircraft Division
3901 Broadway
Hawthorne, CA 90250